

TECHNICAL UNIVERSITY OF CRETE
SCHOOL OF MINERAL RESOURCES ENGINEERING
MSc in PETROLEUM ENGINEERING



**BASIN MODELING STUDY OF POTENTIAL SOURCE ROCK
FORMATIONS IN NORTH IONIAN SEA**

MASTER THESIS

GEORGIA MOSCHOU

Examination committee:

Prof. N. Pasadakis (Supervisor)

Dr. S. Bellas (Principal Researcher IPR-FORTH, Scientific Advisor)

Dr. I. Oikonomopoulos (Senior Geoscientist, HELPE Upstream)

Chania

October, 2021

*A Master Thesis submitted in partial fulfillment of the requirements for the degree of
Master of Science in Petroleum Engineering.*

*The MSc Program in Petroleum Engineering of the Technical University of Crete was
attended and completed by Mrs. Moschou Georgia due to the HELPE Group of
Companies Scholarship award.*

ABSTRACT

This study will focus on the basin modeling of potential source rock formations in western Greece. Its main purpose is to evaluate the potential source rock formations in two wells within the Ionian basin using PetroMod (version 2017.1) software. The first one is the Agios Georgios-3, an onshore well in Epirus area. The second one is the offshore East Erikoussa-1 well drilled to the east of the island Ereikoussa (part of the Diapontia Islands complex) in the northern Ionian Sea. The main goal of 1D basin modeling is to simulate the basin evolution (burial history, thermal history, maturity history, potential hydrocarbon generation, expulsion). The 1D basin modeling software was used to reconstruct the temperature and maturity histories of the formations penetrated by the studied wells, giving attention to the maturity, transformation ratio (TR) and hydrocarbon potential generation of the source rock formations. In addition, a sensitivity analysis using various scenarios was conducted for the Agios Georgios-3 well in order to monitor the influence of erosion thickness and boundary conditions and to assess the results.

In Agios Georgios-3 well three source rock formations were identified of different stratigraphic levels (the Posidonia shales of Jurassic age, the Vigla shales A and the Vigla shales B, both of Cretaceous age). Posidonia shales is the most mature source rock formation of this well. Despite references in the literature on the extensive dolomitization in the area, a fact that may have seriously affected this source rock, our model showed that Posidonia shales presented the highest transformation ratio and potential oil and gas generation masses of all source rock formations of this well. Vigla formation developed very good quality hydrocarbon source rocks as well. It consists of two main source rock formation zones, Vigla shales A (upper horizon) and Vigla shales B (lower horizon). The second one (older) is more mature than the first, with higher transformation ratio and potential hydrocarbon generation mass than the other.

In East Erikoussa-1 well only one source rock formation (the Vigla shales) was identified. The transformation ratio and potential oil and gas generation masses of Vigla are very low, indicating an immature source rock formation.

Our models provided that neither of the two studied wells reached the peak oil expulsion in the specific areas although the Posidonia shales show to be more mature with higher transformation ratio than the Vigla source rocks in the Agios Georgios-3 well.

Sensitivity analysis applied on the Agios Georgios-3 well, due to the fold and thrust belt (FTB) of the western Hellenides, which is affecting the well area. Results displayed that the thickness of eroded surface at 0m depth affects positively the transformation ratio values and potential hydrocarbon generation mass values of the source rock formations, with standard heat flow. It is also shown that among the boundary condition parameters which applied, only the heat flow plays an important role to the temperature and maturity modeling.

ΠΕΡΙΛΗΨΗ

Η συγκεκριμένη μελέτη εστιάζει στη μοντελοποίηση σχηματισμών μητρικών πετρωμάτων στη δυτική Ελλάδα. Κύριο σκοπό της αποτελεί η αξιολόγηση πιθανών μητρικών πετρωμάτων σε δύο γεωτρήσεις εντός της Ιόνιας λεκάνης χρησιμοποιώντας το λογισμικό PetroMod (έκδοση 2017.1). Η γεώτρηση Άγιος Γεώργιος-3 (χερσαία γεώτρηση) αποτελεί την πρώτη που εξετάζεται, η οποία και εντοπίζεται στην Ήπειρο. Η δεύτερη είναι η γεώτρηση Ανατολική Ερεϊκούσσα-1 (θαλάσσια γεώτρηση) η οποία τοποθετείται ανατολικά του νησιού της Ερεϊκούσσας (Διαπόντια νησιά) στο βόρειο Ιόνιο. Βασικό στόχο της μοντελοποίησης λεκανών σε μια διάσταση (1D) αποτελεί η προσομοίωση της εξέλιξής τους σε σχέση με το δυναμικό σε υδρογονάνθρακες που διαθέτουν (ιστορικό ταφής, θερμοκρασίας και ωριμότητας, δυνατότητα παραγωγής υδρογονανθράκων, εξαγωγή-αποβολή υδρογονανθράκων). Το λογισμικό μοντελοποίησης λεκάνης σε μια διάσταση (1D) χρησιμοποιήθηκε για την αναπαράσταση των ιστορικών θερμοκρασίας και ωριμότητας των σχηματισμών που διατρήθηκαν από τις ως προς εξέταση γεωτρήσεις, δίνοντας ιδιαίτερη βάση στην ωριμότητα, στο λόγο μετατροπής (TR) και στη δυνατότητα παραγωγής υδρογονανθράκων από τους σχηματισμούς των μητρικών πετρωμάτων. Επιπροσθέτως, πραγματοποιήθηκε ανάλυση ευαισθησίας για τη γεώτρηση Άγιος Γεώργιος-3 ερευνώντας διάφορα σενάρια σχετικά με την επιρροή του πάχους διάβρωσης και των οριακών συνθηκών που εισάγονται στο λογισμικό (boundary conditions), καθώς και η αξιολόγηση των αποτελεσμάτων.

Στη γεώτρηση Άγιος Γεώργιος-3 εντοπίζονται τρεις σχηματισμοί μητρικών πετρωμάτων διαφορετικών στρωματογραφικών επιπέδων (οι σχίστες με Ποσειδώνιες ηλικίας Ιουρασικού, οι σχίστες της Α ζώνης του σχηματισμού της Βίγλας και οι σχίστες της Β ζώνης του σχηματισμού της Βίγλας, και οι δυο ηλικίας Κρητιδικού). Ο σχηματισμός των σχιστών με Ποσειδώνιες χαρακτηρίζεται ως το πιο ώριμο μητρικό πέτρωμα αυτής της γεώτρησης. Μολονότι οι βιβλιογραφικές αναφορές επισημαίνουν την εκτεταμένη δολομιτίωση στην περιοχή, γεγονός που θα μπορούσε να έχει επηρεάσει σε μεγάλο βαθμό το συγκεκριμένο μητρικό πέτρωμα, το μοντέλο μας υποδεικνύει πως οι σχίστες με Ποσειδώνιες παρουσιάζουν τις υψηλότερες τιμές του λόγου μετατροπής (TR) και της δυνατότητας παραγωγής πετρελαίου και αερίου σε σχέση με τα υπόλοιπα μητρικά πετρώματα της γεώτρησης. Ο σχηματισμός της Βίγλας επίσης διαμόρφωσε μητρικά πετρώματα καλής ποιότητας σε υδρογονάνθρακες. Εντοπίζονται δύο κύριες ζώνες μητρικών πετρωμάτων στο συγκεκριμένο σχηματισμό, οι σχίστες της Α ζώνης (ανώτερος ορίζοντας) και οι σχίστες της Β ζώνης (κατώτερος ορίζοντας). Το μητρικό πέτρωμα της Β ζώνης (παλαιότερο) είναι πιο ώριμο από

αυτό της Α ζώνης, με υψηλότερες τιμές του λόγου μετατροπής (TR) και της δυνατότητας παραγωγής πετρελαίου και αερίου σε σχέση με το άλλο (Α ζώνη).

Στη γεώτρηση Ανατολική Ερεϊκούσσα-1 εντοπίζεται μόνο ένας σχηματισμός μητρικού πετρώματος (οι σχίστες της Βίγλας). Ο λόγος μετατροπής (TR) και η δυνατότητα παραγωγής πετρελαίου και αερίου του σχηματισμού της Βίγλας λαμβάνουν πολύ χαμηλές τιμές, υποδεικνύοντας ένα ανώριμο μητρικό πέτρωμα.

Σύμφωνα με τα μοντέλα που δημιουργήθηκαν, καμία από τις δύο γεωτρήσεις δεν αποβάλλει υδρογονάνθρακες στις συγκεκριμένες περιοχές, παρόλο που ο σχηματισμός των σχιστών με Ποσειδώνιες παρουσιάζεται ως πιο ώριμο μητρικό πέτρωμα και με υψηλότερες τιμές του λόγου μετατροπής (TR) σε σχέση με τα μητρικά πετρώματα της Βίγλας στη γεώτρηση Άγιος Γεώργιος-3.

Ακολούθως, πραγματοποιήθηκε ανάλυση ευαισθησίας στη γεώτρηση Άγιος Γεώργιος-3, λόγω της ζώνης πτυχών και επωθήσεων (fold-and-thrust belt ή σύντομα FTB) των δυτικών Ελληνίδων, η οποία και επηρεάζει την περιοχή της γεώτρησης. Τα αποτελέσματά της δείχνουν πως το πάχος διάβρωσης στα 0m βάθος έχει θετική επιρροή στις τιμές του λόγου μετατροπής (TR) και στις τιμές της δυνατότητας παραγωγής υδρογονανθράκων των μητρικών πετρωμάτων, ενώ παράλληλα η τιμή της θερμικής ροής παραμένει αμετάβλητη. Επίσης, παρατηρείται πως μεταξύ των παραμέτρων των οριακών συνθηκών που εισάγονται στο λογισμικό (boundary conditions) μόνο η θερμική ροή παίζει σημαντικό ρόλο στη μοντελοποίηση της θερμοκρασίας και της ωριμότητας των μητρικών πετρωμάτων του σχηματισμού.

ACKNOWLEDGEMENTS

First of all, I would like to express my sincere gratitude to my supervisor Professor Nikos Pasadakis for his scientific advice and his patience throughout the entire project. Additionally, I want to thank Dr. Spyridon Bellas (Principal Researcher at the Institute of Petroleum Research – IPR of the Foundation for Research and Technology – FORTH) for his scientific directions, guidance and recommendations that arose during this study. Finally, I would like to thank Ms. Vagianna Makri for her comments, continued support and encouragement.

TABLE OF CONTENTS

1 INTRODUCTION.....	1
1.1 Aim of the thesis	1
1.2 Description of the chapters	1
2 BASIN MODELING.....	3
2.1 Introduction	3
2.2 Burial history	5
2.3 Thermal history.....	11
2.4 Modeling maturation, hydrocarbon generation and expulsion	16
2.4.1 Modeling maturation.....	17
2.4.2 Hydrocarbon generation.....	19
2.4.3 Expulsion.....	21
2.5 Modeling maturation.....	22
3 STUDY AREAS	23
3.1 Geological background of Ionian basin.....	23
3.1.1 Tectonostratigraphic evolution	23
3.1.2 Lithostratigraphy.....	24
3.1.3 Petroleum system elements	25
3.2 Geographical location	28
3.2.1 Onshore well location	28
3.2.2 Offshore well location.....	29
3.3 Wells description	29
3.3.1 Agios Georgios-3	30
3.3.1.1 Lithostratigraphic data	30
3.3.1.2 Identification of potential source rocks.....	31
3.3.1.3 Oil window - Timing of oil generation	33
3.3.1.4 Calculation of the eroded formation thickness	33
3.3.1.5 Dolomitization.....	34
3.3.2 East Erikoussa-1	36
3.3.2.1 Lithostratigraphic data	36
3.3.2.2 Identification of potential source rocks.....	37
3.3.2.3 Oil window - Timing of oil generation.....	38
4 1D ONSHORE WELL MODELING.....	39
4.1 Thrust_model_1 and model_erikoussa input parameters	39

4.1.1 Age & Depth.....	39
4.1.2 Event type.....	40
4.1.3 Lithology	40
4.1.4 PSE.....	41
4.1.5 Source Rock Parameters.....	41
4.2 Boundary Conditions	43
4.2.1 Paleo Water Depth (PWD)	43
4.2.2 Sediment Water Interface Temperature (SWIT).....	44
4.2.3 Heat Flow (HF).....	45
4.3 Simulation	47
4.4 Calibration.....	48
4.4.1 Temperature (T).....	48
4.4.2 Vitrinite Reflectance (Ro)	49
5 RESULTS.....	51
5.1 Agios Georgios-3.....	51
5.1.1 Burial history	51
5.1.2 Temperature history	52
5.1.3 Present-day maturity	53
5.1.4 Transformation ratio (TR).....	54
5.1.5 Petroleum generation and Expulsion.....	55
5.1.6 Sensitivity analysis.....	58
5.2 East Erikoussa-1	67
5.2.1 Burial history	67
5.2.2 Temperature history.....	68
5.2.3 Present-day maturity	69
5.2.4 Transformation ratio (TR).....	70
5.2.5 Petroleum generation and Expulsion	71
6 CONCLUSIONS.....	75
6.1 Agios Georgios-3.....	75
6.2 East Erikoussa-1	76
6.3 Correlation.....	76
REFERENCES	79
APPENDIX	88

LIST OF FIGURES

Figure 1: Geological processes in basin modeling (Hantschel and Kauerauf, 2009).....	4
Figure 2: A hypothetical stratigraphic column containing a depositional hiatus and an erosional unconformity to be used in the construction of a burial history (Dembicki, 2017). ..	6
Figure 3: A sedimentation history for the stratigraphic column (Fig. 2) to be used in the construction of a burial history (Dembicki, 2017).	7
Figure 4: The burial history based on the stratigraphic column in Fig. 2 and the sedimentation history in Fig. 3 (Dembicki, 2017).....	8
Figure 5: Depth versus porosity plot for a series of lithologies based on the Sclater and Christie (1980) exponential model using empirically determined initial porosities and compaction factors (Dembicki, 2017).	9
Figure 6: Kozeny–Carman relationship of porosity with permeability (Dembicki, 2017).	10
Figure 7: Burial history curve for a horizon with and without compaction correction (Dembicki, 2017).	10
Figure 8: Boundary value problem for a heat flow analysis (a) of the lithosphere and (b) in the sediments (Hantschel and Kauerauf, 2009).	13
Figure 9: Influence of the Beta factor on the heat flow history during a rifting event (Dembicki, 2017).	14
Figure 10: Summary of the TTI calculation method. After Waples, D.W., 1980, Time and temperature in petroleum formation: application of Lopatin’s method to petroleum exploration. American Association of Petroleum Geologists Bulletin 64 (6), 916–926 (in Dembicki, 2017).	18
Figure 11: The simple (3 component) model for kerogen generation of oil, gas, and a carbon residue (Dembicki, 2017).	19
Figure 12: Detailed location map for Arta-Preveza block (https://www.greekhydrocarbons.gr/en/ArtaPreveza_en.html). The well location is indicated by the black border (AY-3).....	28
Figure 13: Detailed location map for Block 1. (https://www.greekhydrocarbons.gr/en/Block01_en.html). The location of East Erikoussa-1 well is indicated by the black border (E.ER-1).	29
Figure 14: Lithostratigraphic data of the Agios Georgios-3 well (modified from Rigakis, 1999).	30

Figure 15: Vitrinite reflectance (Ro%) vs. depth and Sonic vs. depth diagram for calculation of the eroded formation thickness (Rigakis et al., 2013).	34
Figure 16: Dolomitization effects to the organic matter in the formations drilled by AgiosGeorgios-3 well, Arta syncline (Rigakis et al., 2013).	35
Figure 17: Lithostratigraphic data of the East Erikoussa-1 well (modified from Rigakis, 1999).	36
Figure 18: Petroleum System Elements plot of thrust_model_1 (Agios Georgios-3).	41
Figure 19: Petroleum System Elements plot of model_erikoussa (East Erikoussa-1).	41
Figure 20: Main input data for burial and thermal histories reconstruction in PetroMod for the Agios Georgios-3 well (thrust_model_1).	42
Figure 21: Main input data for burial and thermal histories reconstruction in PetroMod for the East Erikoussa-1 well (model_erikoussa).	43
Figure 22: Diagram showing depositional environments and bathymetric changes used in paleoenvironmental interpretations (modified after Allen, 1965, 1970). Figure form Okosun and Osterloff (2014).	44
Figure 23: Paleo water depth (m) vs. time (Ma) plot of thrust_model_1 (Agios Georgios-3).	44
Figure 24: Paleo water depth (m) vs. time (Ma) plot of model_erikoussa (East Erikoussa-1).	44
Figure 25: Global mean surface temperature at sea level through geological time.	45
Figure 26: SWI-Temperature (°C) vs. time (Ma) plot of thrust_model_1 (Agios Georgios-3).	45
Figure 27: SWI-Temperature (°C) vs. time (Ma) plot of model_erikoussa (East Erikoussa-1).	45
Figure 28: Heat flow mp of Greece by Fytikas and Kolios (1979) in Papadakis et al. (2016). The heat flow values are presented in mW/m ²	46
Figure 29: Heat flow (mW/m ²) vs. time (Ma) plot of thrust_model_1 (Agios Georgios-3).	46
Figure 30: Heat flow (mW/m ²) vs. time (Ma) plot of model_erikoussa (East Erikoussa-1). ..	47
Figure 31: Temperature profiles of (a) thrust_model_1 and (b) model_erikoussa.	49
Figure 32: Temperature calibration plots of (a) thrust_model_1 and (b) model_erikoussa. ...	49
Figure 33: Vitrinite reflectance calibration plot of thrust_model_1.	50
Figure 34: Burial history of Agios Georgios-3well.	51

Figure 35: Burial history of Agios Georgios-3 well with a temperature overlay.....	52
Figure 36: Temperature (°C) vs. time (Ma) plots of the three source rock formations of Agios Georgios-3 well.....	52
Figure 37: Maturity history plot (vitrinite reflectance) of the source rock formations of Agios Georgios-3 well.....	53
Figure 38: Vitrinite reflectance (%Ro) vs. time (Ma) plots of the three source rock formations of Agios Georgios-3 well.	54
Figure 39: Burial history plot of Agios Georgios-3 well with a transformation ratio overlay.	55
Figure 40: Transformation ratio (TR) vs. time (Ma) plots of the three source rock formations of Agios Georgios-3 well.	55
Figure 41: Burial plot with potential oil generation mass overlay by Pepper & Corvi (1995) for the source rock formations of Agios Georgios-3 well.	56
Figure 42: Burial plot with potential gas generation mass overlay by Pepper & Corvi (1995) for the source rock formations of the Agios Georgios-3 well.....	56
Figure 43: Potential oil generation mass by Pepper & Corvi (1995) vs. time (Ma) plots of the three source rock formations of Agios Georgios-3 well.....	57
Figure 44: Potential gas generation mass by Pepper & Corvi (1995) vs. time (Ma) plots of the three source rock formations of Agios Georgios-3 well.....	57
Figure 45: Burial plot of Agios Georgios-3 well with an expulsion onset overlay.....	57
Figure 46: Calibration plots of thrust_model.....	60
Figure 47: Calibration plots of thrust_model_2.....	60
Figure 48: Calibration plots of thrust_model_3.....	60
Figure 49: Calibration plots of thrust_model_4.....	61
Figure 50: Calibration plots of thrust_model_5.....	61
Figure 51: Transformation ratio (TR) vs. time (Ma) plots near to 0Ma of all thrust models at Vigla shales A formation.....	62
Figure 52: Transformation ratio (TR) vs. time (Ma) plots near to 0Ma of all thrust models at Vigla shales B formation.	62
Figure 53: Transformation ratio (TR) vs. time (Ma) plots near to 0Ma of all thrust models at Posidonia shales formation.	62

Figure 54: Potential oil generation mass by Pepper & Corvi (1995) vs. time (Ma) plots near to 0Ma of all thrust models at Vigla shales A formation.....	63
Figure 55: Potential oil generation mass by Pepper & Corvi (1995) vs. time (Ma) plots near to 0Ma of all thrust models at Vigla shales B formation.....	64
Figure 56: Potential oil generation mass by Pepper & Corvi (1995) vs. time (Ma) plots near to 0Ma of all thrust models at Posidonia shales formation.....	64
Figure 57: Potential gas generation mass by Pepper & Corvi (1995) vs. time (Ma) plots near to 0Ma of all thrust models at Vigla shales A formation.....	65
Figure 58: Potential gas generation mass by Pepper & Corvi (1995) vs. time (Ma) plots near to 0Ma of all thrust models at Vigla shales B formation.....	65
Figure 59: Potential gas generation mass by Pepper & Corvi (1995) vs. time (Ma) plots near to 0Ma of all thrust models at Posidonia shales formation.....	66
Figure 60: Burial history of East Erikoussa-1 well.....	68
Figure 61: Burial history of East Erikoussa-1 well with a temperature overlay.....	68
Figure 62: Temperature (°C) vs. time (Ma) plot of the source rock formation of East Erikoussa-1 well.....	69
Figure 63: Maturity history plot (vitrinite reflectance) of East Erikoussa-1 well.....	69
Figure 64: Vitrinite reflectance (%Ro) vs. time (Ma) plot of the source rock formations of East Erikoussa-1 well.....	70
Figure 65: Burial history plot of East Erikoussa-1 well with a transformation ratio overlay.....	70
Figure 66: Transformation ratio (TR) vs. time (Ma) plot of the source rock formation of East Erikoussa-1 well.....	71
Figure 67: Burial plot with potential generation oil mass overlay by Pepper & Corvi (1995) of East Erikoussa-1 well.....	72
Figure 68: Burial plot with potential generation gas mass overlay by Pepper & Corvi (1995) of East Erikoussa-1 well.....	72
Figure 69: Potential generation oil mass by Pepper & Corvi (1995) vs. time (Ma) plots of the source rock formation of East Erikoussa-1 well.....	73
Figure 70: Potential generation gas mass by Pepper & Corvi (1995) vs. time (Ma) plot of the source rock formation of East Erikoussa-1 well.....	73
Figure 71: Burial plot of East Erikoussa-1 well with an expulsion onset overlay.....	74

LIST OF TABLES

Table 1: Boundary condition tables of thrust_model_1 (Agios Georgios-3).....	47
Table 2: Boundary condition tables of model_erikoussa (East Erikoussa-1).	47
Table 3: Vitrinite reflectance and hydrocarbon generation stages	53
Table 4: Transformation ratio (TR) values of all the thrust models of Agios Georgios-3 well.	63
Table 5: Potential oil generation masses (mgHC/gTOC) of all the thrust models of Agios Georgios-3 well.....	66
Table 6: Potential gas generation masses (mgHC/gTOC) of all the thrust models of Agios Georgios-3 well.....	67

1 INTRODUCTION

1.1 Aim of the thesis

Basin modeling is dynamic modeling of geological processes in sedimentary basins over geological time spans (Hantschel and Kauerauf, 2009). Simulation of basin models starts with the sedimentation of the oldest layer until the entire sequence of layers has been deposited and present-day is reached. Deposition, heat flow analysis, petroleum generation, expulsion, migration and accumulation are the most important geological processes which are calculated during simulation.

This type of modeling has been an important part of oil and gas exploration studies since the 1970s. It is known that the best way to decrease investment risk in petroleum exploration is to determine the types and volumes of hydrocarbons before drilling. Companies have become more conscious with time to investment risk, especially for big and expensive projects, so basin and petroleum modeling became one of their main tools.

This study will focus on the basin modeling of potential source rock formations in western Greece. Its main purpose is to evaluate the potential source rock formations in two wells using Schlumberger's PetroMod (version 2017.1) petroleum systems modeling software. The first one is the Agios Georgios-3, an onshore well, while the second is the offshore East Erikoussa-1 well. The software used to construct their 1D basin models, giving attention to the maturity, transformation ratio (TR) and hydrocarbon potential generation of the source rock formations.

1.2 Description of the chapters

The study starts with the introduction in the first chapter. The second chapter presents the theoretical background of basin modeling, giving the main information about the processes taking place in basin modeling and the type of data to run the simulation. The third one presents an overview of the geological background of Ionian basin and a more detailed description about the two examined wells.

Next is the fourth chapter that describes the entire procedure which was followed for building the 1D model for the onshore and offshore wells and running the simulation using Schlumberger's PetroMod (version 2017.1) petroleum systems modeling software. Following,

the fifth chapter presents the results of 1D basin modeling in wells Agios Georgios-3 and East Erikoussa-1 with the best matching between measured and calculated (model) data. The sensitivity analysis results of Agios Georgios-3 well are presented as well. The final chapter summarizes the 1D basin modeling output for the source rock formations of both wells and presents the correlation between them.

2 BASIN MODELING

This chapter presents the theoretical background of basin modeling. Main information about the processes taking place in basin modeling and the type of data to run the simulation that are available, leads the modeler to follow the correct order of steps to construct the final model.

2.1 Introduction

Basin modeling has been an important part of oil and gas exploration studies since the 1970s. It is known that the best way to decrease investment risk in petroleum exploration is to determine the types and volumes of hydrocarbons before drilling. Seismic interpretation can identify potential subsurface traps but they cannot predict their content with absolute certainty. On the other hand, drilling on a closed structure does not guarantee that similar type of fluids will be found. So, a profitable exploration requires a methodology to predict the probability of success according to the available data.

After years of studies, the term “petroleum system” started to be used by the industry. It includes the geologic elements and processes needed for oil and gas to accumulate. The necessary elements are an effective source rock, reservoir, seal and overburden rock. The processes include trap formation, generation, migration and accumulation of petroleum. All of them must occur in the proper order for the organic matter in a source rock to be converted into petroleum and then to be stored and preserved. If a single element or process is missing or occurs out of the required sequence, a prospect loses viability (Al-Hajeri et al., 2009).

Companies have become more conscious with time to investment risk, especially for big and expensive projects, so basin and petroleum modeling became one of their main tools. Petroleum industry became the major sponsor for basin modeling development. Gradually, more specialized tools and various types of basin modeling simulators have been developed. Following them new terminologies have been introduced, such as “Petroleum Systems Modeling”, “Exploration Risk Assessment” or “Prospect and Play Analysis” (Hantschel and Kauerauf, 2009). In addition, these models became more and more sophisticated with time thanks to the geochemical parameters which have played a major role in their development. There are two sides of basin modeling: thermal and fluid flow modeling. Thermal modeling deals with maturation, generation and cracking (Philp, 2003).

According to Welte and Yalcin (1988), the methodical approach of basin modeling offers two distinct advantages. Firstly, it makes possible a logical, quantitative treatment of very complex geological and geochemical processes and secondly it allows these processes to be examined on the basis of an absolute geological time scale. The distance scale typically is tens to hundreds of kilometers, and the periods covered may reach hundreds of millions of years (Al-Hajeri et al., 2009).

Based on Hantschel and Kauerauf (2009), basin modeling is dynamic modeling of geological processes in sedimentary basins over geological time spans. Simulation of basin models starts with the sedimentation of the oldest layer until the entire sequence of layers has been deposited and present-day is reached. Deposition, heat flow analysis, petroleum generation, expulsion, migration and accumulation are the most important geological processes which are calculated during simulation (Fig. 1).

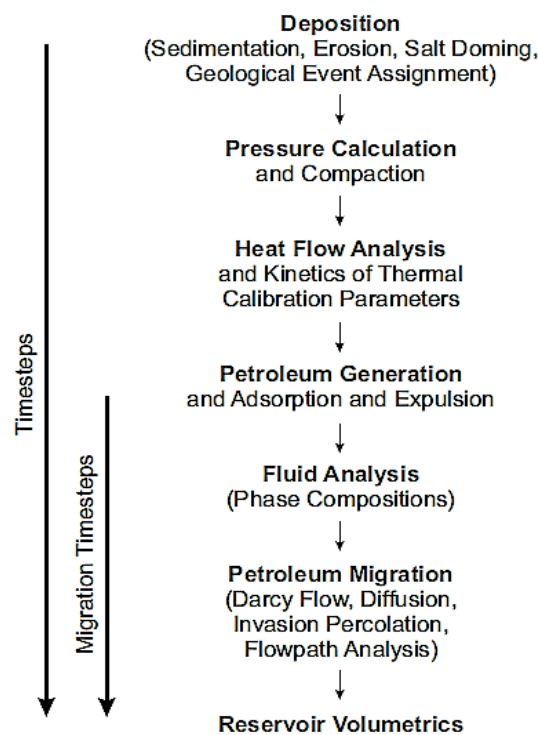


Figure 1: Geological processes in basin modeling (Hantschel and Kauerauf, 2009).

It uses the depth, age, and lithologic description of a stratigraphic sequence, cross section, or an entire basin in conjunction with information about the thermal history of the basin setting to simulate its geologic history and predict petroleum generation, expulsion, migration, and accumulation (Dembicki, 2017). In addition, the charge or the volume of hydrocarbons available for entrapment can be calculated by basin and petroleum system modeling, as well

as the fluid flow, to predict the volumes and locations of accumulation and their properties (Al-Hajeri et al., 2009).

Al-Hajeri et al (2009) mention, that basin and petroleum system modeling brings together several dynamic processes, including sediment deposition, faulting, burial, kerogen maturation kinetics and multiphase fluid flow. All these processes could be examined at several levels, while the complexity of modeling increases with spatial dimensionality. The simplest, 1D modeling, examines burial history at a point location. Two-dimensional (2D) modeling, either in map or cross section, can be used to reconstruct oil and gas generation, migration and accumulation along a cross section. Three-dimensional (3D) modeling is used to rebuild petroleum systems at reservoir and basin scales and to display the output in 1D, 2D, 3D and through time. In this study we emphasize on 1-D models.

The primary goals of basin modeling are to (1) determine if, when, where, how much, and what type of hydrocarbons have been generated and expelled by a source rock; (2) to be able to compare the timing of generation and expulsion with the timing of trap development; (3) to be able to trace potential migration pathway from source areas to trap areas; and (4) to be able to estimate the amount of hydrocarbons that are filling a trap (Dembicki, 2017).

In addition, basin and petroleum system modeling consists of two main stages: model building and forward modeling. Model building involves the construction of a structural model and the identification of the deposition and physical properties chronology of each layer. Forward modeling performs calculations on the model in order to simulate sediment burial, pressure changes, temperature changes, kerogen maturation, hydrocarbon expulsion, migration and accumulation. Calibration compares model results with independent measurements to allow refinement of the model (Al-Hajeri et al., 2009).

2.2 Burial history

The burial history of a basin contains information about burial depth and preservation of organic material. These two are related to pressures and temperatures the sediments were exposed to and the durations of exposure. Pressure is vital for migration of fluids and temperature is the main variable in conversion of kerogen to petroleum. Key inputs for building a burial history include sedimentation rate, compaction, uplift, erosion and depositional environment (Al-Hajeri et al., 2009).

According to Dembicki (2017), a burial history simulates the sedimentation events represented in a stratigraphic column. This stratigraphic column can be based on actual well data, deduced from seismic data or postulated from outcrop data. The burial history will consist of a depth–time plot that will represent the geologic events that define the stratigraphic sequence. The curves in the burial history represent the tops and/or bottoms of stratigraphic intervals (formations) or unconformity surfaces. The sedimentation events portrayed by each segments of a burial history curve represent deposition, erosion, or non-deposition (depositional hiatus).

To demonstrate how burial history curves are constructed, we use the following hypothetical stratigraphic column (Fig. 2) of the theoretical well. The following column consists of five depositional events (A to E) and two unconformities. Depth (i.e. thicknesses) is given in feet (ft). The first unconformity, at 2000ft, is a depositional hiatus with a time gap from 2 to 3MYBP (1 Myrs) where no sediment deposition occurred. The second unconformity, at 6000ft, has a time gap of 4 Myrs (from 8 to 12MYBP). It is an erosional unconformity where from 12 to 10MYBP, 2000ft of sediment was deposited followed by 2000ft of erosion from 10 to 8MYBP.

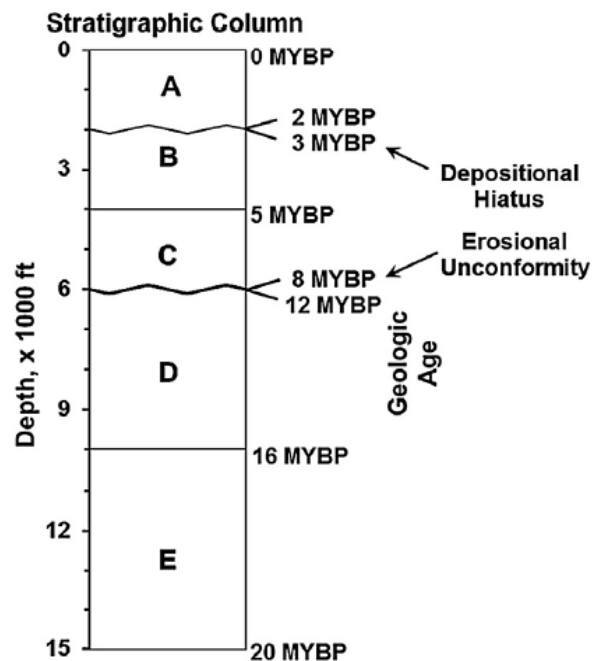


Figure 2: A hypothetical stratigraphic column containing a depositional hiatus and an erosional unconformity to be used in the construction of a burial history (Dembicki, 2017).

To display the previous stratigraphic column in a burial history, it is useful to break it down into a sedimentation history (Fig. 3). Each one of the depositional events is shown as an amount of sediment over a certain time period. Erosional events are negative sedimentation

events and depositional hiatus events plot along the zero line. To build a burial history diagram, we start on the left side of the sedimentation history plot and move right one step at a time.

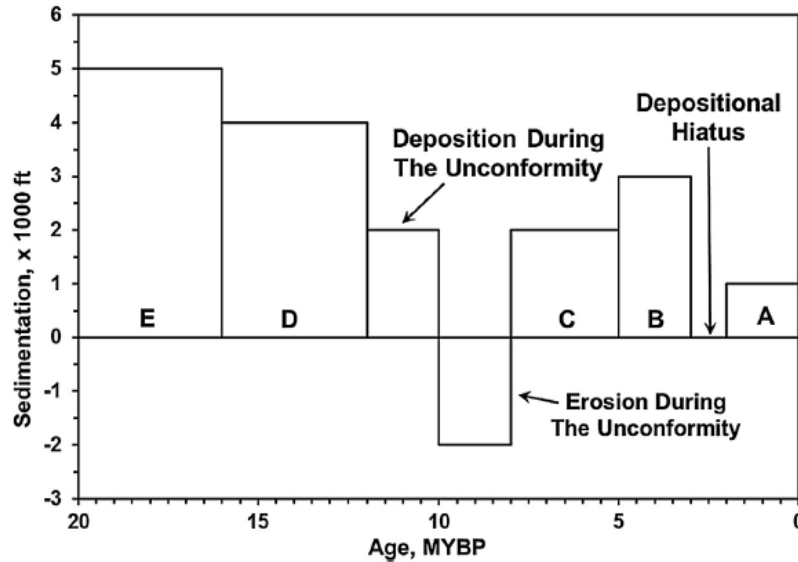


Figure 3: A sedimentation history for the stratigraphic column (Fig. 2) to be used in the construction of a burial history (Dembicki, 2017).

Following to the previous figure, depositing interval E starts at 0ft and 20MYBP on the burial history diagram (Fig. 4). The burial history curve segment ends at a depth of 5000ft at 16MYBP and interval E deposits 5000ft of sediment in 4 million years. Next is the deposition of interval D, 4000ft of sediment in 4 million years. The second segment of the burial history curve ends at 12MYBP at a depth 9000ft. The erosional unconformity is between intervals D and C. Deposition of 2000ft of sediment occurs between 12MYBP and 10MYBP, so that the third segment of the burial history curve ends at a depth of 11,000ft at 10MYBP. This is followed by the erosional phase of the unconformity where 2000ft of sediment is removed between 10MYBP and 8MYBP. This brings the end of the fourth segment of the burial history curve to a depth of 9000ft at 8MYBP. This is followed by the deposition of intervals C and B bringing the burial history curve to 11,000ft at 5MYBP and 14,000ft at 3MYBP, respectively. After the deposition of interval B, a period on non-deposition occurs between 3 and 2MYBP (i.e. strong bottom currents that did not allow for deposition of marine sediments). This part of the burial history curve remains at 14,000ft for this time period. The deposition of interval A is 1000ft of sediment between current time and 2MYBP in order to complete the burial history curve at 0MYBP at a depth of 15,000ft. To draw the other burial history curves (Fig. 4) we can continue this process by moving to the right one depositional interval for each successive curve.

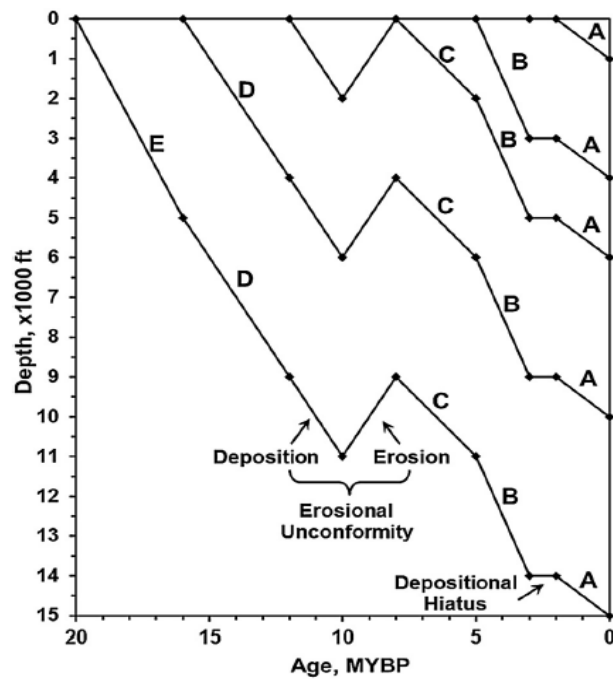


Figure 4: The burial history based on the stratigraphic column in Fig. 2 and the sedimentation history in Fig. 3 (Dembicki, 2017).

In spite of the fact that the resulting burial history plot is helpful, the depiction of the sedimentation events is not accurate. As a result, it is necessary to do compaction corrections to the sediment thicknesses as the overburden is added to the sediment column.

To correct for compaction, researchers have developed empirical relationships to help predict changes in porosity, such the exponential model of Sclater and Christie (1980), the reciprocal model of Falvey and Middleton (1981) and the argillaceous sediment model of Butler and Baldwin (1985).

The Exponential Model of Sclater and Christie (1980): (2.1)

$$P = P_0 \exp(-Kz)$$

The Reciprocal Model of Falvey and Middleton (1981): (2.2)

$$1/P = 1/P_0 + Kz$$

The Argillaceous Sediment of Bulter and Baldwin (1985): (2.3)

$$z = 6.02 S^{6.35}$$

Where P is the porosity, P_0 is the initial porosity, K is the lithology's compaction factor, z is the depth and S is solidity, the inverse of porosity ($1-P$).

These relationships recognize that different lithologies will have different initial porosities and different rates of compaction with increasing burial (Fig. 5).

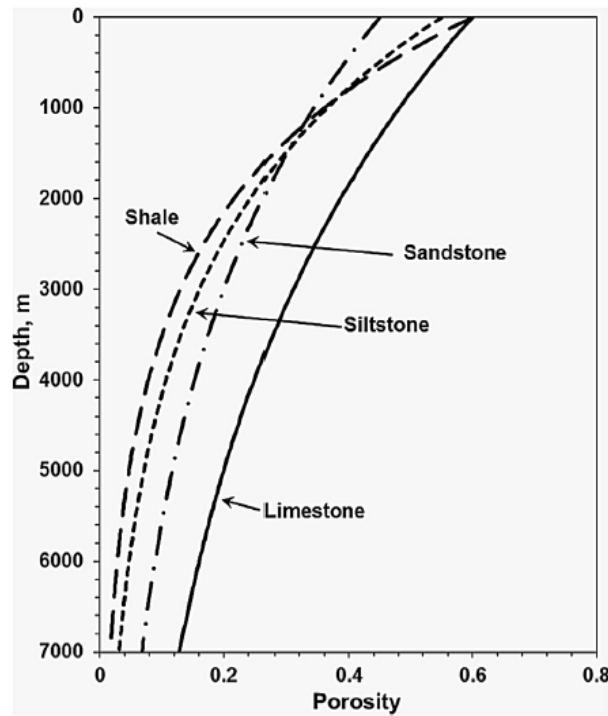


Figure 5: Depth versus porosity plot for a series of lithologies based on the Sclater and Christie (1980) exponential model using empirically determined initial porosities and compaction factors (Dembicki, 2017).

The sediment must have sufficient permeability to let fluids loose during compaction. To properly correct for compaction, the permeability of the sediments must be factorized into the process. Most compaction models use a porosity–permeability relationship, usually the Kozeny–Carman equation (Ungerer et al., 1990) for the sediment and apply Darcy's law to predict a fluid flow rate. An example of a set of porosity–permeability relationships used in compaction correction is shown in Fig. 6.

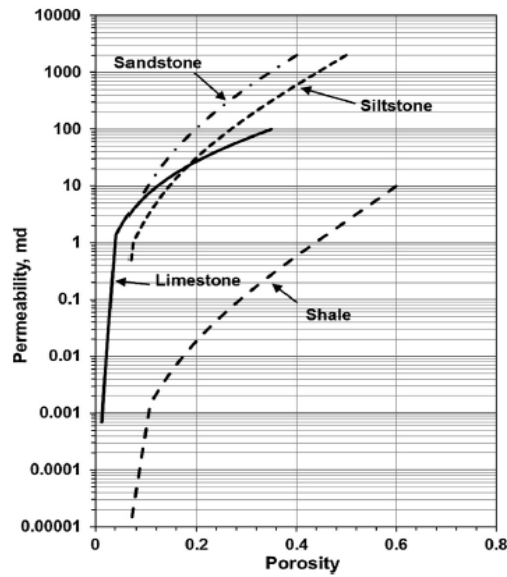


Figure 6: Kozeny–Carman relationship of porosity with permeability (Dembicki, 2017).

The main cause of porosity loss and volume reduction in sediments is mechanical compaction. Other factors that may also influence the process are low-permeability sediments (e.g., shales) which may not be able to lose fluid at high enough rates during rapid burial, resulting in excess fluid pressure (overpressure) and higher porosities than expected. In addition, cementation can result in a more rigid grain framework halting compaction. And finally, clay diagenesis and authigenic mineral growth can fill pores, while pressure solution (stylolitization) can eliminate pore space and reduce rock volume. All these processes are difficult to be predicted in basin modeling, so they are repeatedly ignored.

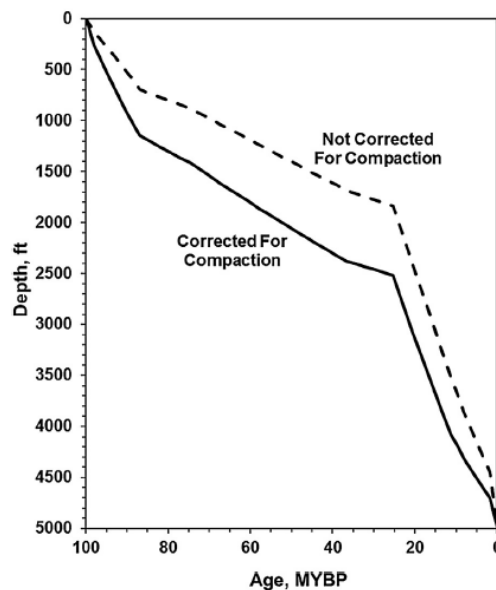


Figure 7: Burial history curve for a horizon with and without compaction correction (Dembicki, 2017).

The actual process of compaction correction is a complex mathematical procedure, especially for mixed lithologies and is usually handled by basin modeling software. On previous figure (Fig. 7) we can clearly see why the correction for compaction is essential.

Having both the corrected and uncorrected burial history curves, we notice that they have the same starting and ending points. However, the uncorrected curve is consistently greater than the corrected curve. As temperature increases with depth, the temperature experienced by the compaction uncorrected curve is always deeper than that experienced by the corrected curve. This will have a significant impact on the maturation and hydrocarbon generation modeling.

2.3 Thermal history

After burial history, the next important part of basin modeling is thermal history. Modeling of thermal history is used for the estimation of the temperature history of stratigraphic layers in a sedimentary basin. Time and temperature controls the organic matter maturation and hydrocarbon generation (kinetic processes). So, to model maturation and generation, it will be necessary to convert the depth in the burial history to temperature to arrive at a thermal history.

The thermal history of a basin is linked to the history of the crust in which it formed. Basin subsidence, uplift and heat flow are determined by the crustal behavior. Modeling the petroleum potential of a basin requires reconstruction of the temperature over geologic time and across the basin (Al-Hajeri et al., 2009).

According to Dembicki (2017), the thermal history is a simulation of the heat flow and temperatures experienced by sediments in a stratigraphic column during their burial history. It is usually expressed as the time–temperature histories of geologic events in a stratigraphic sequence. The thermal history is controlled by the surface temperature, heat flow, and thermal properties of the sediments, as well as influences from igneous bodies and/or circulating fluids.

During early days of basin modeling development, a simplistic method for approximating the thermal history was used. This method employed the surface temperature and bottom hole temperature (BHT) to calculate a geothermal gradient according to the following equation:

$$\text{Geothermal Gradient} = (\text{BHT} - \text{Surface Temperature}) / \text{Depth} \quad (2.4)$$

The bottom hole temperature is measured during wire line logging runs and reported in the log headers. It needs to be adjusted for the chilling of the borehole by circulating drilling fluids using a correction such as Horner Plot method (Horner, 1951; Fertl and Wichmann, 1977).

Geothermal gradients consider the thermal properties of the sediments in the stratigraphic sequence are constant with depth. In comparison with high-resolution temperature profiles in wells, they do not deliver accurate estimations of depth. As a result, it is more convenient to examine the thermal history of sediments from the perspective of heat flow.

Heat flow

Heat can be transferred by convection, conduction and radiation in sediments (Beardsmore and Cull, 2001; Hantschel and Kauerauf, 2009). The primary boundary conditions for heat flow analysis in sediments are the sediment water interface temperature and the basal heat flow. Mechanical and thermal processes of the crust and mantle are used for the determination of magnitude, orientation and distribution of the heat inflow at the base of the sediments (Allen and Allen, 2005). Two processes result in permanent heat flow from the Earth's interior to its surface: earth cooling and radiogenic heat production with a ratio of 17% to 83% respectively (Turcotte, 1980).

The heat conductivity law states, that a temperature difference between two locations causes a heat flow q . Its magnitude depends on the thermal conductivity of the material and the distance between these locations (Hantschel and Kauerauf, 2009). In mathematical notation it becomes:

$$\mathbf{q} = -\lambda \cdot \nabla T \quad (2.5)$$

with the temperature gradient ∇T and the thermal conductivity tensor λ .

The tensor λ is often assumed to have only two independent components: the conductivity along a geological layer λ_h and the conductivity across a geological layer λ_v . The heat flow vector at any location is mainly directed along the steepest decrease of temperature from a given location. In the lithosphere, it is mostly caused by the difference between its top and base temperatures: the surface temperature or sediment water interface (SWI) temperature at the top and the asthenosphere–lithosphere boundary temperature at its base (Hantschel and Kauerauf, 2009).

As Hantschel and Kauerauf (2009) mention, the sediment water interface temperature T_{swi} or bottom water temperature is the upper boundary for the heat flow problem. It can be determined with estimated paleo mean surface or air temperatures T_s and corrections for water depths. The annual mean ground surface temperature is primarily obtained from mean air temperatures (www.worldclimate.com), which depends on (paleo-) latitude.

The derivation of the paleo SWI temperatures from average surface temperature is very difficult to estimate. A decrease of 1.5°C per 100m in shallow water was proposed by Wygrala (1989). The temperature in water depths deeper than 400m is primarily controlled by the coldest arctic water temperatures T_n , which are presently affected by polar glaciations.

Heat flow analysis problem is commonly subdivided into two sectors: the consideration of the crustal model to calculate the heat in-flux into the sediments and the temperature calculation in the sediments afterwards (Fig. 8).

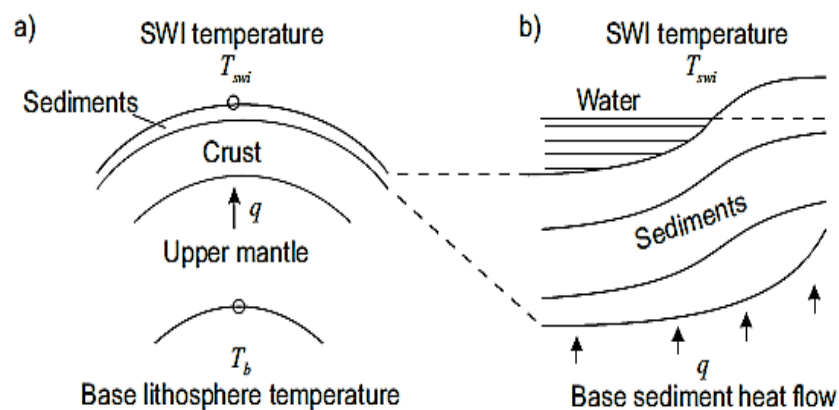


Figure 8: Boundary value problem for a heat flow analysis (a) of the lithosphere and (b) in the sediments (Hantschel and Kauerauf, 2009).

In one dimensional models (1D) all heat flow vectors considered as vertical. In general, they provide good temperature estimations except for local areas of extraordinary high thermal conductivities like salt domes which cannot be modeled. They bundle heat flow vectors from adjacent areas along highly conductive avenues.

Surface temperature

Onshore, the mean annual surface temperature is often suggested for the surface temperature (Gretener, 1981). Although, solar heating at the surface, climatic conditions and the thermal properties of the surface sediments may make the mean annual surface temperature an

inaccurate estimator for the surface temperature in some settings. Guidance may be gained from near surface groundwater and cave air temperatures to help constrain the surface temperature (Dembicki, 2017).

The temperature at the sediment–water interface is the surface temperature in offshore settings. This temperature will vary with latitude and water depth (Pickard, 1963). Below about 500m, where most exploration activity is currently focused, typical deep ocean temperatures will vary from -1° to 10°C , with the colder temperatures usually occurring in the higher latitudes or at depths greater than 4000m (Beardsmore and Cull, 2001). An estimate of the sediment–water interface temperature can be calculated from latitude and depth using an equation proposed by Beardsmore and Cull (2001).

The surface temperature and heat flow can change through time. Surface temperature could change with changing water depth or latitude. Heat flow can change with geologic events too. The rifting model put forward by McKenzie (1978) is a classic example of heat flow changing with time.

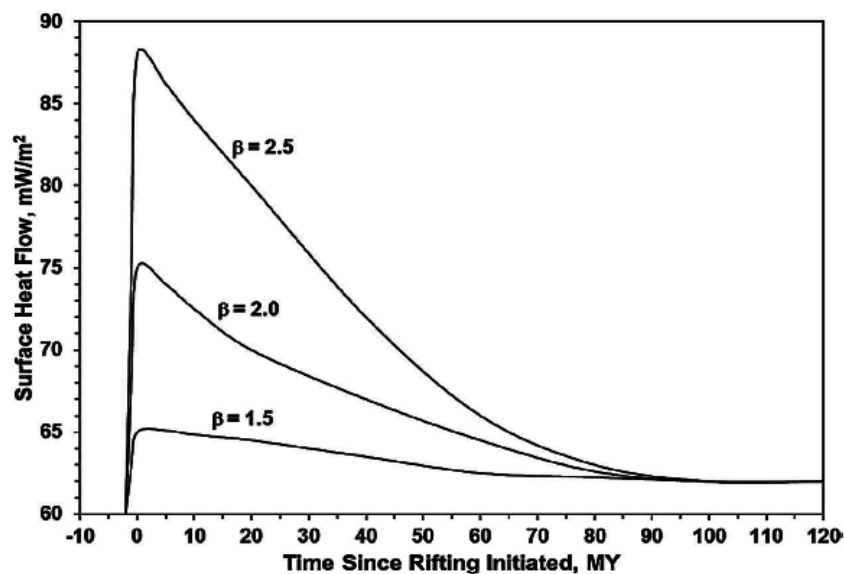


Figure 9: Influence of the Beta factor on the heat flow history during a rifting event (Dembicki, 2017).

Based on Dembicki (2017), at the start of rifting, a heat spike occurs (Fig. 9), due to the upwelling of the asthenosphere and accompanying crustal thinning. This heat flow spike is described by the Beta factor (β), which represents the amount of stretching that the crust underwent prior to faulting, breakup, and subsidence. As the amount of stretching increases, the heat flow receives higher values and the amount of crustal thinning is increasing too. The

model estimates the rate of decay of the heat flow spike as it returns to lower heat flows. Often, it is necessary to change the value of Beta factor to arrive at a reasonable heat flow history for the rifting event.

Thermal conductivity

Dembicki (2017) mention that, for a stratigraphic sequence, the movement of heat is from within the earth to the surface, where it is dissipated into the atmosphere, surface water, and eventually space by radiation. If we consider the geothermal gradient as the change in temperature (dT) over a depth interval (dz), or dT/dZ , under steady state conditions, then the heat flow, Q , is equal to $k (dT/dz)$, where k is the thermal conductivity. The thermal conductivity is a measure of the ability of a substance to conduct heat. Low thermal conductivity indicates an insulator, while high thermal conductivity indicates a good heat conductor. The unit for thermal conductivity is W/m/K.

Under steady state conditions, the local geothermal gradient is inversely proportional to the local thermal conductivity, while the conductive heat flow is considered constant from the bottom to the top of a sediment interval. However, basin development is a dynamic set of processes that are rarely constant through time. As a result, most stratigraphic sequences are deposited under transient heat flow conditions with the potential for brief period of steady state conditions. During transient conditions, the conductive heat flow is not constant from the bottom to the top of the sediment interval.

Heat capacity

Heat capacity is a measure of how heat flow affects the temperature of a system and is usually expressed as the amount of heat required to increase the temperature of a mass by a given number of degrees. Low heat capacity indicates that temperature will change more quickly with additional heating (less heat can be adsorbed) while high heat capacity indicates that temperature will change more slowly with additional heating (more heat can be adsorbed). The thermal inertia, I , is a measure of the responsiveness of the material to variations in temperature and represents the ability of a material to conduct and store heat. It is defined as $I = (k \rho c)^{1/2}$, where k is the thermal conductivity, ρ is the material's density, and c is the heat capacity (Dembicki, 2017).

The thermal conductivity and heat capacity are dynamic units, so it is essential to examine the matrix and bulk properties. The bulk thermal conductivity and heat capacity change with the

porosity and fluid content, but matrix thermal conductivity and heat capacity are constant with depth for a specific lithology.

To calculate the thermal history using the basin modeling software, it is necessary to have surface temperature, heat capacity and thermal conductivity data. For the calculations of thermal conductivity and heat capacity, the lithologic definitions of the stratigraphy with the porosity predictions from the burial history are used as input. The software uses these data with the surface temperature to estimate the basal heat and finally to calculate the thermal history.

Radiogenic heat

Most of the heat flow is the result of heat conducted up from the mantle, but there can also be a significant contribution from radioactive decay within crust from both basement and sediments. Basement rocks composed of granite and rhyolite have an average radiogenic heat production of $2.5 \mu\text{W}/\text{m}^3$, while basalt and gabbro have an average radiogenic heat production of about $0.3 \mu\text{W}/\text{m}^3$ (Pollack, 1982). Radiogenic heat contributions from sediment depend on the uranium, thorium, and potassium contents and can be estimated from gamma ray log response (Bucker and Rybach, 1996).

Short-term heat

Short-term heat sources such as circulating fluids (e.g., hydrothermal fluids) and igneous intrusives (dikes and sills) can also influence the thermal history. They can result in volatilization of sediment pore fluids and diagenetic effects up to metamorphism (Esposito and Whitney, 1995).

Evaporites

Diapiric salt column can also affect the heat flow. Evaporitic minerals have exceptionally high thermal conductivities as compared to other sediments (Dembicki, 2017). This high thermal conductivity can draw heat away from surrounding sediments by providing a low resistance conduit for heat flow (Beardsmore and Cull, 2001).

2.4 Modeling maturation, hydrocarbon generation and expulsion

Following the thermal history modeling, the next stage of basin modeling is the simulation of the maturation, hydrocarbon generation and hydrocarbon expulsion histories of the source rocks. Maturation modeling can predict a stratigraphic layer's current maturity and built its maturation history in the geologic period. Commonly, it is expressed as estimated vitrinite

reflectance, given in %Ro equivalence. On the other hand, hydrocarbon generation modeling can estimate the quantity, the type and the time of oil and/or gas generation in the source rocks. Expulsion modeling can predict when and how much of the generated hydrocarbon can move from a source rock toward a carrier bed (reservoir) using the results of the hydrocarbon generation model and the estimated porosity and permeability values.

2.4.1 Modeling maturation

Maturation (or maturity), sometimes called thermal maturation, is the process of chemical changes in the organic matter of sediments or sedimentary rocks under the influence of increasing temperature over geologic time due to burial (Dembicki, 2017). During the early days of basin modeling, the scientific development of maturity models was in the hands of petroleum geochemists. Maturation in petroleum geochemistry is a technical term used to address thermally induced changes in the nature of organic matter during catagenesis (Welte et al., 1997). Early models, such as the one proposed by Connan (1974), consisted of time-temperature relationships based on Arrhenius equation. Meanwhile, the petroleum companies were trying to develop computer-based modeling software using burial and thermal histories and developed the early kinetic models.

According to Dembicki (2017), a major step in the progress of basin modeling appeared in the '80s with the publication of Waples (1980), the interpretation of the Lopatin (1971) method and the arrival of the personal computer(s). Lopatin had developed an approach to predict coal rank (maturity) using its time-temperature history. This time-temperature index, or TTI, of Lopatin was adapted by Waples to predict maturity in source rocks (Fig. 10). Waples used basic burial and temperature histories that could be constructed with a pencil, straightedge, graph paper, and a calculator using stratigraphic columns and geothermal gradients. He also simplified the Lopatin calculation and provided a conversion of TTI to equivalent vitrinite reflectance.

TTI calculation method: (2.6)

$$\text{TTI} = \sum(\Delta T_n)(r^n)$$

where T_n is the time spent in each 10°C temperature interval and r^n is the temperature factor for that interval.

Time spent during any reduction in temperature (e.g. during an uplift) is not included in the calculation.

Temperature Intervals in °C	Temperature Factor
30-40	2 ⁻⁷
40-50	2 ⁻⁶
50-60	2 ⁻⁵
60-70	2 ⁻⁴
70-80	2 ⁻³
80-90	2 ⁻²
90-100	2 ⁻¹
100-110	2 ⁰
110-120	2 ¹
etc.	etc.

TTI	Interpretation	% Ro
15	Onset of oil generation	0.65
75	Peak oil generation	1.00
160	End oil generation	1.30
~500	40° oil preservation deadline	1.75
~1,000	50° oil preservation deadline	2.00
~1,500	Wet gas preservation deadline	2.20
>65,000	Dry gas preservation deadline	4.80

Figure 10: Summary of the TTI calculation method. After Waples, D.W., 1980, Time and temperature in petroleum formation: application of Lopatin’s method to petroleum exploration. American Association of Petroleum Geologists Bulletin 64 (6), 916–926 (in Dembicki, 2017).

Basin and maturation modeling had a quick progress after the Waples (1980) paper. A prime example is the work by McKenzie (1981) that he used a simple modification of the Waples (1980) method to calculate TTI values based on an integration of the time–temperature history. This integration is more geologically accurate accounting for periods of erosion and depositional hiatus as well as depositional events and eliminated the need for the 10°C temperature windows. McKenzie’s model also included methods to construct burial histories accounting for compaction and thermal histories using heat flow.

The integrated TTI approach was an improvement but it still relied on some form of “calibration” in order to convert the simulated time–temperature histories of sediments into equivalent vitrinite reflectance, and it did not address the actual chemical evolution of the vitrinite itself. This problem required the development of kinetic models for vitrinite reflectance prediction to be solved. The development of kinetic models for hydrocarbon generation began in the late 1960s. Later on, a number of kinetic schemes for prediction of vitrinite reflectance were proposed including Burnham and Sweeney (1989), Larter (1989), Sweeney and Burnham (1990), and Suzuki et al. (1993). Among them, the EASY%Ro model of Sweeney and Burnham (1990) has gained the most widespread acceptance. The kinetic parameters for this model are a condensed version of an earlier VITRIMAT model (Burnham and Sweeney, 1989) and require a less complex set of calculations. EASY%Ro has been shown to be a robust model for predicting vitrinite reflectance in a variety of sedimentary

basin settings and can handle special circumstances such as the influences of igneous intrusion and hydrothermal fluids.

2.4.2 Hydrocarbon generation

The burial and thermal histories of a sediment column are used in hydrocarbon generation modeling to simulate the oil and gas generating chemical reactions in source rock formations. Hydrocarbon generation is the alteration of the kerogen in a sediment under the influence of time and temperature to form gas, oil, and a carbon-rich residue (char) (Dembicki, 2017) as shown in Fig. 11.

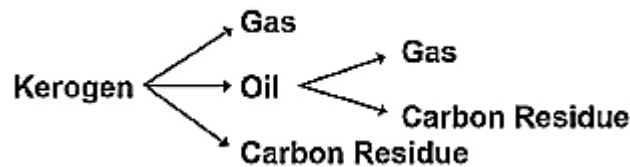


Figure 11: The simple (3 component) model for kerogen generation of oil, gas, and a carbon residue (Dembicki, 2017).

Even though more complex models for the generation of oil and gas exist, this simple model is the basis of one of the fundamental concepts in petroleum geochemistry, the oil window.

The oil window is the cumulative result of several processes acting simultaneously. Kerogen is converted to oil and gas and then oil is converted to gas, as shown in the previous simple model (Fig. 11). Although not yet observed in nature, there is also the thermodynamically theoretical potential for gas to be destroyed (Barker and Takach, 1992). The so-called oil window is therefore the summed total of all these processes.

The reactions that produce oil and gas have been observed in nature to approximately follow first-order Arrhenius kinetics (Tissot, 1969).

First-Order Arrhenius Reactions:

$$dX/dt = -kX \quad (2.7)$$

$$\text{where } k = A \exp(-E/RT) \quad (2.8)$$

X is the amount of the unreacted material

t is the time

k is the reaction rate constant

A is the frequency or pre-exponential factor

E is the activation energy

R is the universal gas constant

T is temperature, in degrees Kelvin

Based on Dembicki (2017), the first-order reactions, it is assumed that the reaction is irreversible. If the amount of the reactive material in equation 2.7 is X and time is t, the change in the concentration of the reactant over time, dX/dt , is governed by the reaction rate constant, k. The reaction rate constant (2.8) is defined as the product of the frequency factor, A, and the exponential function raised to the power of $-E/RT$. The frequency factor is a statistical estimate of how often the reaction can take place. The activation energy, E, is the amount of energy required to overcome the free energy barrier in order for the reaction to occur, R is the gas constant, and T is the temperature. The progress of chemical reactions governed by first-order Arrhenius kinetics is monitored by tracking the consumption of the reactant, in this case kerogen.

Early work to define the hydrocarbon generation kinetic parameters, such as Tissot (1969) and Tissot and Espitalie (1975) laid the groundwork for the understanding of the hydrocarbon generation process and how it could be simulated. Following that, the development of computational methods for efficiently solving initial value differential equations, such as Gear (1971) and Balarin (1977), made it possible to use the first-order Arrhenius kinetics to model hydrocarbon generation (Dembicki, 2017).

Some of the investigations that have contributed kinetic parameters for modeling hydrocarbons generation for the major chemical kerogen types, are Tissot et al. (1987), Braun et al. (1991), Behar et al. (1992), Tegelaar and Noble (1994), Pepper and Corvi (1995) and Behar et al. (1997). All these kinetic parameters are for the simple hydrocarbon generation model (Fig. 11). The more complex models (five-component models) required special compositional kinetic parameters to be derived for individual kerogens. They use complex series of analyses such as those described by Behar et al. (1997), Vandenbroucke et al. (1999) and Dieckmann et al. (2000).

There are two key parameters that will determine the results from hydrocarbon generation models. The first parameter is the type of organic matter in the source rock and the second is the amount of it. Model inputs should be estimated for the immature sediment based on analogs or based on measurements from immature samples. The source rock input parameters

usually consist of the Rock-Eval S2 or hydrogen index (HI) and the total organic carbon (TOC).

2.4.3 Expulsion

Expulsion from a source rock takes place when hydrocarbons move out into the pore spaces and form a closely connected oil-wet migration pathway along which hydrocarbons can leave the source rock. Any hydrocarbons generated above the amount needed to maintain the minimum hydrocarbon saturation that formed the pathway are available for expulsion. Expulsion can be aided when pore fluids, both water and petroleum, become overpressured due to compaction, tectonic stress, thermal expansion of water, and hydrocarbon generation (Dembicki, 2017).

Expulsion is controlled by many factors such as the type and the amount of organic matter in the source rock, the type of the sediment and the sedimentation rate. Some kerogen types generate more or less hydrocarbons than others and different kerogen types generate hydrocarbons at different points in their time-temperature history. The lithology governs the porosity and permeability evolution of the sediment which also governs the pore volume needed to be filled by the hydrocarbons. In addition, the thermal history, overpressure development and rate of hydrocarbons generation are influenced by sedimentation rate.

Some of the early basin models connected expulsion to maturity indicators, such as vitrinite reflectance or transformation ratio. Later, the main expulsion model used in 1D basin modeling software is the porosity saturation model. The porosity saturation model uses an estimate of the hydrocarbon saturation of the pore spaces in a source rock formation (Ungerer et al., 1988b) based on hydrocarbon generation and porosity reduction/ compaction model results. Once the saturation exceeds a threshold value, usually 20–25%, any additional hydrocarbon generated is expelled (Dembicki, 2017).

A more rigorous approach to expulsion uses capillary entry pressure and permeability in Darcy type flow to calculate if and how much fluid might be expelled from a sediment (Hantschel and Kauerauf, 2009). This approach requires accurate permeability predictions and some knowledge of the fluid's viscosity. There are versions of this expulsion modeling approach suited for 1D applications (Nakayama, 1987), but it is usually employed in 2D and 3D basin models.

2.5 Modeling maturation

Migration modeling is used for the prediction of the pathways by which hydrocarbons move from the source rock to traps and from one trap to another to form multiple accumulations. When the newly generated hydrocarbons moves out of their source rock the primary migration is occurred (expulsion). Following, the movement of hydrocarbons into the reservoir rock, in a trap or in another area of accumulation is called secondary migration. This process can be local or can occur along distances of hundreds of kilometers in sedimentary basins.

2D and 3D modeling can demonstrate potential migration pathways, which is not the case in the present study. More precisely, 2D modeling can demonstrate potential migration pathways either on a surface (in map view) for lateral movement in a specific carrier bed or in cross section for limited observations of both horizontal and vertical migration in a single plane. And 3D modeling can demonstrate potential migration pathways within a volume and represents the only true form of migration modeling. On the other hand, 1D modeling can only estimate if, when and how much petroleum has been expelled from the source rock and is available for migration at a specific location and geological conditions.

There are three main approaches to simulate petroleum migration from source rock to trap, ray-path modeling, Darcy flow and invasion percolation. In this study we emphasize on 1-D models, so we will not analyze it farther.

3 STUDY AREAS

This chapter presents an overview of the geological background of Ionian basin and a more detailed description about the two examined wells. More specifically, the geographical location of the onshore and offshore wells and the available information from Rigakis (1999) study are presented as further described below.

3.1 Geological background of Ionian basin

3.1.1 Tectonostratigraphic evolution

Subduction of NeoTethyan oceanic crust which separated the African and Eurasian Plates during the Late Cretaceous resulted in the formation of the Dinarides-Albanides-Hellenides fold-and-thrust belt (e.g. Jacobshagen, 1986; Doutsos et al., 1993; Papanikolaou, 2009). The Hellenides fold belt dominates Western Greece (Karakitsios, 1995; Karakitsios and Rigakis, 2007). The external (western) part of the Hellenides fold belt can be divided into three thrust-bound tectonostratigraphic zones which extend north into Albania. From east to west these are the Gavrovo, Ionian and pre-Apulian (or Paxi) zones (e.g. Aubouin, 1959 & 1965; Doutsos et al., 1993; Karakitsios and Rigakis, 1996; Rigakis and Karakitsios, 1998; Zelilidis et al., 2002). The Ionian zone in Greece is further divided into three partly thrust-bound belts or sub-zones (internal, middle and external) (Aubouin, 1959; IFP, 1966; Bellas, 1997; Zelilidis et al., 2003).

The tectonostratigraphic evolution of the Ionian zone is reflected on the deposition of four distinct geological sequences each one indicative of a different tectonic regime (Karakitsios, 1995; Bellas, 1997; Karakitsios, 2013):

1. A pre-rift sequence is represented by the Early Jurassic platform Pantokrator Limestones, which overly Early to Mid-Triassic evaporites through Foustapidima Limestones of Ladinian-Rhetian age (Kontakiotis et al., 2020).
2. A syn-rift sequence (Pliensbachian-Tithonian) deposited during extensional faulting and halokinesis of the Triassic evaporites, which caused the formation of the Ionian basin and its internal syn-rift differentiation into smaller sub-basins characterized by asymmetric half-graben geometry and different carbonate

thickness accumulation (Karakitsios, 1995; Bourli et al., 2019). Complete Toarcian-Tithonian syn-rift pelagic sequences such as Siniais and lateral equivalent Louros Limestones, Ammonitico Rosso or lower Posidonia beds, Limestone with filaments, Upper Posidonia beds are located in the deeper part of the half-grabens, while unconformities interrupt these sequences in the rift shoulders.

3. A post-rift sequence (Early Cretaceous-Eocene) deposited after the cessation of extensional faulting and it is defined by a synchronous throughout the basin Early Berriassian break-up. It is marked by an unconformity at the base of the pelagic Vigla Limestones.
4. The Mesozoic to Eocene carbonate succession passes upwards through the transitional beds (Bellas & Frydas, 1996) to the Flysch synorogenic sedimentation (mostly siliciclastic turbidites), which began at the Eocene–Oligocene boundary and revealed progressively diminishing grain-size and thicknesses from the internal to the external areas (IFP, 1966; Bellas, 1997; Kontakiotis et al., 2020). Until the Early Miocene, the basin was filled with submarine fan deposits, in response to movement of Pindos thrust, compressional structures, deformation of the external Hellenides which migrated westwards, uplift of the entire Hellenides orogenic belt, and development of a foreland basin at the edge of the Apulian microcontinent (Bellas, 1997; Avramidis and Zelilidis, 2001; Karakitsios et al., 2017). Periodically, the basin received input from the western part of the Ionian as well (Bellas et al., 1995).

3.1.2 Lithostratigraphy

A first thorough study of the Ionian geotectonic zone in Epirus was given by Aubouin & Brunn (1958) and followed by IFP (1966). Karakitsios (1995) and Rigakis (1999) provided a detailed overview of the Mesozoic stratigraphy of the Ionian, including the Jurassic Posidonia and the Cretaceous Vigla beds and later on Zelilidis et al. (2015) described the Upper Posidonia beds to include yellow to green chert-rich intervals with thin-bedded siliceous argillites containing abundant pelagic bivalves and radiolarians (Danelian and Baudin, 1990). The lower part consists of thin intervals of chertified lumachelles and large planktonic bivalves. In some other places the Lower and Upper Posidonia Beds are separated by some

meters of Limestones-with-Filaments. The Lower Posidonia beds consist of green to grey marly limestones intercalated with thin-bedded, dark-grey, marly siliceous sand intervals rich in radiolaria and large pelagic bivalves (e.g. *Bositra*) (Zelilidis et al., 2015). The formation top is dominated by black chert-rich intervals.

The Vigla Limestones formation consists of thinly-bedded packstones grey in color, with chert intervals and intercalations of shales. The Vigla Shales member of the Vigla Limestones formation consists of limestones with chert intervals and interbeds of dark grey to green or red shales. The next two shale horizons consist of thinly-bedded marly limestones and are followed by 15 shale intervals. It is not clear if these shale horizons continue in the subsurface.

Upper Cretaceous (Senonian) limestones, which rest in the Vigla Limestones, comprise two facies: (a) limestones with rudist fragments and *Globotruncanidae*, and (b) micro-brecciated intervals with limestones and rudist fragments within a calcareous matrix containing pelagic fauna. This period corresponds to subdivision of the basin into a central, topographically-high area with reduced sedimentation, and two surrounding talus slopes with increased sedimentation (Zelilidis et al., 2015).

During the Paleocene-Eocene, erosion of Cretaceous carbonates from both the Gavrovo platform (to the east) and the Apulian platform (to the west) provided the Ionian Basin with a source of micro-breccia materials (Bellas et al., 1995; Zelilidis et al., 2015). The supply of clastic sediment diminished significantly during the Eocene, especially in the central Ionian Basin. The main depositional facies during this period consisted of platy wackestone/mudstones with *Globigerinidae* and siliceous nodules, analogous to the Vigla Limestones but lacking continuous cherty intervals (Zelilidis et al., 2015).

3.1.3 Petroleum system elements

As it is defined from Magoon and Beaumont (2013), a petroleum system encompasses a pod of an active source rock and all genetically related oil and gas accumulations. Petroleum system consists of all the geologic elements and processes that are essential in order for an oil and gas accumulation to exist.

All the essential petroleum system elements are the effective source rock, reservoir, seal and overburden rock. Time is of essence too. The petroleum systems have two processes, the trap

formation and the generation, migration and accumulation of hydrocarbons. All these essential elements and processes should occur in the proper order and appropriate duration for the organic matter in a source rock to be converted into petroleum and then to be stored and preserved. If a single element or process is missing or occurs out of the required sequence, a prospect loses viability (Al-Hajeri et al., 2009).

Source rocks

The source and reservoir rocks of the Ionian zone have been mainly documented by following authors (e.g. Karakitsios, 1995; Karakitsios and Rigakis, 1996; Rigakis and Karakitsios, 1998; Rigakis, 1999; Karakitsios and Rigakis, 2007; Karakitsios, 2013). During the promotion for the greek hydrocarbons international round in 2012, a number of talks and presentations including relevant posters have been given. The first one was that of Georgalas et al. (Jan. 2012), providing all necessary data for the Oil companies. Four main potential source rock intervals have been reported plus another one at the L. Miocene (Mavromatidis, 2009; Lie et al., 2013), namely:

- 1) Albian-Turonian (Cretaceous) Vigla shales
- 2) Callovian-Tithonian (Jurassic) *Upper* Posidonia beds
- 3) Toarcian (Jurassic) *Lower* Posidonia beds and time equivalent marls at the base of the Ammonitico Rosso
- 4) Shallow-water organic-rich shales within the Triassic evaporites

Based on pyrolysis data from well samples (Rigakis and Karakitsios, 1998), the potential source rocks are oil-prone (type I to II kerogen) and they have good hydrocarbon generation potential. The Lower Posidonia beds are probably the most significant oil source rocks in the Ionian zone, having TOC content ranges up to 19.1% (average, 2.7%), kerogen type I to II, and petroleum potential up to 125.85 mg HC/g of rock. The Vigla Shales have TOC content up to 6 wt% and average Hydrogen Index of 321 mg/g (Zelilidis et al., 2015).

Based on Rock Eval analysis, kerogen is classified into the four following types (Pasadakis, 2015):

- I. Kerogen type I is a highly oil-prone organic matter. The thermally immature type I kerogens have high H/C index (~1.5) and HI (>600mgHC/gTOC). They are poor to oxygen (O/C<0.1).
- II. Kerogen type II is an oil-prone organic matter. The thermally immature type II kerogens have high H/C index (1.2-1.5) and high HI (300-600mgHC/gTOC).

- III. Kerogen type III is a gas-prone organic matter. This type of kerogen has low H/C index (0.7-1.0) and low HI (50-200mgHC/gTOC).
- IV. Kerogen type IV is an inert organic matter. This type of kerogen has low H/C index (<0.7) and low HI (5<0mgHC/gTOC). It does not produce hydrocarbons.

Published burial histories indicate that the oil window in the Ionian basin deepens eastwards (Karakitsios and Rigakis, 2007), while Triassic shale source rocks may therefore have reached the gas window in the deeper parts of sub-basins. The Lower and Upper Posidonia beds as well as the marls at the base of the Ammonitico Rosso are within the oil generation window (Rigakis and Karakitsios, 1998; Karakitsios and Rigakis, 2007). The Vigla Shales are early mature in the west and central sub-basins and mature further east (Zelilidis et al., 2015).

Reservoir rocks

Potential reservoir rocks in the Ionian zone successions (Karakitsios and Rigakis, 2007; Maravelis et al., 2012; Zelilidis et al., 2015), include:

- 1) Triassic breccias (porosity up to 13%)
- 2) Pantokrator Limestone (average porosity, 10%, thickness >1500 m)
- 3) Vigla Limestones (porosity~1.7%) and with variable thickness up to 250m in central Epirus (Karakitsios, 2007)
- 4) Senonian limestones
- 5) Paleocene–Eocene limestones (e.g. the reservoir in West Katakolo oilfield, with porosity up to 8%)
- 6) sandstone-dominated intervals in the Eocene–Oligocene Pindos foreland basin succession (Flysch thicknesses range up to 4km)
- 7) sandstone intervals in post-Alpine (Neogene) siliciclastics.

Seal rocks

Flysch is considered to be the first seal rock in western Greece, because stratigraphically is the first impermeable formation after the permeable carbonates sequence (Rigakis, 1999). Fine-grained intervals in the Eocene–Oligocene Pindos foreland basin succession are considered to be regional cap rocks (Karakitsios and Rigakis, 2007). Thick, mud-rich intervals, described by Avramidis and Zelilidis (2001), exposed in the middle Ionian zone, may serve as effective seals for underlying reserves. According to Karakitsios (2013), Upper Miocene and Pliocene marls are also proven seals, as documented at the West Katakolo oilfield. Additional cap rocks may include Triassic evaporites, especially for potential sub-thrust plays (Schjeldsøe Berg et al., 2014; Zelilidis et al., 2015).

Migration

The timing of maturation of the main Mesozoic source rocks within the Ionian basin has been described by Karakitsios and Rigakis (2007), who proposed that organic-rich Triassic shales entered the oil window in the Late Jurassic. The Lower and Upper Posidonia beds probably entered the oil window during the Miocene (Serravallian), and the Vigla Shales after the Serravallian in the internal Ionian zone (Zelilidis et al., 2015).

3.2 Geographical location

In the present work we study two wells which are both located in northwestern Greece. The first one is an onshore well named Agios Georgios-3 and the second one is an offshore well named East Erikoussa-1.

3.2.1 Onshore well location

The Agios Georgios-3 well, is an onshore well drilled in the Arta syncline, near Platanoussa village (Apostolidis, 1990). Platanoussa is a village in the wider Preveza area, Epirus (Fig. 12).

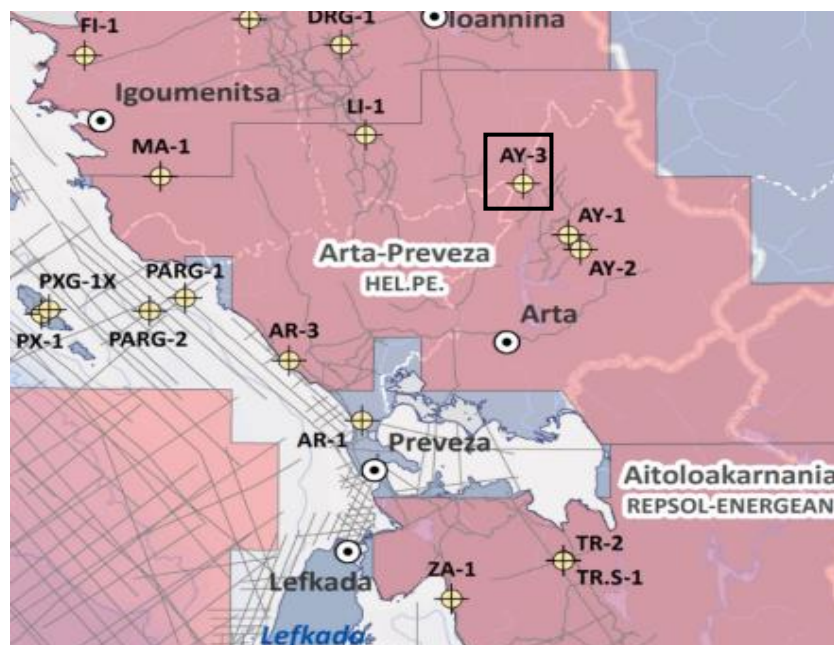


Figure 12: Detailed location map for Arta-Preveza block

(https://www.greekhydrocarbons.gr/en/ArtaPreveza_en.html). The well location is indicated by the black border (AY-3).

3.2.2 Offshore well location

The East Erikoussa-1 well, is an offshore well drilled to the east of the island Ereikoussa (Fig. 13). Ereikoussa is one of the Diapontia Islands, an island complex to the northwest of Corfu. It is the northernmost island of the group, almost equidistant from Corfu to the southeast, Mathraki to the southwest and Othonoi to the west.

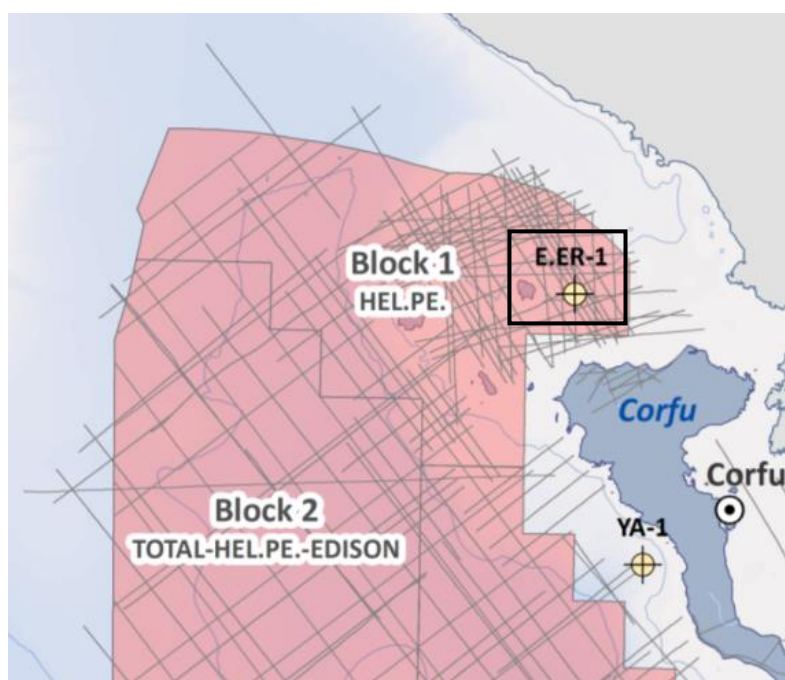


Figure 13: Detailed location map for Block 1.

(https://www.greekhydrocarbons.gr/en/Block01_en.html). The location of East Erikoussa-1 well is indicated by the black border (E.ER-1).

3.3 Wells description

Both study areas are parts of the Ionian geotectonic zone depositional paleo-basin and exclusively composed of Ionian zone formations. According to Rigakis (1999), East Erikoussa-1 is placed in the external part of the Ionian zone while Agios Georgios-3 in the internal Ionian zone. But according to a recent study of Kontakiotis et al. (2020), Agios Georgios-3 is located on the border of middle and internal Ionian zones (Fig. 12). Apparently, the borders of the sub-zones differentiation of the Ionian Basin are a matter of debate and not concrete but rather transitional.

3.3.1 Agios Georgios-3

3.3.1.1 Lithostratigraphic data

The lithostratigraphic column of Agios Georgios-3 well (Fig. 14) is presented bellow.

RIFT PHASE	AGE		FORMATION	SOURCE ROCKS	THICKNESS (m)
	PERIOD	EPOCH			
POST-RIFT	QUATERNARY	HOLOCENE	#### #####		210
	PALEOGENE	OLIGOCENE	FLYSCH A		840
			=====		450
			FLYSCH B		460
		MIDDLE-UPPER EOCENE	EOCENE LIMESTONES		140
	CRETACEOUS	LOWER EOCENE-UPPER SENONIAN	SENONIAN LIMESTONES		580
TURONIAN-LOWER CRETACEOUS		VIGLA	★	1280	
SYN-RIFT	JURASSIC	UPPER JURASSIC	POSIDONIA SHALES	★	250
PRE-RIFT	JURASSIC	LOWER JURASSIC	PANTOKRATOR		77+



Figure 14: Lithostratigraphic data of the Agios Georgios-3 well (modified from Rigakis, 1999).

1) Debris; 2A) Clay, siltstones, sandstones and conglomerate; 2B) Clay, siltstones, sandstones and conglomerate; 3) Limestones breccia; 4) Limestones (micrite); 5) Micrite limestones, shales, cherts and black marly limestones (organic rich) and after 3220m dolomitic limestones, shales and dolomites; 6) Marly limestones, dolomites, shales and cherts; 7) Dolomites;

According to Rigakis (1999), the Agios Georgios-3 well consists of 7 formations.

1. Debris
2. Flysch
3. Eocene Limestones
4. Senonian Limestones
5. Vigla
6. Posidonia Shales
7. Pantokrator

The lithostratigraphic column (Fig. 14) starts with an erosion surface at 0m depth. The first layer starts at 0m and ends at 210m depth. Flysch formation follows until 1960m, while a thrust sheet is detected at 1050m. Eocene Limestones and Senonian Limestones have a thickness equal to 140m and 580m respectively. The fifth and sixth layers are Vigla at 2680m and Posidonia Shales at 3960m depth. The final layer is Pantokrator at 4210m depth.

3.3.1.2 Identification of potential source rocks

The identification of potential source rocks is described according to the study of Rigakis (1999).

➤ FLYSCH

The results of the formation samples analysis show that Flysch presents a low amount of organic matter. TOC and petroleum potential values are poor to fair and the kerogen type is III. Ro values range between 0.40 and 0.50%, so gas could be generated if the formation was not immature. There are not potential source rocks in this formation.

➤ **EOCENE-SENONIAN**

According to the analysis results, the HI values are high while OI values are low. Such type of values combination indicates a kerogen type II. There are not potential source rocks on Eocene and Senonian Limestones, which is usual for formations like them.

➤ **VIGLA**

Vigla has rich to very rich source rocks. These rocks correspond to the shale member. The richest horizon starts at 3120m and ends at 3580m depth. It is divided up into two zones with an intermediate layer of limestone. The first zone (A') and second zone (B') have thicknesses equal to 150m (3120-3270m) and 205m (3375-3580m) respectively. The formation in the second zone is more mature than the first one. The high HI and low OI values indicate a kerogen type II. Some samples of the very rich source rock zones indicate kerogen type I – II.

Shale members of Vigla formation are rich in TOC with a very good hydrocarbon generation potential. As a result, they form very good hydrocarbon source rocks.

➤ **POSIDONIA SHALES**

In external and middle Ionian zone there are very rich source rocks in the Posidonia Shales formation. The opposite stands for the internal Ionian zone. According to the analysis results, most of the samples are poor to fair in TOC and poor in PP. There are two samples rich in TOC but their potential does not increased proportionally. This indicates an oxidation.

The formation samples have low to medium HI values and low OI values which indicate a kerogen type II although the formation is oxidized from dolomitization. The samples that are rich in TOC detected on the lower formation layers, which correspond to the lower shale members (rich source rocks) of middle Ionian zone. But if dolomitization extends to the whole Arta sub-basin, significant quantities of oil that comes from Posidonia shales formation should not be expected.

➤ **PANTOKRATOR**

TOC and petroleum potential are poor to fair while PP values are not analogous to TOC. This is an effect of dolomitization. The low HI values and the medium to high OI values indicate a kerogen type III. The formation is oxidized from dolomitization. There are not potential source rocks in this formation.

3.3.1.3 Oil window - Timing of oil generation

As Rigakis (1999) mentioned, the maturity of the organic matter is defined by the Ro-depth diagram (Fig. 15). The oil window (Ro = 0.5%) starts at 2000m depth while the beginning of significant oil generation (Ro = 0.6%) is at 2950m depth. The oil generation ends (Ro = 1.3%) at 7200m depth.

For the maturity definition the previous author used the TTI-depth diagram as well. According to this diagram, the beginning of oil generation (Ro = 0.6%) is at 2900m depth and it ends (Ro = 1.3%) at 5900m depth.

3.3.1.4 Calculation of the eroded formation thickness

The postulated flysch thickness that was eroded, was calculated by the vitrinite reflectance (Ro) and sonic methods, by using the indigenous flysch horizons (Fig. 15) (Rigakis, 1999; Rigakis et al., 2013).

Based on the vitrinite reflectance method (Dow, 1977), the eroded formation thickness can be calculated by the extrapolation of the Ro (%) vs. depth curve till the depth corresponding to the value Ro= 0.25%. The Ro value corresponds to the maturity degree of the recent-immature sediments.

The first step was the selection of the proper vitrinite values and the drawing of the correct maturity-depth curve. The second step was the extrapolation of this curve till the depth which corresponds to the value Ro= 0.25%, the maturity degree of the recent-immature sediments. The depth found was -1780m. As a result, the eroded formation thickness calculated at 1780m (Rigakis, 1999; Rigakis et al., 2013). By studying the maturity-depth curve, the presence of a thrust block of flysch was detected at 1050m depth (Fig. 15).

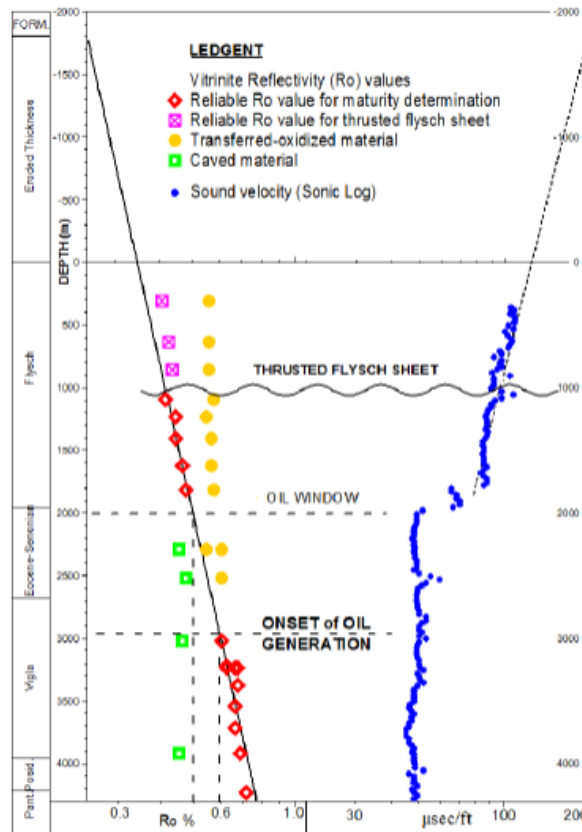


Figure 15: Vitrinite reflectance (Ro%) vs. depth and Sonic vs. depth diagram for calculation of the eroded formation thickness (Rigakis et al., 2013).

The vitrinite reflectance method is similar to the sonic one (Magara, 1978) for calculation of the eroded formation thickness. A sonic vs. depth curve was created and extrapolated till the value of 200µsec/ft (Rigakis, 1999; Rigakis et al., 2013). The depth that found was -1780m. The eroded formation thickness is equal to 1780m, which is exactly the same with the depth calculated by the vitrinite reflectance (Ro) method.

3.3.1.5 Dolomitization

According to Rigakis et al. (2013), dolomitization is strong in the case of Agios Georgios-3 well. The percentage of the Magnesium Carbonate (MgCO₃) in the well samples is strongly associated with the reduction of the organic matter quantity by depth.

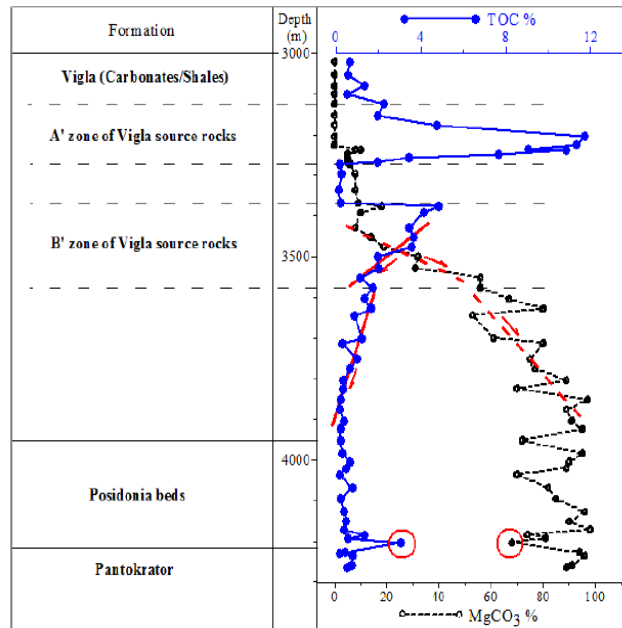


Figure 16: Dolomitization effects to the organic matter in the formations drilled by AgiosGeorgios-3 well, Arta syncline (Rigakis et al., 2013).

From Figure 16 which presents the percentage of the Total Organic Carbon (TOC) and the percentage of the MgCO₃ by depth, following conclusions have been extracted by the author:

1. In the A' zone of Vigla source rocks the MgCO₃ is almost equal to zero and the source rocks are richer in TOC than the source rocks of zone B'. In the B' zone of Vigla source rocks the MgCO₃ ranges between 8 and 56%.
2. In the interval between 3476 and 3576m of zone B', where the percentage of MgCO₃ appears significant increase from 19 to 56%, it is observed a corresponding significant decrease in the TOC content from 4.84 to 1.13%.
3. In the deeper horizons where the MgCO₃ increase shows a lower rate (from 67 to 94%), the rate of the TOC content decrease is also lower.
4. Posidonia Beds appear low TOC content, obviously due to the dolomitization. But, whenever some Posidonia horizons appear high TOC content, the corresponding MgCO₃ percentage is low.

The oil generation from the Posidonia Beds started during Lower Oligocene and continued till Burdigalian (Rigakis, 1999), so these source rocks would had generated their whole petroleum potential before the oxidation of their organic matter. Part of this oil may have been lost during orogenesis processes but it is not anticipated oil from this formation (Rigakis et al., 2013).

3.3.2 East Erikoussa-1

3.3.2.1 Lithostratigraphic data

The lithostratigraphic column of East Erikoussa-1 well (Fig. 17) is presented bellow.

RIFT PHASE	AGE		FORMATION	SOURCE ROCKS	THICKNESS (m)
	PERIOD	EPOCH			
POST-RIFT	QUATERNARY	HOLOCENE	ALLUVIAL		69
	NEOGENE	PLIOCENE	LOWER PLIOCENE		440
		MIOCENE	MIOCENE		810
	PALEOGENE	OLIGOCENE	FLYSCH		390
		EOCENE	EOCENE LIMESTONES		220
	CRETACEOUS	UPPER CRETACEOUS	SENONIAN LIMESTONES		185
VIGLA			★	100	
SYN-RIFT	JURASSIC	LOWER JURASSIC	SINIAIS		107+
PRE-RIFT			PANTOKRATOR		

1	2	3	4	5	6	7	8
---	---	---	---	---	---	---	---

Figure 17: Lithostratigraphic data of the East Erikoussa-1 well (modified from Rigakis, 1999).

- 1) Alluvial sediments; 2) Clay, siltstones, conglomerate and coal; 3) Clay, siltstones and a layer of sandstones; 4) Clay, sandstones, siltstones and limestones; 5) Limestones; 6) Limestones; 7) Limestones, shales, cherts and marls; 8) Limestones;

According to Rigakis (1999), the East Erikoussa-1 well consist of 8 formations.

1. Alluvial
2. Lower Pliocene
3. Miocene
4. Flysch
5. Eocene Limestones
6. Senonian Limestones
7. Vigla
8. Siniais-Pantokrator

The lithostratigraphic column (Fig. 17) starts with alluvial sediments at 71m depth. The second layer of Lower Pliocene age starts at 140m and ends at 580m depth. Miocene formation follows until 1390m. Flysch, Eocene Limestones and Senonian Limestones have a thickness equal to 390m, 220m and 185m respectively. The seventh layer is Vigla formation at 2185m depth. The final layer is Siniais-Pantokrator formation at 2285m depth.

3.3.2.2 Identification of potential source rocks

The identification of potential source rocks is described according to the study of Rigakis (1999).

➤ FLYSCH

According to the results of the formation samples analysis, the total organic carbon of Flysch is poor (TOC = 0.15-0.49%) and the kerogen type is III. It is not considered a potential hydrocarbon source rock.

➤ EOCENE-SENONIAN

Eocene and Senonian limestones are very poor in organic matter. They are not considered as potential hydrocarbon source rocks.

➤ **VIGLA**

The Vigla shale member in the upper part of the formation, consist of potential hydrocarbon source rocks and it is an organic rich formation. TOC ranges between 1.04 and 6.30% (average value 3.25%) and petroleum potential between 3.86 and 32.08 mg HC/g rock (average value 8.9 mg/g). Kerogen is type I – II according to the high HI and low OI values. T_{max} ranges between 420 and 425°C. Vigla limestones are poor in TOC and they cannot generate hydrocarbons.

➤ **SINIAIS-PANTOKRATOR**

Siniaais-Pantokrator is an organic poor formation. It is not a potential hydrocarbon source rock.

3.3.2.3 Oil window - Timing of oil generation

As Rigakis (1999) mentioned, the “potential” source rocks of East Erikoussa-1 well are not within the oil window (immature) and the beginning of significant oil generation is at 3400m depth.

4 1D ONSHORE WELL MODELING

This chapter describes the entire procedure that followed for building the 1D model for the onshore and offshore wells and running the simulation using Schlumberger's PetroMod (version 2017.1) petroleum systems modeling software.

Most of the required input data for the 1D basin modeling of the Agios Georgios-3 and East Erikoussa-1, such as depth surfaces of the formations, type of the events, lithological properties and source rocks parameters are derived from Rigakis (1999) PhD thesis. His work was about the study of the stratigraphy of the Alpine formations of the Ionian, the Preapoulian and the Gavrovo zones and the research on the presence of possible oil source rocks in these formations. Furthermore he worked on the maturity, the timing of oil generation and the origin of the oil shows in the Western Greece.

4.1 Thrust_model_1 and model_erikoussa input parameters

The thrust_model_1 is the final model of the Agios Georgios-3 well that ensued from many different trials. This model consists of twelve layers, an erosion surface and a thrust sheet. The erosion surface and the thrust sheet depths have been chosen according to Rigakis (1999), while the specific erosion thickness results from this study.

The model_erikoussa is the final model of the East Erikoussa-1 well based on the study of Rigakis (1999). It consists of ten layers. No erosional surface was used, since no such data are provided by the previous author, nor relevant stratigraphic or tectonic hiatus was observed from the available stratigraphic column of the well.

4.1.1 Age & Depth

The first step of 1D modeling in PetroMod software is to import the layers and depths of the well. Every layer corresponds to a different type of formation. For Agios Georgios-3, first we defined the layers according to its lithostratigraphic data (Fig. 14) and then we divided the Vigla formation into five parts. Every single layer of Vigla formation has different characteristics.

For East Erikoussa-1, we followed the same procedure as the one in onshore well modeling. We defined the layers according to its lithostratigraphic data (Fig. 17) and then we divided the Miocene formation into three parts (Miocene A, Gas layer, Miocene B).

For the importation of depths, the software allows modeler to enter either the top depth or the thickness of the layer while it calculates the other. The formations depths are known from Rigakis (1999) study. After defining all layers in the main input tables of the models, depositional ages were assigned to them by specifying a depositional period to each layer between the upper and lower boundaries. The age of each horizon is based on data from Rigakis (1999) with the help of PetroMod Time-Scale Editor.

4.1.2 Event type

The second step is to define the type of the event that took place in every layer of the two models and the paleodeposition or erosion thickness if we have imported an erosion surface. There are four different types of events,

- the deposition,
- the erosion,
- the hiatus and
- the thrusting.

The thrust_model_1 consists of twelve deposition events (twelve layers), one erosion event at 0m depth with erosion thickness equal to 150m and one thrusting at 1050m depth with thickness equals to 450m.

The model_erikoussa consist of ten deposition events (ten layers).

4.1.3 Lithology

The third step is to import the lithology of every recorded formation based on the available data from Rigakis (1999). PetroMod's Lithology Editor allows modeler to create new lithologies by mixing lithologies from the software database.

For the thrust_model_1, nine mixed lithologies have been created (Debris, Flysch, Vigla lim-sh, Vigla sh A, Vigla lim, Vigla sh B, Vigla dol. Lim-sh, Posidonia) and three more have been added from the database.

Five mixed lithologies have been created for model_erikoussa (Alluvial, Pliocene, Miocene, Flysch, and Vigla) and another four have been added from the database.

4.1.4 PSE

The forth step is to define the Petroleum System Elements of the models. The Petroleum System Elements (PSE) are based on the concept introduced and described by Magoon and Dow (1994). The modeler can assign PSEs either from the list of PSEs in the PetroMod database or by copy and paste from other applications. The PetroMod's PSEs database consist of the underburden rock, source rock, reservoir rock, seal rock and overburden rock. The PSEs of the thrust_model_1 (Fig. 18) and model_erikoussa (Fig. 19) have been selected according to Rigakis (1999).

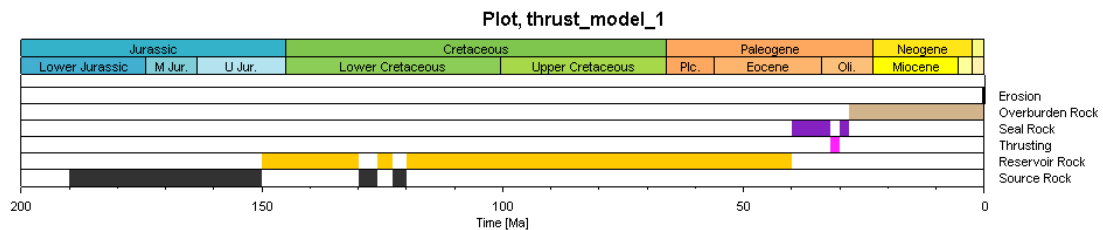


Figure 18: Petroleum System Elements plot of thrust_model_1 (Agios Georgios-3).

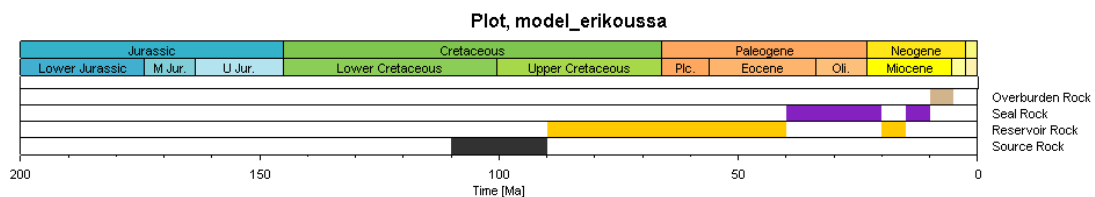


Figure 19: Petroleum System Elements plot of model_erikoussa (East Erikoussa-1).

4.1.5 Source Rock Parameters

The final step is to import the source rock parameters. The source rocks identification and their total organic carbon (TOC) and hydrocarbon index (HI) values are of great importance for the hydrocarbons generation modeling. So, the source rock parameters in PetroMod include TOC, HI and petroleum kinetic model. The TOC and HI for the three source rock

formations of the thrust_model_1 and the one source rock formation of the model_erikoussa were obtained from the study of Rigakis (1999).

As far as petroleum kinetics, PetroMod separates them into bulk, kerogen oil and gas, compositional, compositional for phase separation, miscellaneous reactions, biogenic and secondary reactions. For this study, the kerogen oil and gas have been selected according to the type of kerogen. The hydrocarbon generation from the Vigla shales A, Vigla shales B and Posidonia shales formations of thrust_model_1 is determined by Pepper&Corvi(1995)_TII(B) kinetic model, while Pepper&Corvi(1995)_TI(C) is also examined.

The hydrocarbon generation from Vigla formation of model_erikoussa is also determined by Pepper&Corvi(1995)_TII(B) kinetic model, while Pepper&Corvi(1995)_TI(C) is examined as well. These generation kinetic models have been chosen according to the available data and their correspondence between the age, the lithology and the kerogen type of the source rocks.

All the input parameters of thrust_model_1 (Fig. 20) and model_erikoussa (Fig. 21) are presented below.

Age [Ma]	Name top/well pick	Depth [m]	Thickness [m]	Event type	Name layer/event	Paleodeposition/erosion [m]	Lithology	PSE	Kinetic	TOC [%]	HI [mgHC/gTOC]
0.00	Erosion	0									
0.01	Debris	0		↑ Erosion	Erosion	-150					
			210	↓ Deposition	Debris	150	Debris	Overburden Rock			
28.00	Flysch A	210									
			840	↓ Deposition	Flysch A		Flysch	Seal Rock			
30.00	Thrusting	1050									
			450	← Thrusting	Thrusting						
32.00	Flysch B	1500									
			460	↓ Deposition	Flysch B		Flysch	Seal Rock			
40.00	Mid-Upper Eocene	1960									
			140	↓ Deposition	Eocene		Limestone (micrite)	Reservoir Rock			
50.00	Senonian-Lower Eocene	2100									
			580	↓ Deposition	Senonian		Limestone (micrite)	Reservoir Rock			
80.00	Vigla limestones-shales	2680									
			440	↓ Deposition	Vigla limestones-shales		Vigla lm-sh	Reservoir Rock			
120.00	Vigla shales A	3120									
			150	↓ Deposition	Vigla shales A		Vigla sh A	Source Rock	Pepper&Corvi(1995)_TII(B)	0.79	262.00
123.00	Vigla limestones	3270									
			102	↓ Deposition	Vigla limestones		Vigla lm	Reservoir Rock			
126.00	Vigla shales B	3372									
			208	↓ Deposition	Vigla shales B		Vigla sh B	Source Rock	Pepper&Corvi(1995)_TII(B)	0.20	255.00
130.00	Vigla dol. limestones-shales	3580									
			380	↓ Deposition	Vigla dol. limestones-shales		Vigla dol. lm-sh	Reservoir Rock			
150.00	Posidonia shales	3960									
			250	↓ Deposition	Posidonia shales		Posidonia	Source Rock	Pepper&Corvi(1995)_TII(B)	0.24	92.00
190.00	Pantokrator	4210									
			77	↓ Deposition	Pantokrator		Dolomite (typical)				
200.00	Jurassic	4287									

Figure 20: Main input data for burial and thermal histories reconstruction in PetroMod for the Agios Georgios-3 well (thrust_model_1).

Age [Ma]	Name top/well pick	Depth [m]	Thickness [m]	Event type	Name layer/event	Paleodeposition/erosion [m]	Lithology	PSE	Kinetic	TOC [%]	HI [mgHC/gTOC]
0.00	Alluvial	71	69	↓ Deposition	Alluvial		Alluvial				
5.00	Lower Pliocene	140	440	↓ Deposition	Lower Pliocene		Pliocene	Overburden Rock			
10.00	Miocene A	580	360	↓ Deposition	Miocene A		Miocene	Seal Rock			
15.00	Gas layer	940	70	↓ Deposition	Gas layer		Sandstone (typical)	Reservoir Rock			
20.00	Miocene B	1010	380	↓ Deposition	Miocene B		Miocene	Seal Rock			
25.00	Flysch	1390	390	↓ Deposition	Flysch		Flysch	Seal Rock			
40.00	Eocene Limestones	1780	220	↓ Deposition	Eocene Limestones		Limestone (micrite)	Reservoir Rock			
70.00	Senonian Limestones	2000	185	↓ Deposition	Senonian Limestones		Limestone (micrite)	Reservoir Rock			
90.00	Vigla	2185	100	↓ Deposition	Vigla		Vigla	Source Rock	Pepper&Corvi(1995)_TII(B)	6.10	441.00
110.00	Siriais - Pantokrator	2285	107	↓ Deposition	Siriais-Pantokrator Lim.		Limestone (micrite)				
160.00	Pantokrator	2392									

Figure 21: Main input data for burial and thermal histories reconstruction in PetroMod for the East Erikoussa-1 well (model_erikoussa).

4.2 Boundary Conditions

Based on the PetroMod1D_UserGuide there are three boundary conditions in PetroMod 1D:

- Paleo water depth (PWD),
- Sediment water interface temperature (SWIT)
- Basal heat flow (HF)

The boundary conditions define the basic energetic conditions for the temperature development for all layers, especially the source rock and, consequently, for the maturation of organic matter through time. The modeler can only have one set of boundary conditions per model.

All three boundary conditions are necessary for the calculation of the temperature history.

4.2.1 Paleo Water Depth (PWD)

Paleo water depth (PWD) shows the water depth during deposition of each chronostratigraphic unit. No PWD data were available from the study of Rigakis (1999) and from literature so the assigned PWD values in the models are estimated. Based on the geotectonic evolution of the basin, the lithologies, the depositional environment at each phase of the development of the basin and the studies of Getsos et al. (2018) and Kontakiotis et al. (2020), it was attempted to create two general trends of the paleo water depth, one for the Agios Georgios-3 well (Fig. 23) and one for the East Erikoussa-1 well (Fig. 24).

According to the available information about depositional environments, the following figure (Fig. 22) was used as a guide.

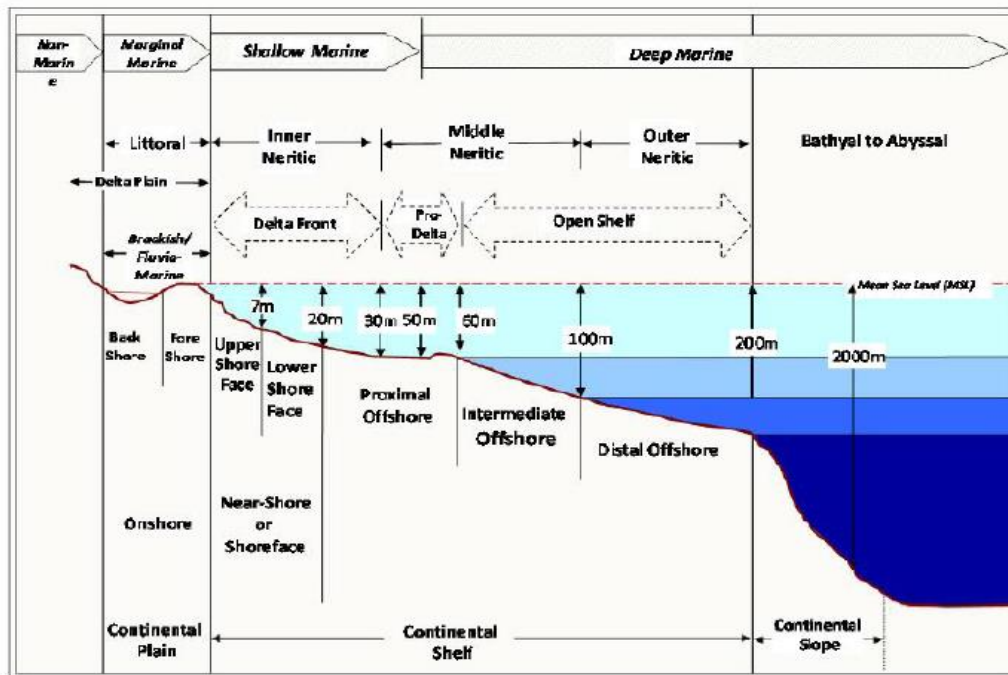


Figure 22: Diagram showing depositional environments and bathymetric changes used in paleoenvironmental interpretations (modified after Allen, 1965, 1970). Figure from Okosun and Osterloff (2014).

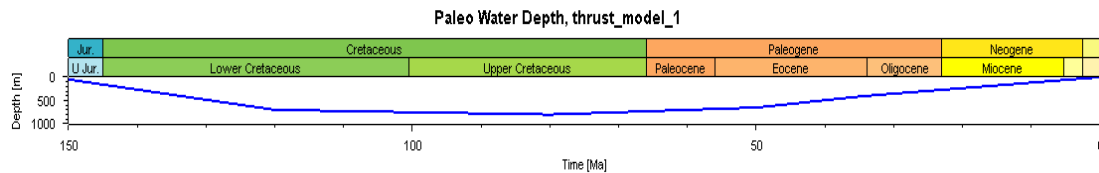


Figure 23: Paleo water depth (m) vs. time (Ma) plot of thrust_model_1 (Agios Georgios-3).

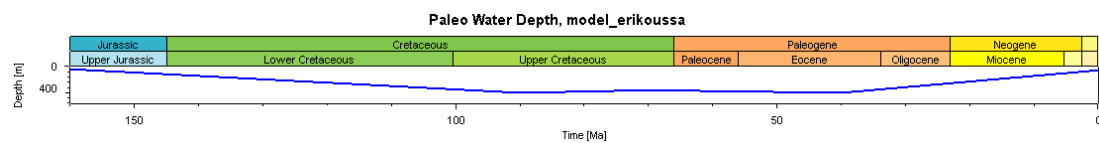


Figure 24: Paleo water depth (m) vs. time (Ma) plot of model_erikoussa (East Erikoussa-1).

4.2.2 Sediment Water Interface Temperature (SWIT)

The Sediment Water Interface (SWIT) is calculated based on Wygrala (1989). More specifically, the SWIT values were entered in the models via the ‘Calc. Settings’ function of PetroMod 1D from the option of ‘From global mean temperature at sea level’ using the ‘Auto

SWIT' tool. The location was set at latitude of 39° in Southern Europe (Fig. 25). The SWIT plots for the thrust_model_1 (Fig. 26) and model_erikoussa (Fig. 27) are presented below.

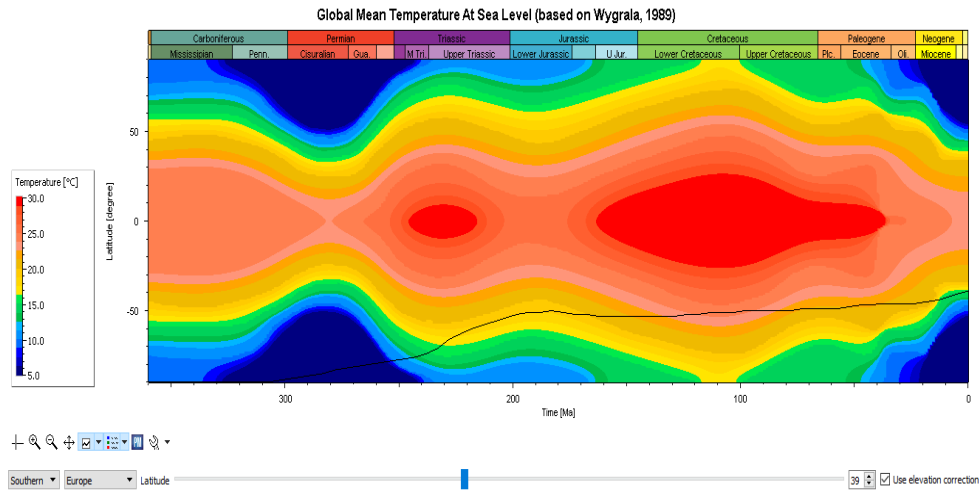


Figure 25: Global mean surface temperature at sea level through geological time.

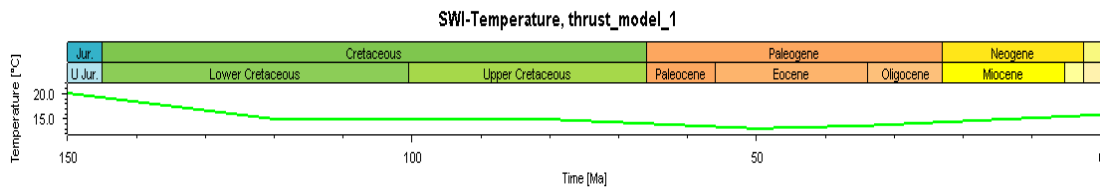


Figure 26: SWI-Temperature (°C) vs. time (Ma) plot of thrust_model_1 (Agios Georgios-3).

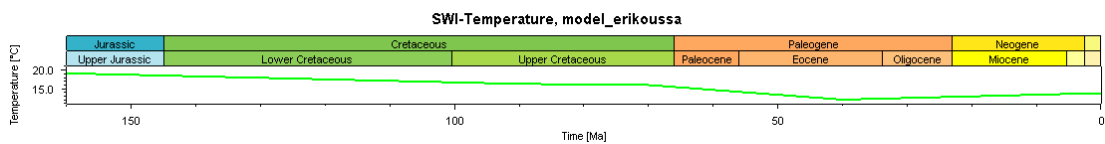


Figure 27: SWI-Temperature (°C) vs. time (Ma) plot of model_erikoussa (East Erikoussa-1).

4.2.3 Heat Flow (HF)

The Heat Flow (HF) is the third boundary condition. The selection of paleo-HF values was according to Mavromatidis (2009), who has suggested a 50mW/m² value for the pre-rift phase, 80mW/m² for the syn-rift phase and 35mW/m² for the post-rift phase of the Ionian Basin. In addition, Fytikas and Kollios (1979) have created a preliminary heat flow map of Greece (Fig. 28) which proposed a present day heat flow ranging from 23 to 41mW/m² for Agios Georgios-3 well area and a heat flow equal to 30mW/m² for East Erikoussa-1 well area.

Fytikas and Kollios (1979) constructed the heat flow map of Greece (Fig. 28) using data from Erickson et al. (1976), Hsu et al. (1975), Jongasma (1974) as well as additional data of their

own. In places where the available heat flow data were not adequate, measurements of surface hydrothermal phenomena (thermal springs, fumaroles and hot grounds) and thermal measurements in drill holes done for geothermal investigations were taken into consideration by Fytikas and Kolios in order to characterize the heat flow pattern and complete the heat flow isocurves map (Papadakis et al., 2016).

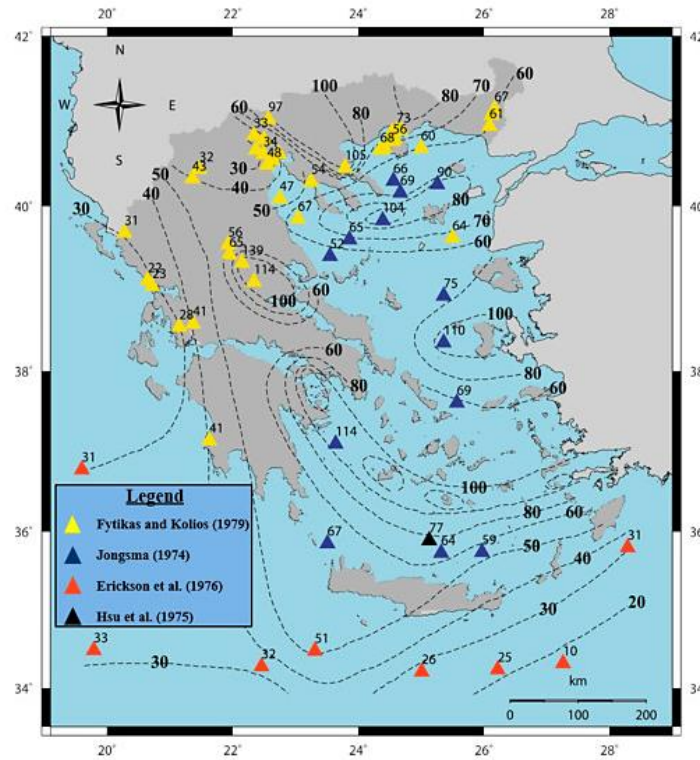


Figure 28: Heat flow map of Greece by Fytikas and Kolios (1979) in Papadakis et al. (2016). The heat flow values are presented in mW/m^2 .

The HF plots for the thrust_model_1 (Fig. 29) and model_erikoussa (Fig. 30) are presented below.

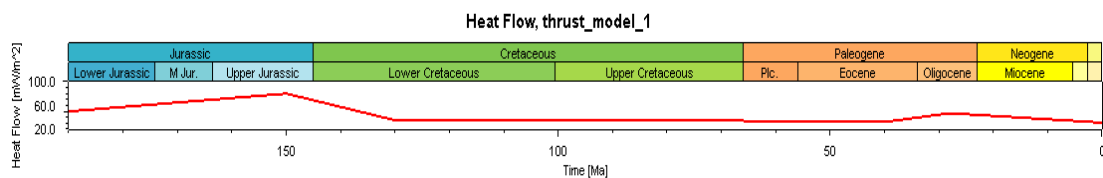


Figure 29: Heat flow (mW/m^2) vs. time (Ma) plot of thrust_model_1 (Agios Georgios-3).

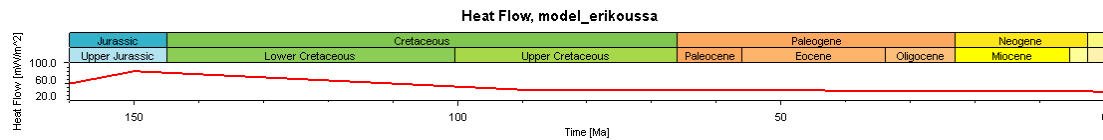


Figure 30: Heat flow (mW/m^2) vs. time (Ma) plot of model_erikoussa (East Erikoussa-1).

The boundary condition tables of thrust_model_1 (Table 1) and model_erikoussa (Table 2) are presented below.

Table 1: Boundary condition tables of thrust_model_1 (Agios Georgios-3).

Age [Ma]	PWD [m]	Age [Ma]	SWIT [$^{\circ}\text{C}$]	Age [Ma]	HF [mW/m^2]
0.00	0	0.00	15.84	0.00	31.00
34.00	400	34.00	13.69	28.00	47.00
50.00	650	50.00	13.13	40.00	34.00
80.00	800	80.00	14.93	50.00	33.00
120.00	700	120.00	15.00	80.00	35.00
150.00	50	150.00	20.10	120.00	35.00
				130.00	35.00
				150.00	80.00
				190.00	50.00

Table 2: Boundary condition tables of model_erikoussa (East Erikoussa-1).

Age [Ma]	PWD [m]	Age [Ma]	SWIT [$^{\circ}\text{C}$]	Age [Ma]	HF [mW/m^2]
0.00	71	0.00	13.84	0.00	30.00
40.00	500	40.00	12.09	5.00	32.00
70.00	450	70.00	16.01	15.00	32.00
90.00	500	90.00	16.32	25.00	32.00
160.00	50	160.00	19.16	40.00	33.00
				70.00	34.00
				90.00	35.00
				150.00	80.00
				160.00	50.00

4.3 Simulation

After input parameters and boundary conditions the next step is the simulation. The simulation options consist of the run control and petroleum parameters, the parameters that have to be enabled, the calibration and pressure parameters and the tools. For the run control, the number of runs was set to two, the maximum cell thickness to 50m and the maximum

time step duration to 1Ma. Generation/Migration on Petroleum parameters was set to Generation only with Expulsion factor equal to 100% and Peng Robinson equation of state. Radiogenic heat was enabled, the standard calibration kinetics and all the tools was selected.

4.4 Calibration

The final part after simulation is the calibration of the model. The simulation output needs to be calibrated with measured well data. The calibration takes place by trying to match the calculated data from the model with the measured ones.

On this study, vitrinite reflectance (Ro) and temperature (T) data are used for the calibration of the thrust_model_1 and only temperature data (T) for the model_erikoussa due to lack of available data. During the calibration it was noticed that vitrinite reflectance and temperature trends were only affected by the first two heat flow (HF) values and the value of erosion thickness at 0m depth.

4.4.1 Temperature (T)

Temperature was the first type of data that used for the calibration of the models. There weren't available temperature measurements from the examined wells but according to Rigakis (1999) there were geothermal gradient approximations for the formations. From these approximations a temperature trend for each model was build. The calibration took place by changing the first and second value of the heat flow table.

The temperature trends for thrust_model_1 and model_erikoussa are presented bellow (Fig. 31).

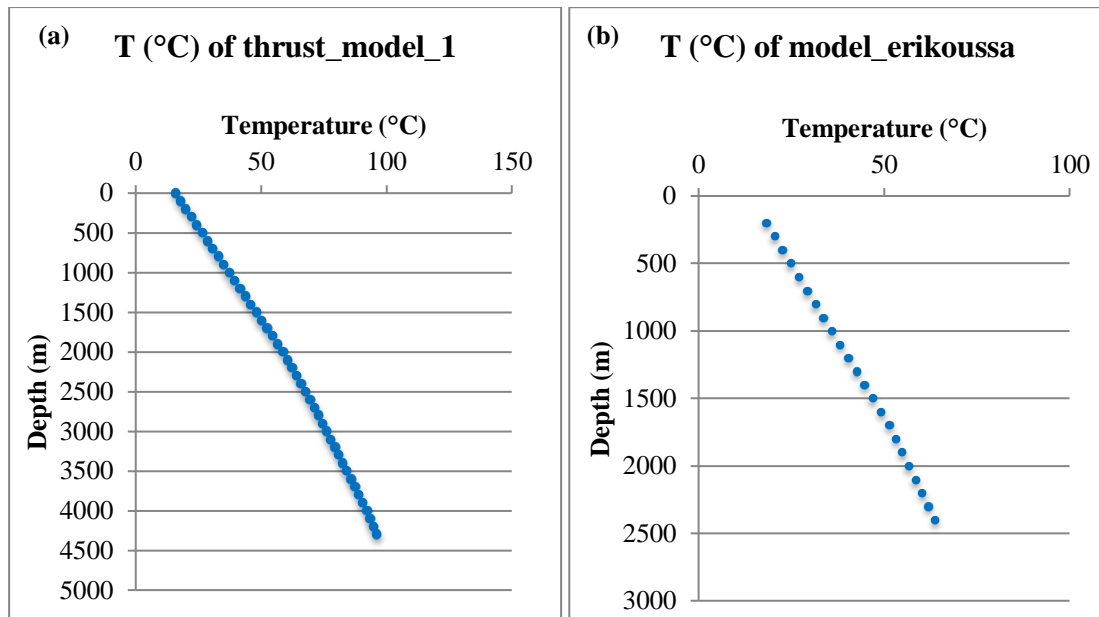


Figure 31: Temperature profiles of (a) thrust_model_1 and (b) model_erikoussa.

The results of temperature calibration are presented by the figure below (Fig. 32).

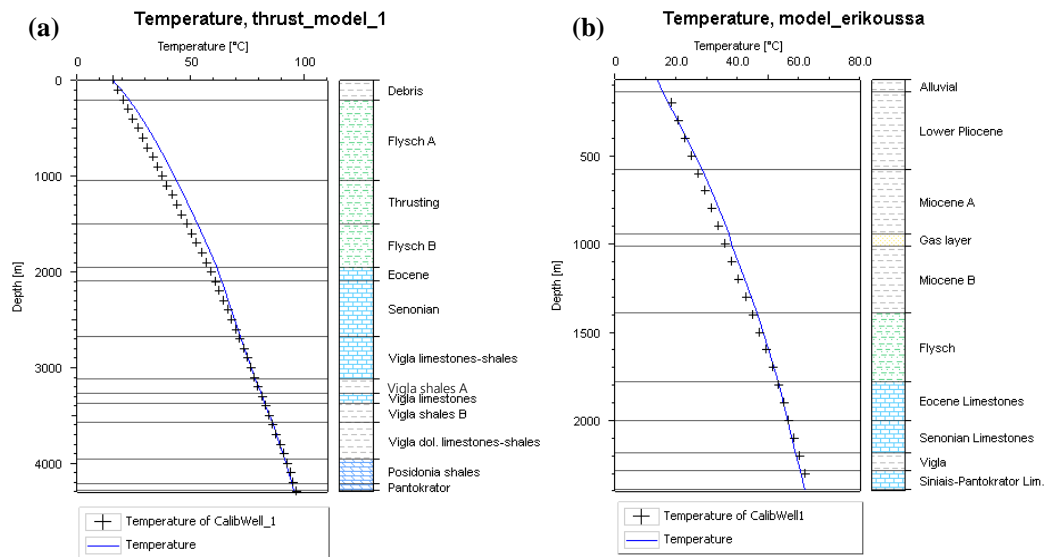


Figure 32: Temperature calibration plots of (a) thrust_model_1 and (b) model_erikoussa.

4.4.2 Vitrinite Reflectance (Ro)

Vitrinite reflectance was the second type of data that used for the calibration of the thrust_model_1. The data were available from the study of Rigakis (1999), while the calibration took place by changing the first and second values of the heat flow table. The results of vitrinite reflectance calibration are presented below (Fig. 33).

Sweeney&Burnham(1990)_EASY%Ro, thrust_model_1

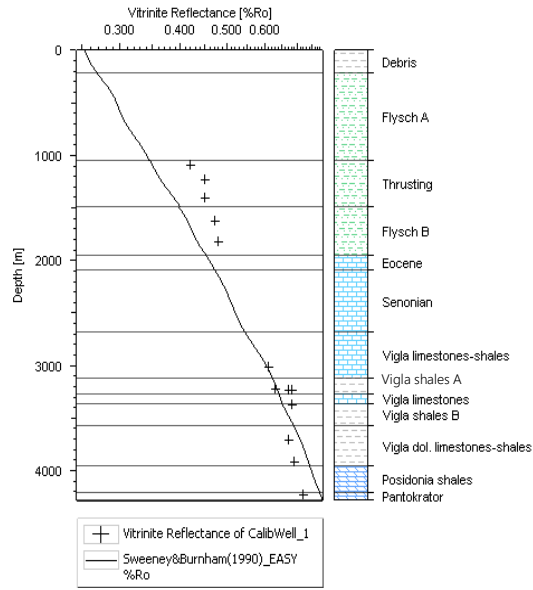


Figure 33: Vitrinite reflectance calibration plot of thrust_model_1.

5 RESULTS

This chapter presents the results of ID modeling in wells Agios Georgios-3 and East Erikoussa-1 with the best matching between measured and calculated model data. As mentioned before, these cases correspond to thrust_model_1 for the Agios Georgios-3 well and to model_erikoussa for East Erikoussa-1 well.

5.1 Agios Georgios-3

The thrust_model_1 is the final model of the Agios Georgios-3 well, but several models have been tested before that. More specifically, the models have been tested by changing the boundary conditions and parameters in the input table in order to monitor how these changes affect the simulation outputs. The outcome from this process will be described after the presentation of thrust_model_1 results.

5.1.1 Burial history

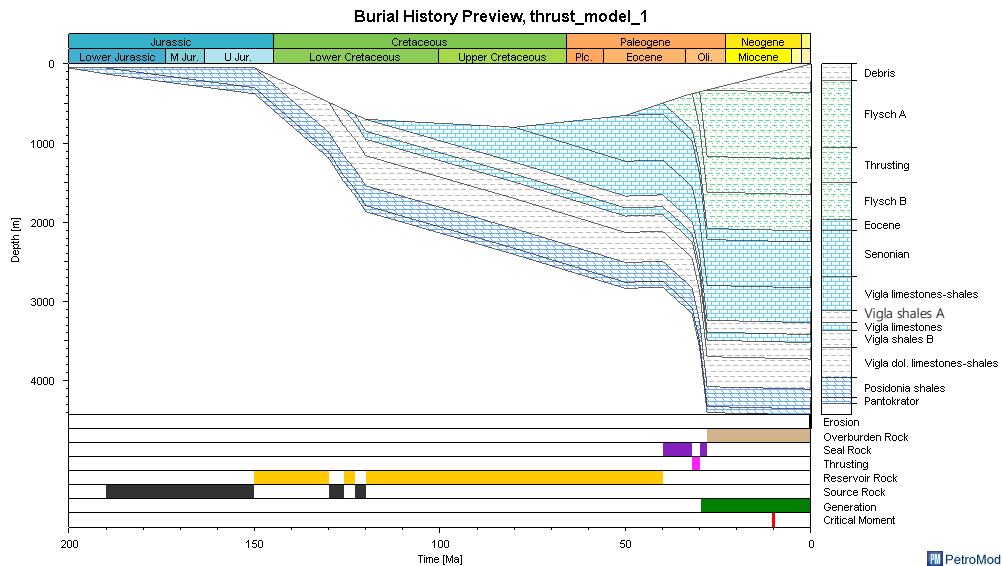


Figure 34: Burial history of Agios Georgios-3well.

The previous figure (Fig. 34) presents the burial history reconstruction for the thrust_model_1, accompanied by the petroleum system elements plot (PSE) which displays the time of depositions, erosion, thrusting, hydrocarbon generation and the critical moment. Detailed results about the hydrocarbon generation and the critical moment will be presented later on.

5.1.2 Temperature history

Figure 35 presents the temperature evolution of the Agios Georgios-3 well and Figure 36 presents the temperature profile of the source rock formations. The higher temperature was reached at 28.00Ma. In particular, the deeper part of Pantokrator formation reached a temperature up to 121.52°C. The source rock formations reached their higher temperature at 28Ma as well. More precisely, Posidonia shales formation reached a temperature up to 120.03°C, while Vigla shales B and Vigla shales A reached a temperature up to 106.01°C and 98.08°C respectively.

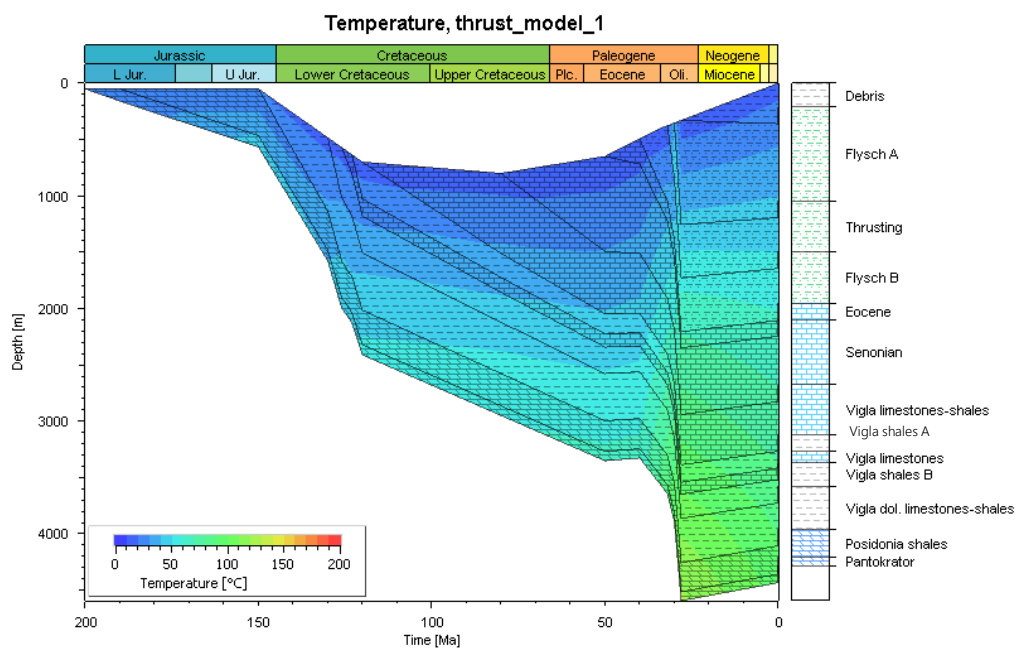


Figure 35: Burial history of Agios Georgios-3 well with a temperature overlay.

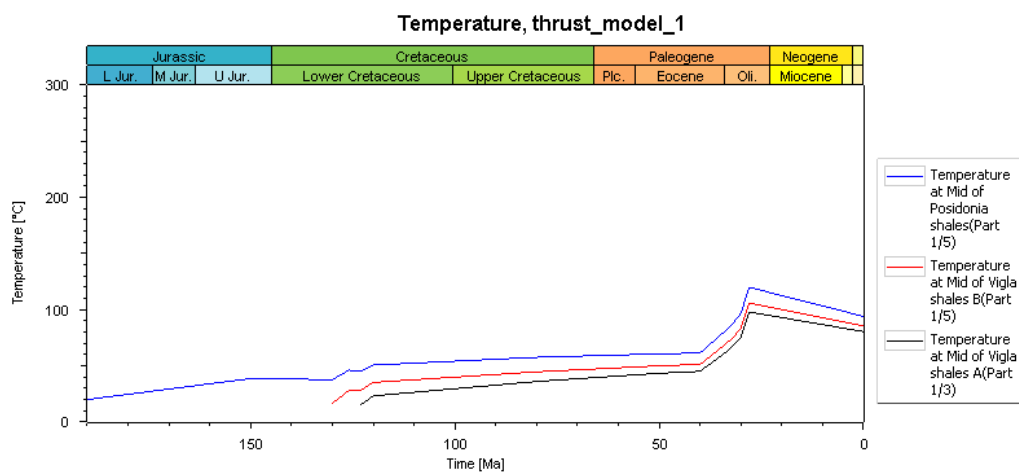


Figure 36: Temperature (°C) vs. time (Ma) plots of the three source rock formations of Agios Georgios-3 well.

5.1.3 Present-day maturity

One of the most common indicators for thermal maturity is the vitrinite reflectance (%Ro). According to Magoon and Dow (1994), the oil-prone generation is divided into five stages based on the Ro values (Table 3).

Table 3: Vitrinite reflectance and hydrocarbon generation stages

Oil-Prone Generation	
Generation Stage	Ro (%)
Immature	0.2 – 0.6
Early oil	0.6 – 0.65
Peak oil	0.65 – 0.9
Late oil	0.9 – 1.35
Postmature	>1.35

The maturity history of Agios Georgios-3 well is presented bellow (Fig. 37; Fig. 38).

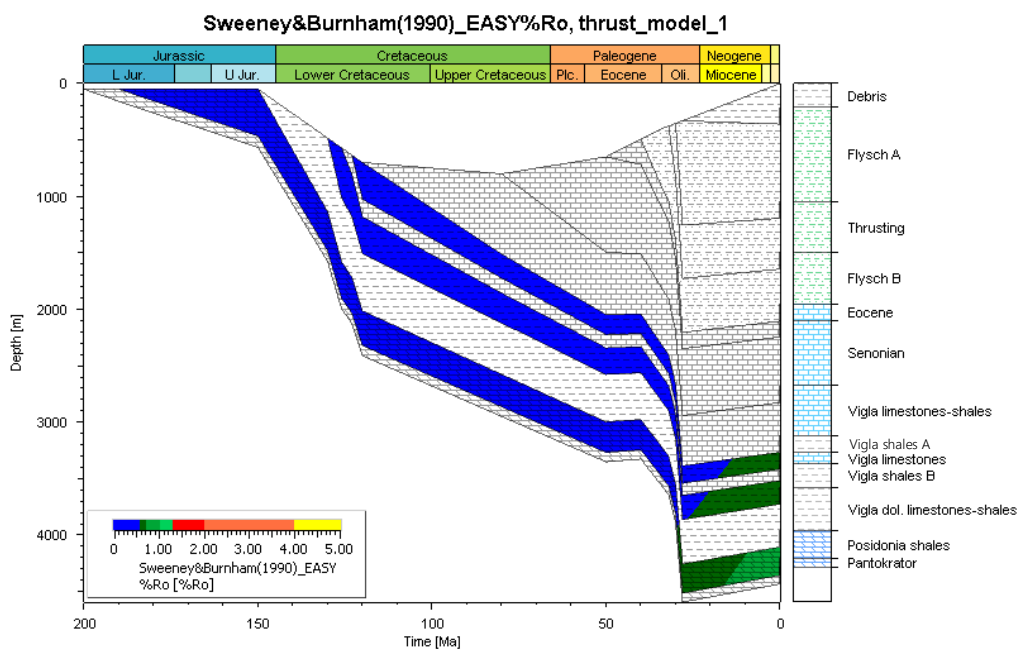


Figure 37: Maturity history plot (vitrinite reflectance) of the source rock formations of Agios Georgios-3 well.

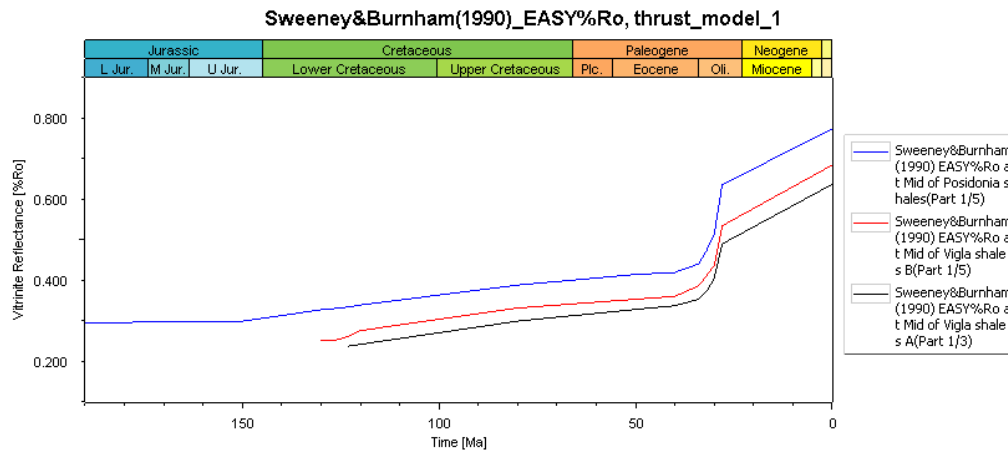


Figure 38: Vitrinite reflectance (%Ro) vs. time (Ma) plots of the three source rock formations of Agios Georgios-3 well.

According to the previous figures, the deepest parts of the Posidonia shales and Vigla shales B formations entered the hydrocarbon generation ranges around the Oligocene, while the Vigla shales B around the Miocene. After that, the maturity keeps increasing up to today. Posidonia shales are the most mature source rocks. The onset of hydrocarbon generation was at 29.53Ma and at 3976m and the zone of main oil was reached at 16.16Ma and at 4448m. On the other hand, the main oil zone was not reached by the other two source rock formations. The onset of hydrocarbon generation for Vigla shales B formation occurred at 26.64 Ma and at 3857m, while for Vigla shales A formation was at 18.12Ma and at 3498m. The present-day vitrinite reflectance value for Posidonia shales, Vigla shales B and Vigla shales A is 0.77%, 0.68% and 0.64% respectively.

5.1.4 Transformation ratio (TR)

The transformation ratio (TR) indicates the percentage of kerogen transformed into petroleum for each source rock (Al-Hajeri et al., 2009) and is one of the main outputs of 1D basin modeling in PetroMod. The critical moment that mentioned before, is the time of generation, migration and accumulation of most of the hydrocarbons in a petroleum system and occurs in the range of 50% to 90% transformation ratio (TR) (Al-Hajeri et al., 2009). Figure 39 and Figure 40 display the results for all the source rocks formations.

Transformation in Posidonia shales source rock formation began at 29.94Ma at a depth of 3830m and it has a present-day TR value equal to 48.95%. Vigla shales B formation is less mature than the Posidonia shales. Transformation began at 28.60Ma at a depth of 3651m and its present-day TR value is 24.05%. The third source rock formation is the most immature.

Transformation in Vigla shales A formation began at 25.17Ma at a depth of 3529m and it has a present-day TR value equal to 13.41%.

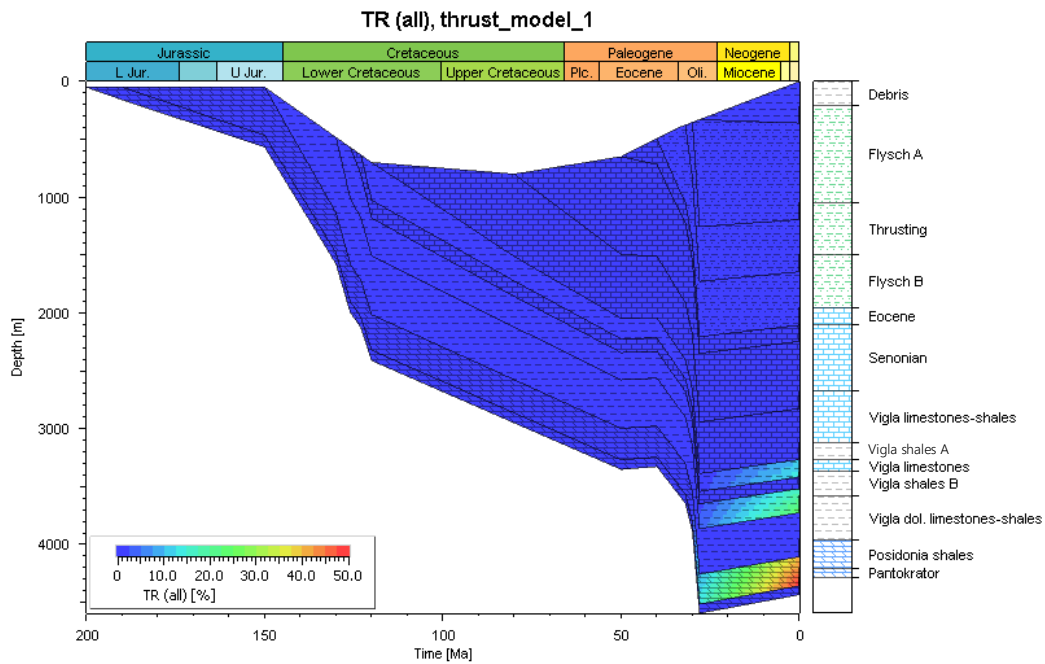


Figure 39: Burial history plot of Agios Georgios-3 well with a transformation ratio overlay.

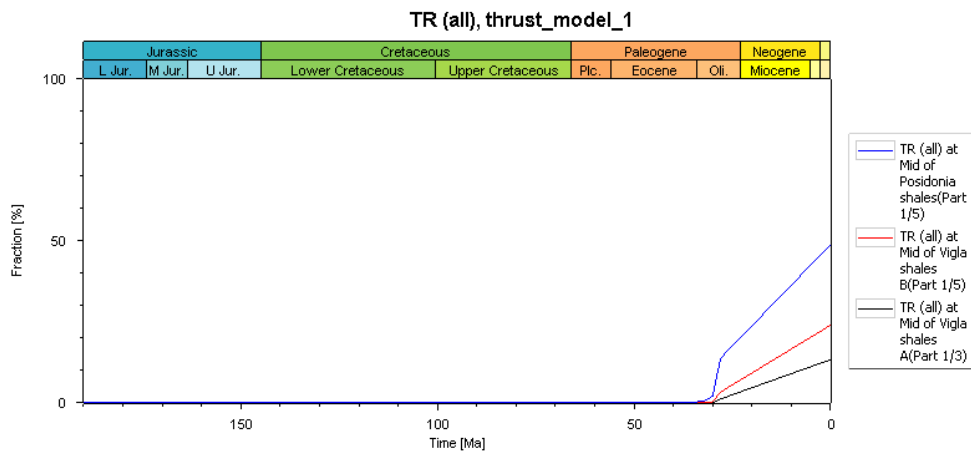


Figure 40: Transformation ratio (TR) vs. time (Ma) plots of the three source rock formations of Agios Georgios-3 well.

5.1.5 Petroleum generation and Expulsion

In this study, no available volume data are defined in 1D modeling, so the generated petroleum mass cannot be predicted. Instead of the generated mass, the potential oil and gas generation masses (mgHC/gTOC) were estimated by using the petroleum kinetics model,

Pepper and Corvi (1995) TII (B). The burial plot with potential oil (Fig. 41) and gas (Fig. 42) generation mass overlay, the potential oil (Fig. 43) and gas (Fig. 44) generation mass plots and the burial plot with an expulsion onset overlay (Fig. 45) are displayed below.

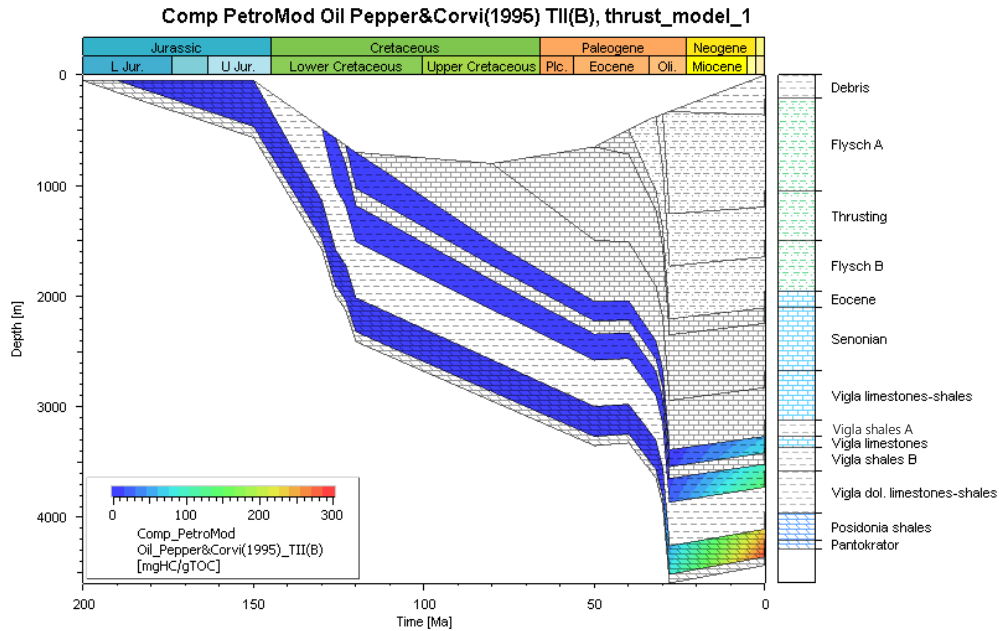


Figure 41: Burial plot with potential oil generation mass overlay by Pepper & Corvi (1995) for the source rock formations of Agios Georgios-3 well.

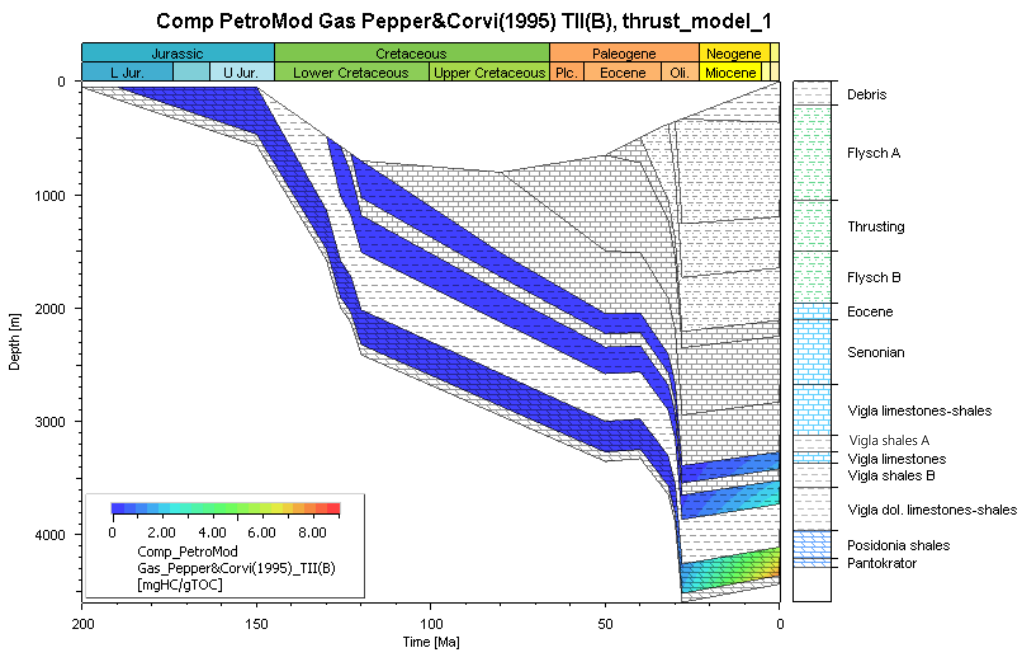


Figure 42: Burial plot with potential gas generation mass overlay by Pepper & Corvi (1995) for the source rock formations of the Agios Georgios-3 well.

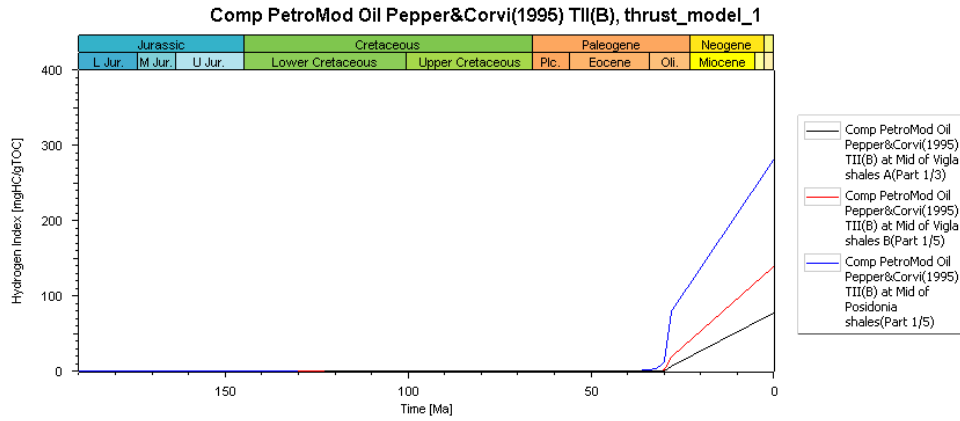


Figure 43: Potential oil generation mass by Pepper & Corvi (1995) vs. time (Ma) plots of the three source rock formations of Agios Georgios-3 well.

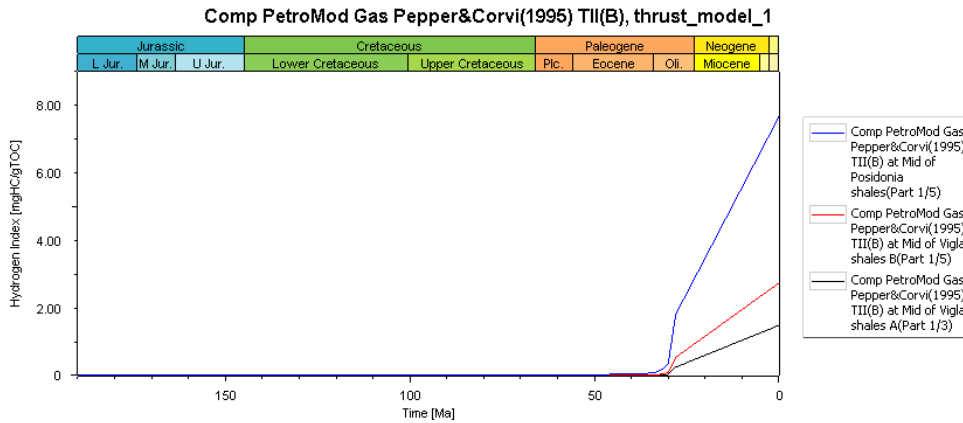


Figure 44: Potential gas generation mass by Pepper & Corvi (1995) vs. time (Ma) plots of the three source rock formations of Agios Georgios-3 well.

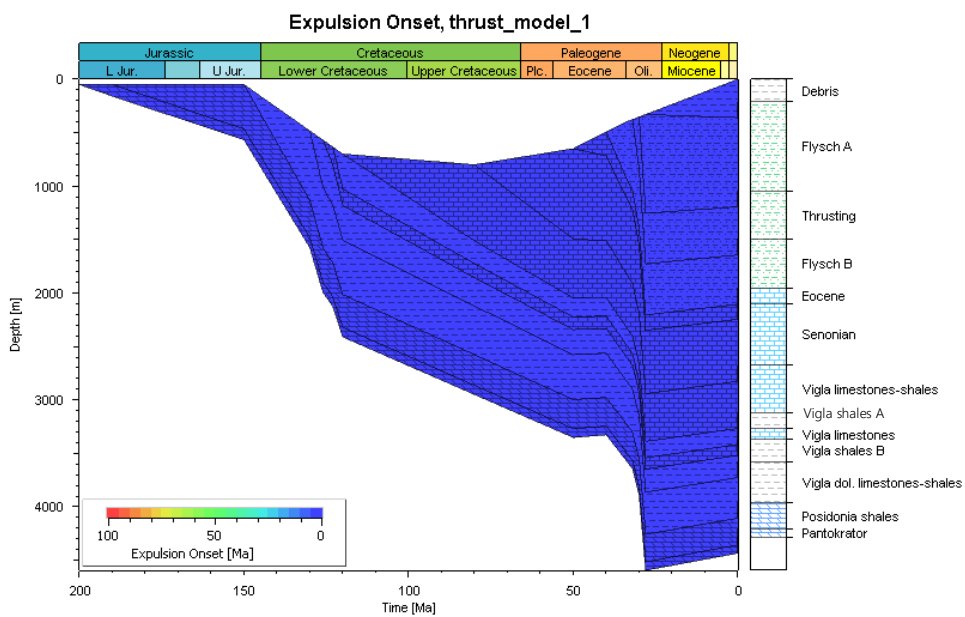


Figure 45: Burial plot of Agios Georgios-3 well with an expulsion onset overlay.

Posidonia shales

Hydrocarbon generation of Posidonia shales formation started at early Oligocene. More specifically, the onset of hydrocarbon generation commenced at 29.53Ma and at 3976m. It is the most mature source rock of Agios Georgios-3 well. The potential oil generation mass is 281.72mgHC/gTOC and the potential gas generation mass is 7.67mgHC/gTOC. The present-day transformation ratio is equal to 48.95% and the present-day vitrinite reflectance value is 0.77%, showing that the formation has not reached the peak oil expulsion in the specific area (Fig. 45).

Vigla shales B

Hydrocarbon generation of Vigla shales B started at late Oligocene with a hydrocarbon generation onset at 26.64 Ma and at 3857m. The potential oil generation mass is 139.67mgHC/gTOC and the potential gas generation mass is 2.74mgHC/gTOC. The present-day transformation ratio is equal to 24.05% and the present-day vitrinite reflectance value is 0.68%. Based on the results, the formation has not reached the peak oil expulsion in the specific area (Fig. 45).

Vigla shales A

Hydrocarbon generation of Vigla shales A started at Miocene, while the hydrocarbon generation onset of the formation is at 18.12Ma and at 3498m. The potential oil generation mass is 78.01mgHC/gTOC and the potential gas generation mass is 1.49mgHC/gTOC. The present-day transformation ratio is equal to 13.41% and the present-day vitrinite reflectance value is 0.64%. According to the available results, the formation has not reached the peak oil expulsion in the specific area (Fig. 45).

5.1.6 Sensitivity analysis

The purpose of this chapter was to monitor the influence of erosion thickness and boundary conditions and to assess the results. It was accomplished by performing a sensitivity analysis. Sensitivity analysis is a study of the sensitivity of a system's response to various disturbances within it (Cao and Lerche, 1989). Using a 1-D fluid flow/compaction model we examine the effects of some of the commonly used parameters (such as depth, age, lithology, porosity, permeability, unconformity, eroded thickness and erosion time, temperature at sediment surface, bottom-hole temperature, present-day heat flow, thermal gradient, thermal conductivity, and kerogen type and content) on the evolution of formation thickness, porosity,

permeability, pressure with time and depth, the “oil window” in terms of time and depth, and the amount of hydrocarbons generated with time and depth (Cao and Lerche, 1989).

The study started with the `basic_model` which consisted of twelve deposition layers. Then according to Rigakis (1999) study, the thrust sheet was added to the input data creating the `thrust_model`. After that, the erosion surface at 0m depth was added creating the `thrust_model_1`. The erosion thickness was imported to the software being equal to 150m. Following the first thrust model with an erosion surface, the `thrust_model_2`, `thrust_model_3`, `thrust_model_4` and `thrust_model_5` were created with erosion thicknesses equal to 100m, 200m, 250m and 300m respectively.

As mentioned before for the `thrust_model_1`, during the calibration of the three new models it was noticed that vitrinite reflectance and temperature trends was only affected by the first two heat flow (HF) values and the value of erosion thickness at 0m depth. The first heat flow value of the table is the present-day heat flow which remained constant. Only the second value changed during the analysis. So, after the calibration of the `thrust_model`, `thrust_model_2`, `thrust_model_3`, `thrust_model_4` and `thrust_model_5`, their new heat flow and erosion thickness values used to monitor how they affect the hydrocarbon generation and transformation ratio.

More precisely, for the `thrust_model` the second value of the heat flow table was set to 48mW/m^2 , while no erosion surface had been imported. For the `thrust_model_1` the second value of the heat flow table was set to 47mW/m^2 and the erosion thickness to 150m. The erosion thickness in the `thrust_model_2` was set to 100m and during the calibration no boundary condition value had to be changed. On the other hand, the erosion thickness in the `thrust_model_3` was set to 200m and during the calibration the second value of the heat flow table had to be changed from 47mW/m^2 to 46mW/m^2 for better calibration of the measured and calculated values. The erosion thickness in the `thrust_model_4` was set to 250m and during the calibration no boundary condition value had to be changed ($= 46\text{mW/m}^2$). The same procedure followed for the `thrust_model_5`. The erosion thickness was set to 300m and during the calibration the second value of the heat flow table had to be changed from 46mW/m^2 to 45mW/m^2 .

The calibration plots of the `thrust_model` (Fig. 46), `thrust_model_2` (Fig. 47), `thrust_model_3` (Fig. 48), `thrust_model_4` (Fig. 49) and `thrust_model_5` (Fig. 50) are presented below.

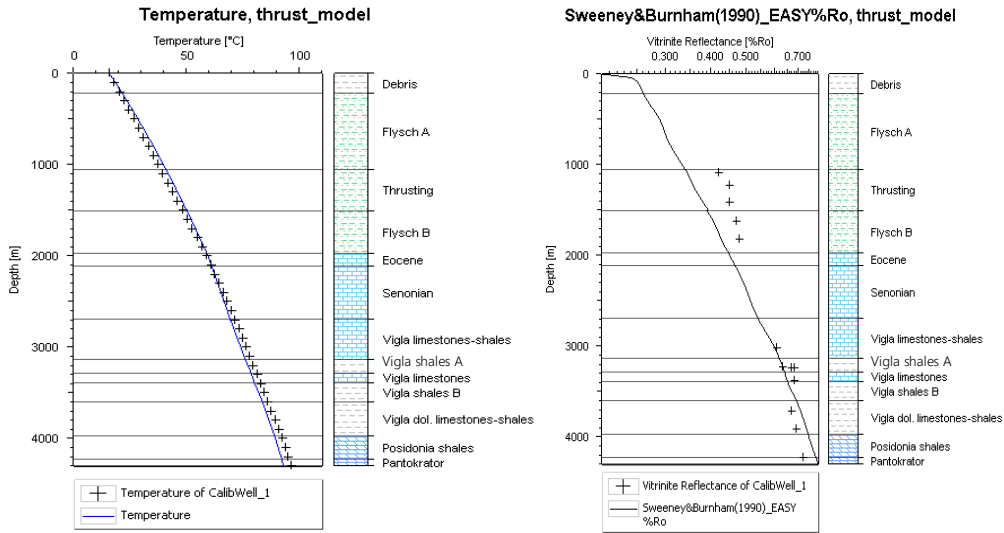


Figure 46: Calibration plots of thrust_model.

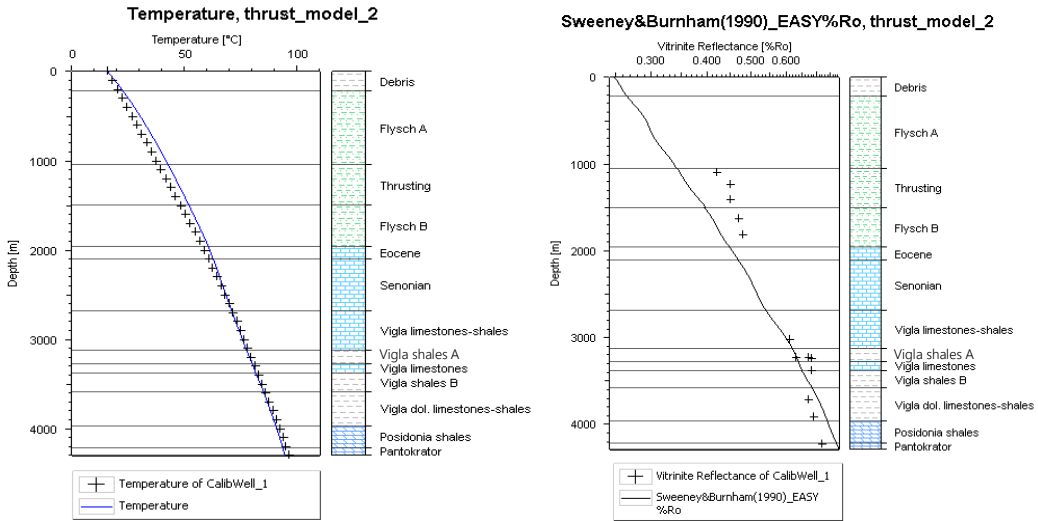


Figure 47: Calibration plots of thrust_model_2.

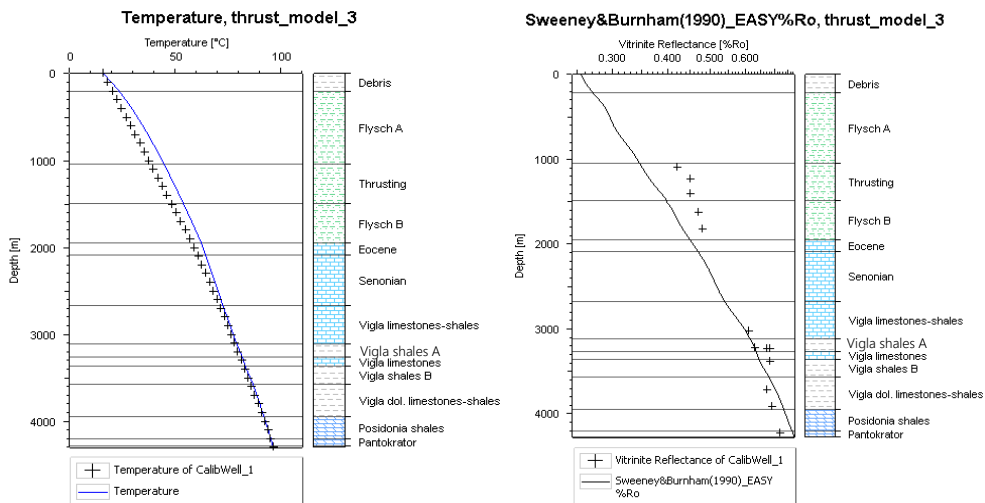


Figure 48: Calibration plots of thrust_model_3.

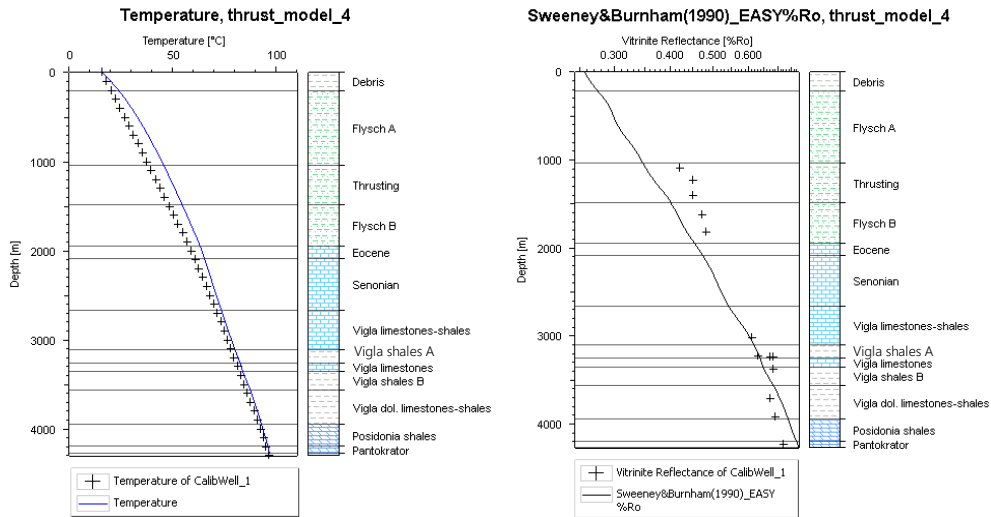


Figure 49: Calibration plots of thrust_model_4.

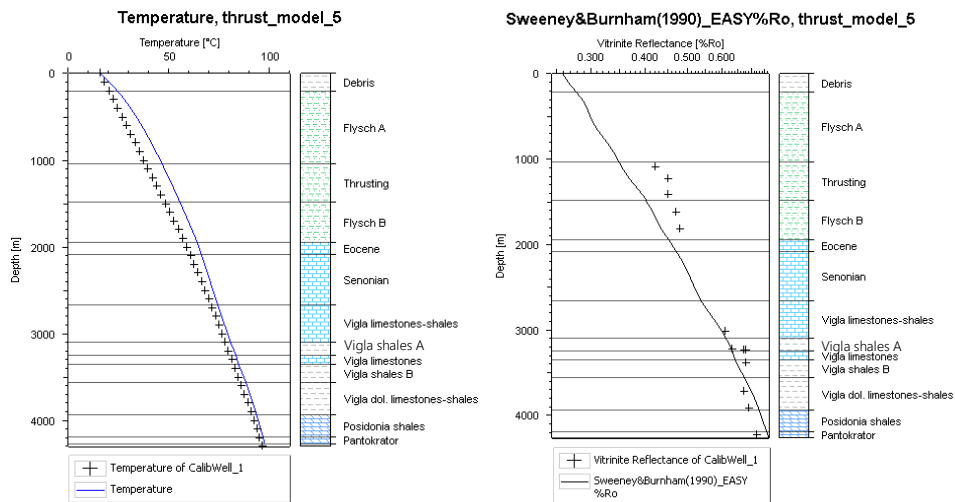


Figure 50: Calibration plots of thrust_model_5.

After the calibration of all thrust models was finished, it was noticed that while the erosion thickness at 0m depth was increasing, both calculated data plots (temperature, vitrinite reflectance) were moving to the right. Then, by changing the second value of the heat flow table in some of them, we noticed a slightly better vitrinite reflectance calibration and a slightly worse temperature calibration than in thrust_model which does not include an erosion surface.

Figure 51, Figure 52 and Figure 53 present the transformation ratio (TR) plots for Vigla shales A, Vigla shales B and Posidonia shales source rock formations of all thrust models.

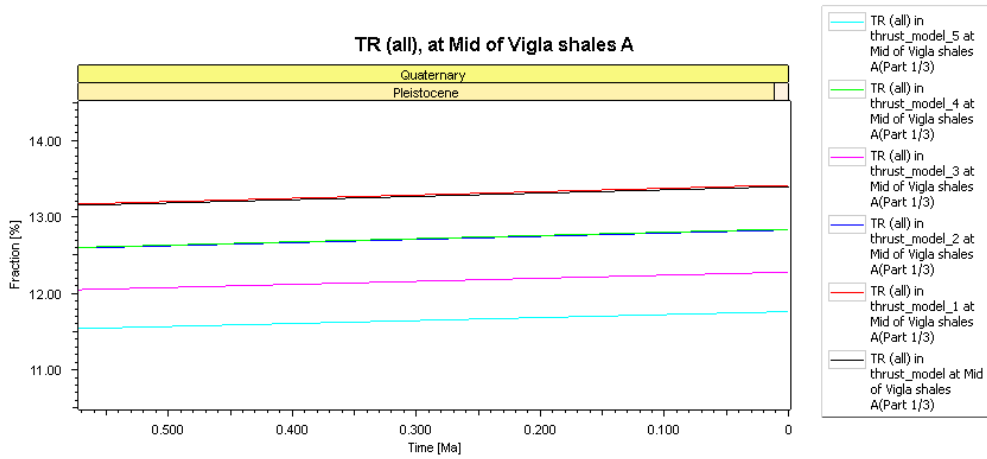


Figure 51: Transformation ratio (TR) vs. time (Ma) plots near to 0Ma of all thrust models at Vigla shales A formation.

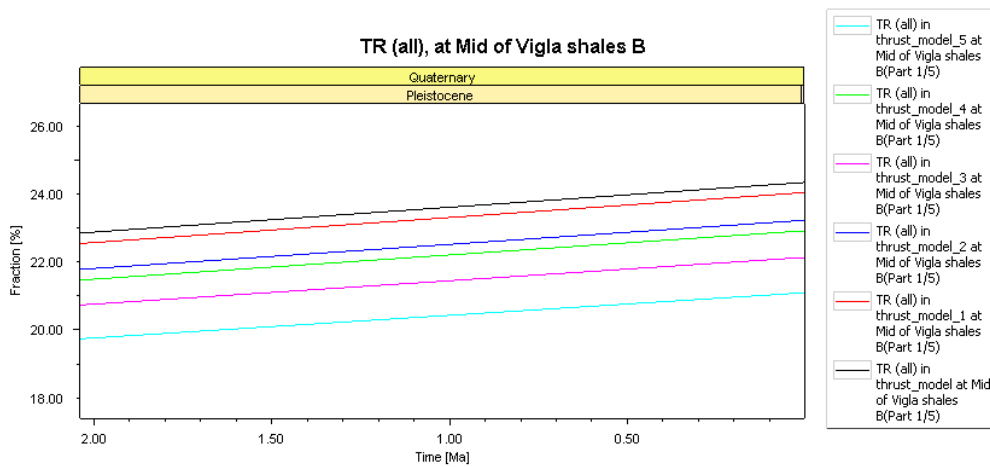


Figure 52: Transformation ratio (TR) vs. time (Ma) plots near to 0Ma of all thrust models at Vigla shales B formation.

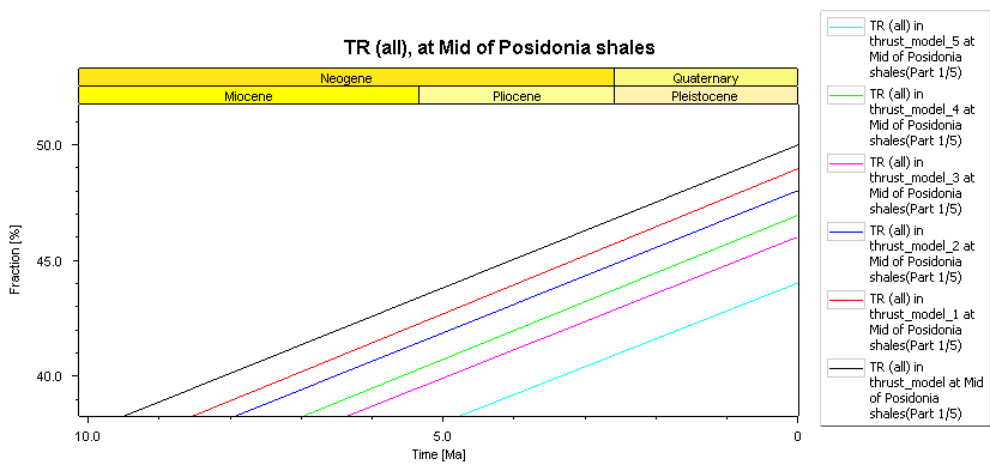


Figure 53: Transformation ratio (TR) vs. time (Ma) plots near to 0Ma of all thrust models at Posidonia shales formation.

According to the previous figures, the present-day transformation ratio values of all the thrust models can be summarized as follows (Table 4).

Table 4: Transformation ratio (TR) values of all the thrust models of Agios Georgios-3 well.

	Erosion thickness (m)	HF [mW/m²]	Vigla shales A	Vigla shales B	Posidonia shales
Thrust_model	0	48	13.40%	24.36%	49.99%
Thrust_model_1	150	47	13.41%	24.05%	48.95%
Thrust_model_2	100	47	12.83%	23.23%	48.01%
Thrust_model_3	200	46	12.27%	22.13%	46.00%
Thrust_model_4	250	46	12.84%	22.92%	46.94%
Thrust_model_5	300	45	11.76%	21.09%	44.01%

Results displayed that the thickness of eroded surface at 0m depth affects positively the transformation ratio values of the source rock formations, with standard heat flow (thrust_model_1, thrust_model_4).

Figure 54, Figure 55, Figure 56, Figure 57, Figure 58 and Figure 59 present the potential oil and gas generation mass plots for Vigla shales A, Vigla shales B and Posidonia shales source rock formations of all thrust models.

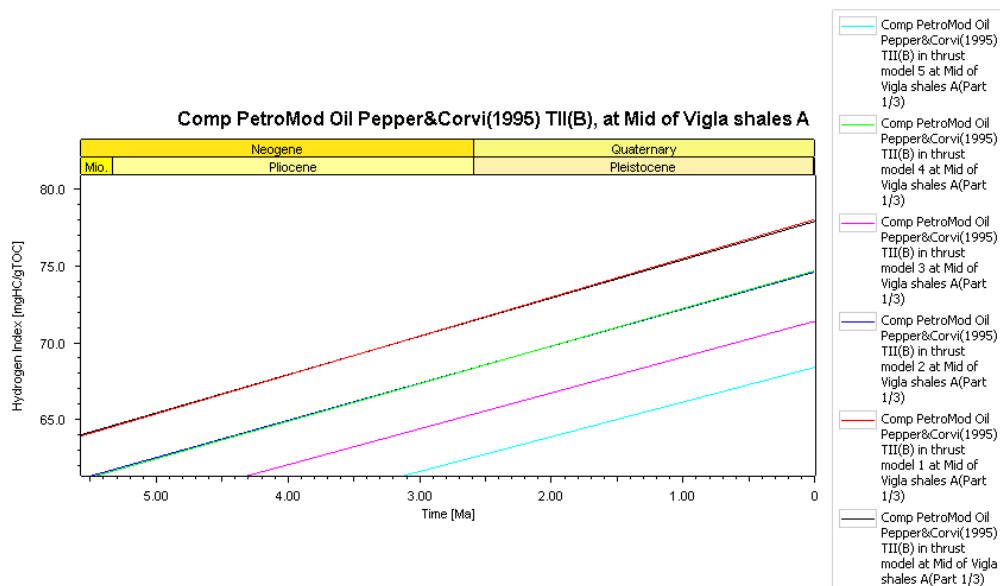


Figure 54: Potential oil generation mass by Pepper & Corvi (1995) vs. time (Ma) plots near to 0Ma of all thrust models at Vigla shales A formation.

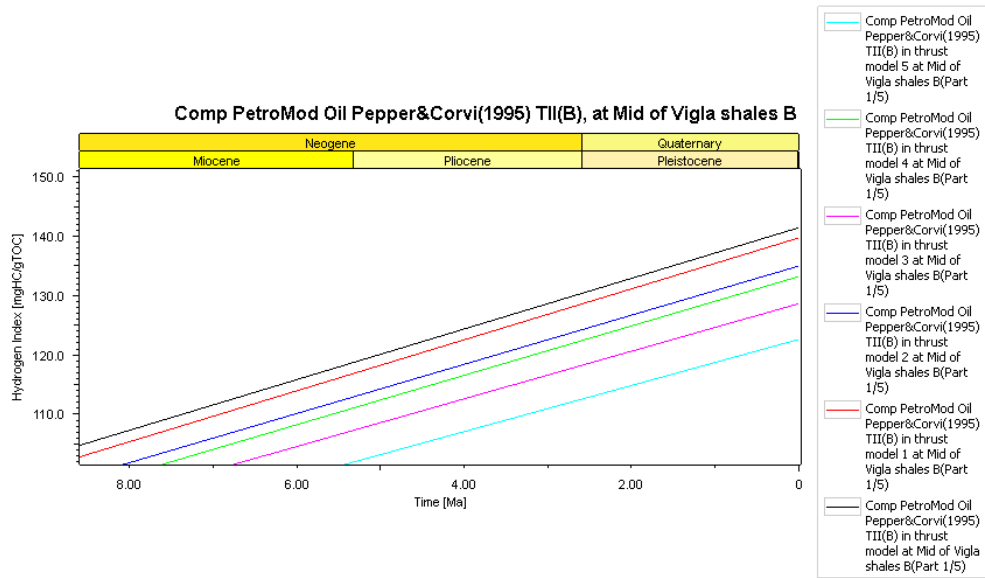


Figure 55: Potential oil generation mass by Pepper & Corvi (1995) vs. time (Ma) plots near to 0Ma of all thrust models at Vigla shales B formation.

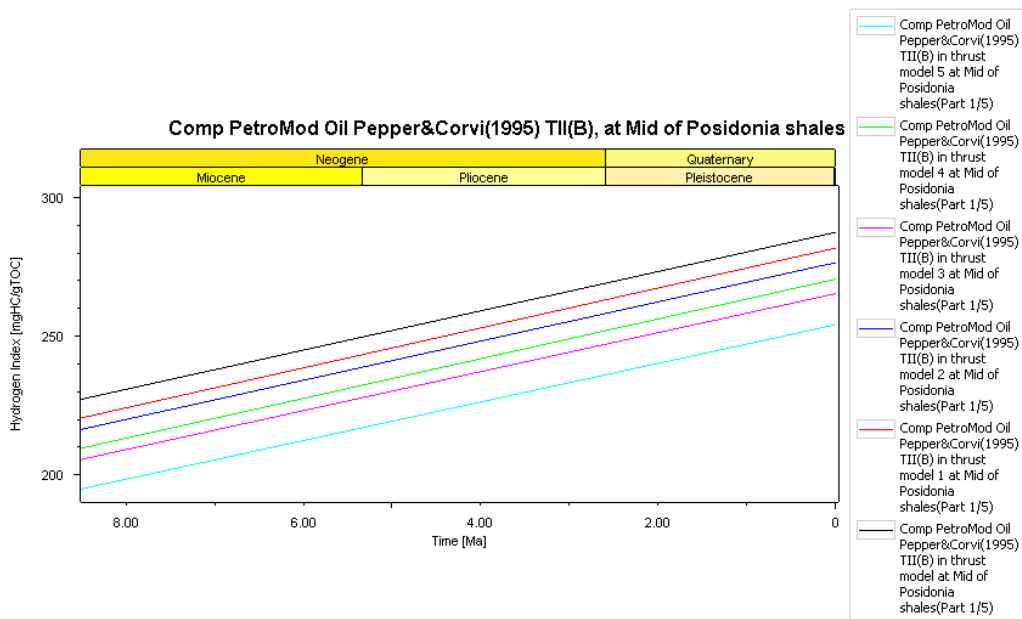


Figure 56: Potential oil generation mass by Pepper & Corvi (1995) vs. time (Ma) plots near to 0Ma of all thrust models at Posidonia shales formation.

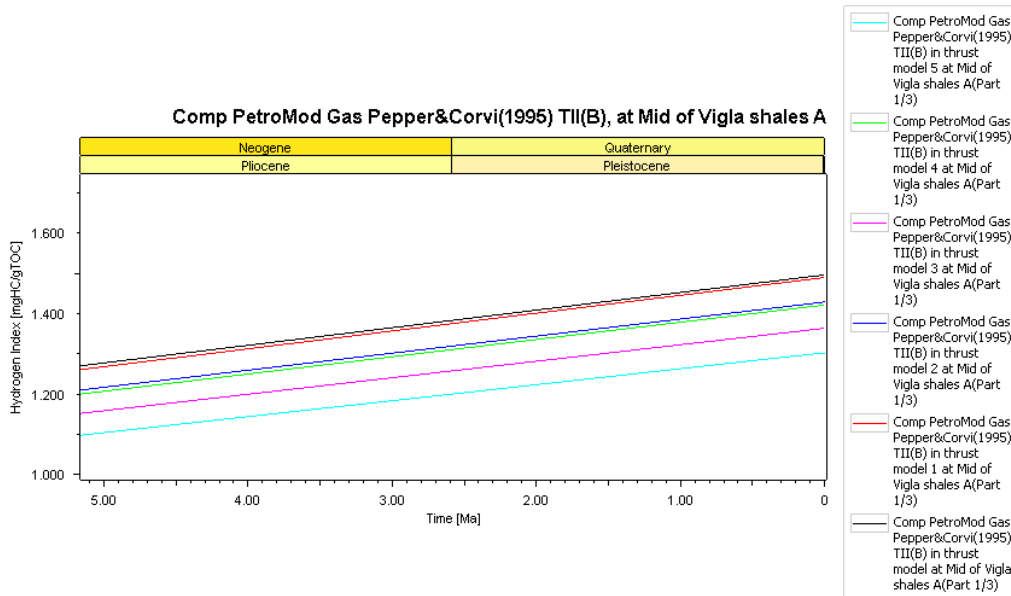


Figure 57: Potential gas generation mass by Pepper & Corvi (1995) vs. time (Ma) plots near to 0Ma of all thrust models at Vigla shales A formation.

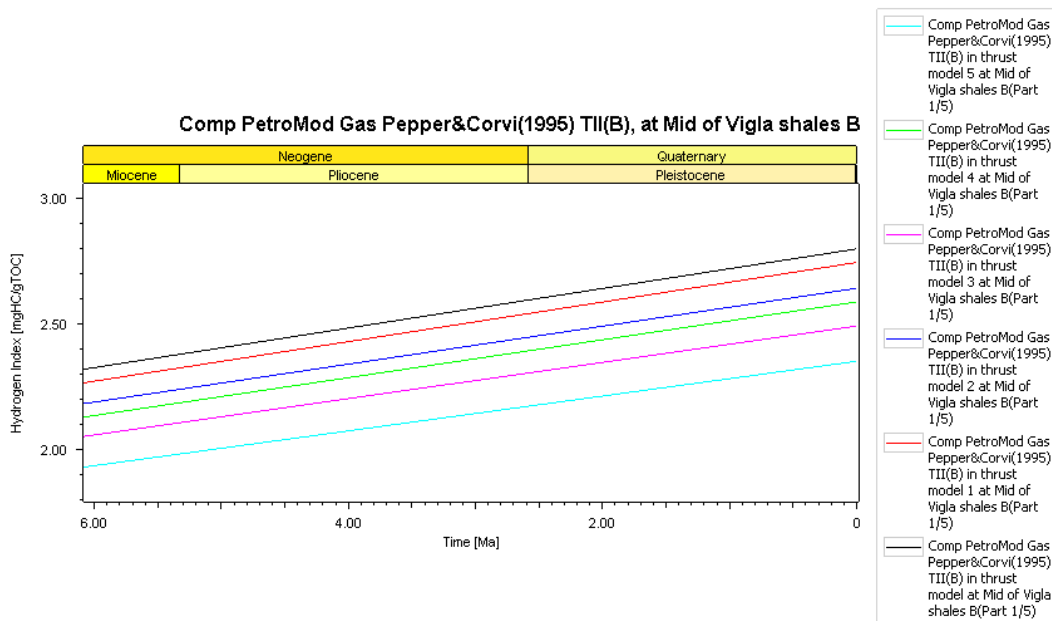


Figure 58: Potential gas generation mass by Pepper & Corvi (1995) vs. time (Ma) plots near to 0Ma of all thrust models at Vigla shales B formation.

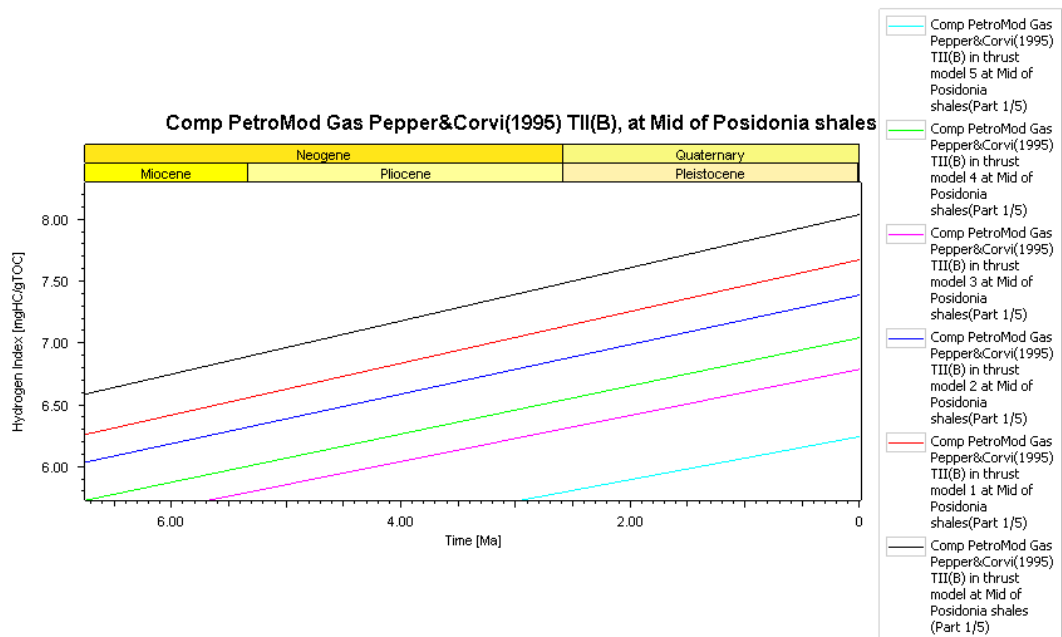


Figure 59: Potential gas generation mass by Pepper & Corvi (1995) vs. time (Ma) plots near to 0Ma of all thrust models at Posidonia shales formation.

According to the previous figures, the potential oil (Table 5) and gas (Table 6) generation masses of all the thrust models can be summarized as follows.

Table 5: Potential oil generation masses (mgHC/gTOC) of all the thrust models of Agios Georgios-3 well.

	Erosion thickness (m)	HF [mW/m²]	Vigla shales A	Vigla shales B	Posidonia shales
Thrust_model	0	48	77.90	141.42	287.44
Thrust_model_1	150	47	78.01	139.67	281.72
Thrust_model_2	100	47	74.59	134.93	276.46
Thrust_model_3	200	46	71.38	128.60	265.27
Thrust_model_4	250	46	74.67	133.15	270.52
Thrust_model_5	300	45	68.38	122.57	254.08

Table 6: Potential gas generation masses (mgHC/gTOC) of all the thrust models of Agios Georgios-3 well.

	Erosion thickness (m)	HF [mW/m²]	Vigla shales A	Vigla shales B	Posidonia shales
Thrust_model	0	48	1.50	2.80	8.04
Thrust_model_1	150	47	1.49	2.74	7.67
Thrust_model_2	100	47	1.43	2.64	7.39
Thrust_model_3	200	46	1.36	2.49	6.79
Thrust_model_4	250	46	1.42	2.58	7.04
Thrust_model_5	300	45	1.30	2.35	6.24

Results displayed that the thickness of eroded surface at 0m depth affects positively the transformation ratio values and the potential oil and gas generation masses of the source rock formations, with standard heat flow (thrust_model_1, thrust_model_4). Thrust_model_1 presents the highest transformation ratio and potential oil and gas generation masses between the thrust models with an erosion surface, while keeping a good match between measured and calculated temperature and vitrinite reflectance values. This is the reason why the thrust_model_1 had been chosen as the final model of Agios Georgios-3 well.

5.2 East Erikoussa-1

This chapter will present the results of the final model of East Erikoussa-1 well.

5.2.1 Burial history

The figure below (Fig. 60) presents the burial history reconstruction for the model_erikoussa, accompanied by the petroleum system elements plot (PSE). Detailed results about the hydrocarbon generation and the critical moment will be presented in the following chapters.

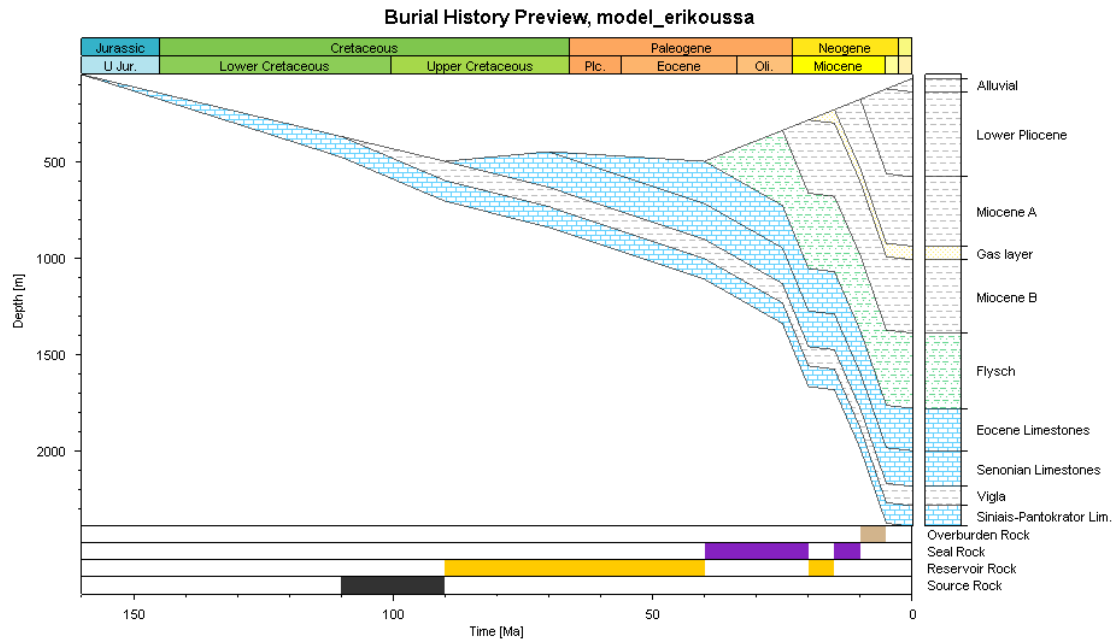


Figure 60: Burial history of East Erikoussa-1 well.

5.2.2 Temperature history

Figure 61 presents the temperature evolution of the East Erikoussa-1 well and Figure 62 presents the temperature profile of the source rock formations. The source rock formation reached its higher temperature at 5Ma. More specifically, Vigla formation reached a temperature up to 62.01°C.

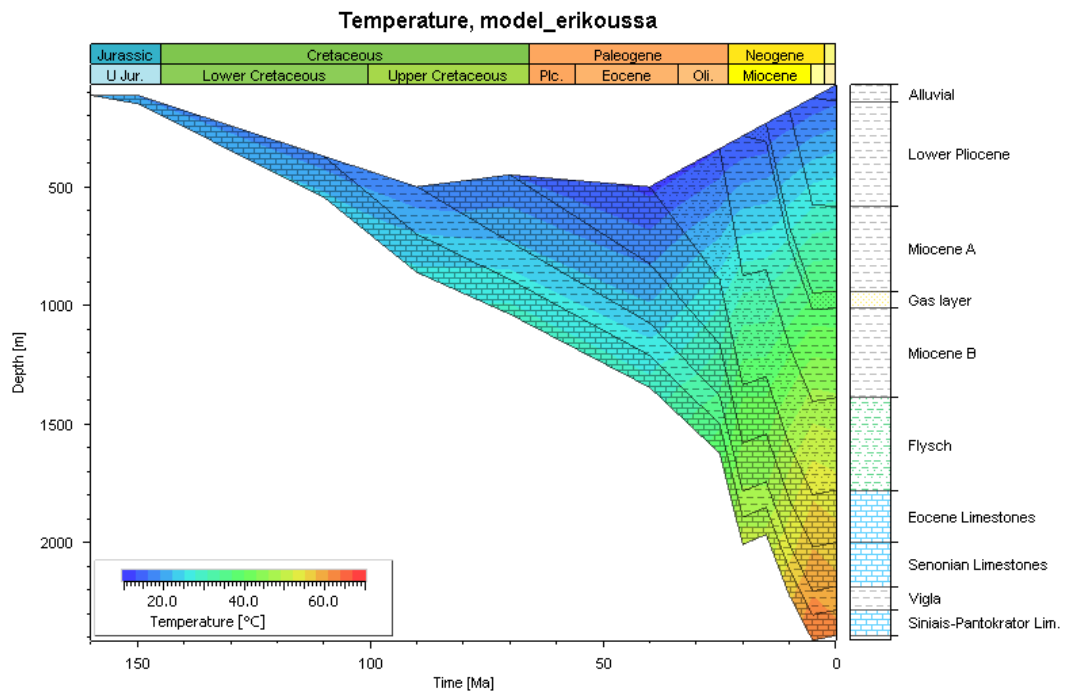


Figure 61: Burial history of East Erikoussa-1 well with a temperature overlay.

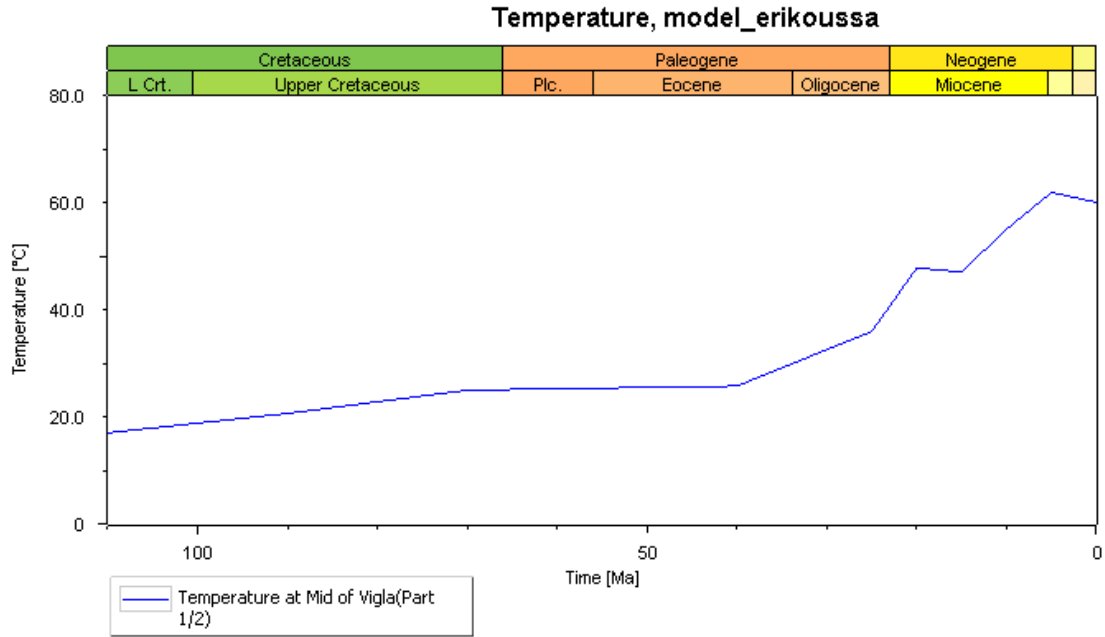


Figure 62: Temperature (°C) vs. time (Ma) plot of the source rock formation of East Erikoussa-1 well.

5.2.3 Present-day maturity

Figure 63 and Figure 64 present the maturity history of East Erikoussa-1 well.

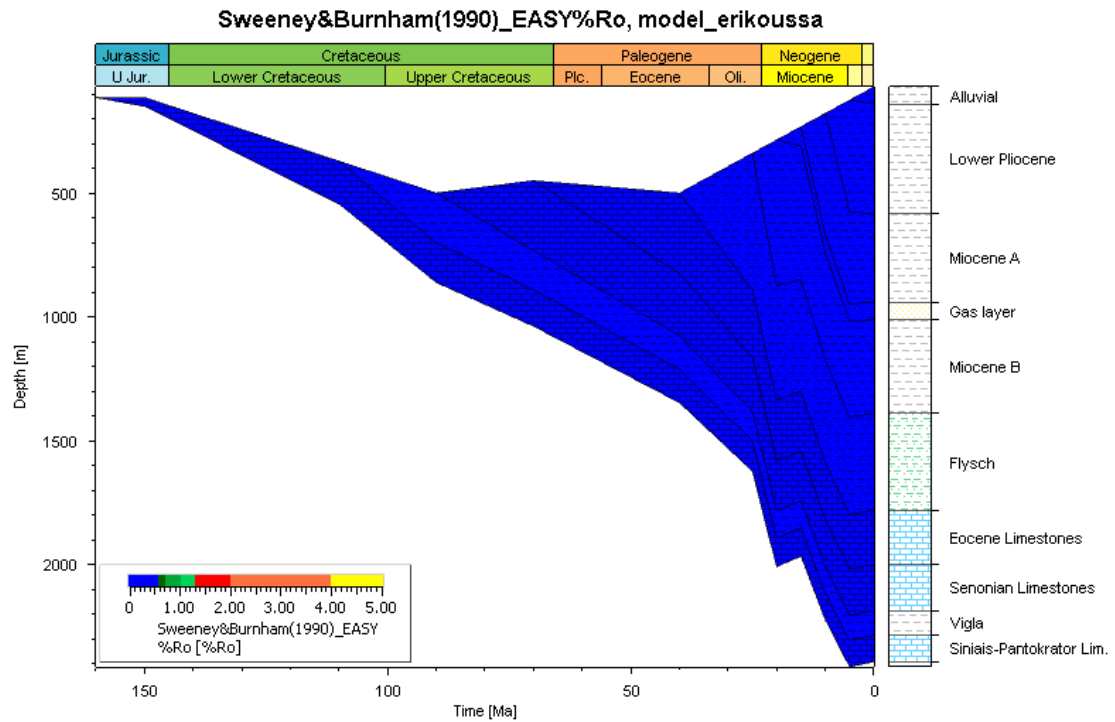


Figure 63: Maturity history plot (vitrinite reflectance) of East Erikoussa-1 well.

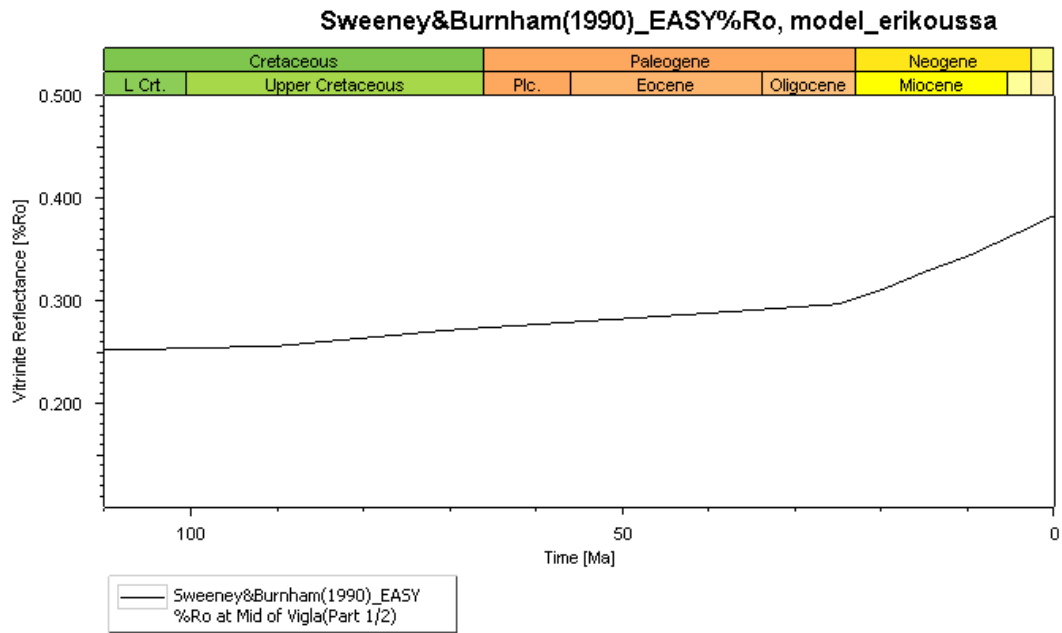


Figure 64: Vitrinite reflectance (%Ro) vs. time (Ma) plot of the source rock formations of East Erikoussa-1 well.

According to the previous figures, the source rock of Vigla formation is immature with a present-day vitrinite reflectance value of 0.38%.

5.2.4 Transformation ratio (TR)

Figure 65 and Figure 66 display the transformation ratio results for the source rock formation.

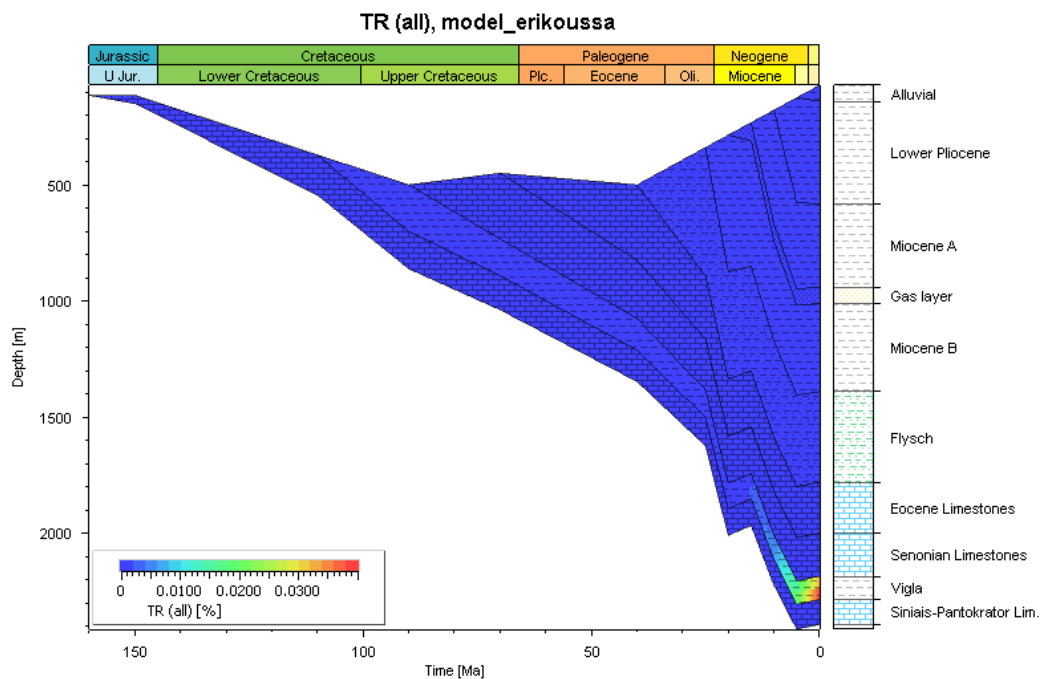


Figure 65: Burial history plot of East Erikoussa-1 well with a transformation ratio overlay.

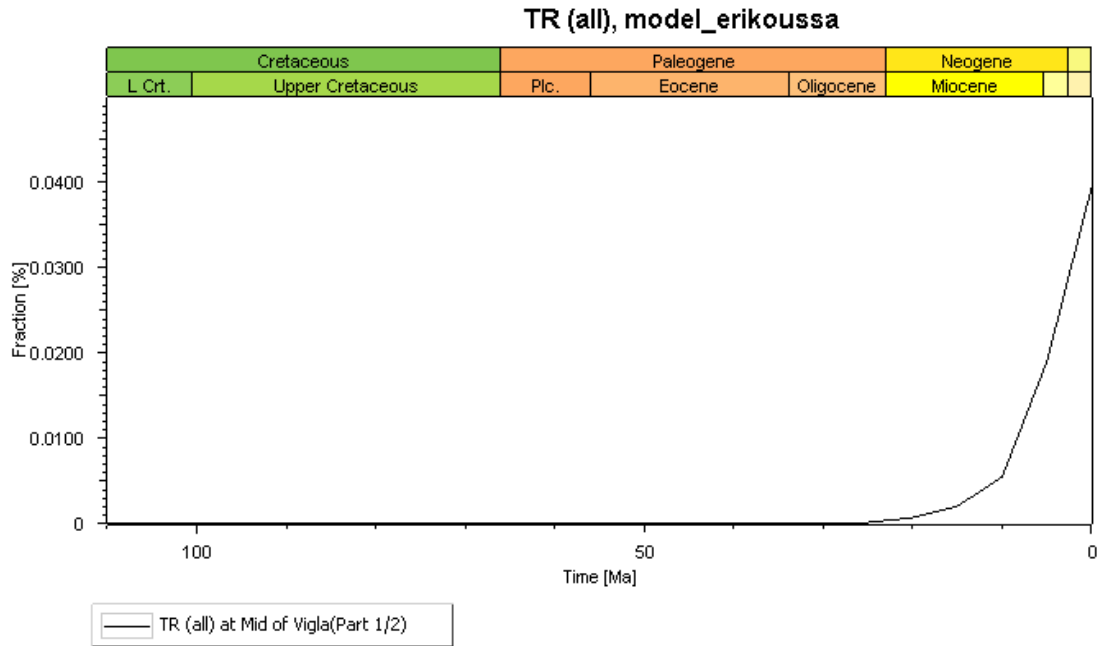


Figure 66: Transformation ratio (TR) vs. time (Ma) plot of the source rock formation of East Erikoussa-1 well.

Transformation in Vigla source rock formation began at 15.44Ma at a depth of 1855m and it has a present-day TR value of 0.04%.

5.2.5 Petroleum generation and Expulsion

As mentioned before, no available volume data are defined in 1D modeling, so instead of the generated mass, the potential generation oil (Fig. 67) and gas (Fig. 68) masses (mgHC/gTOC) were estimated by using the petroleum kinetics model, Pepper and Corvi (1995) TII (B).

The kerogen kinetic classification by Pepper and Corvi (1995) is based on the "organofacies" concept. Being an organofacies defined as "a collection of kerogens derived from common organic precursors, deposited under similar environmental conditions and exposed to similar early diagenetic histories" (Sylwan et al., 2008).

Pepper and Corvi (1995) TII (B) petroleum kinetic model characterized by kerogen type II and organofacies B.

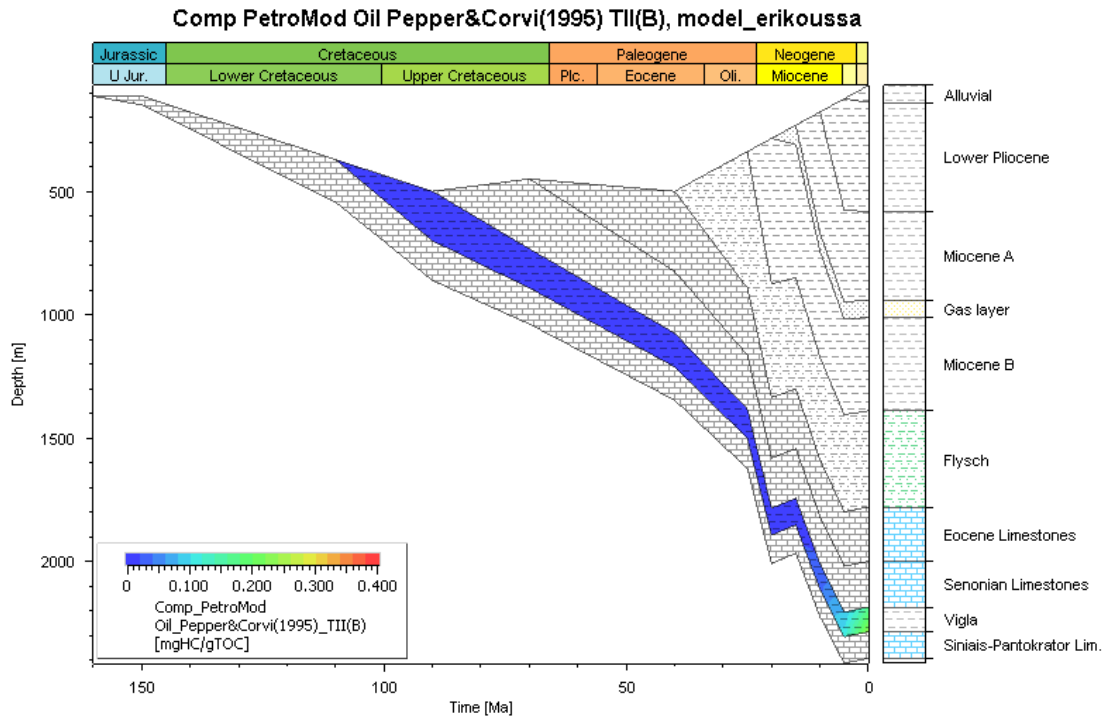


Figure 67: Burial plot with potential generation oil mass overlay by Pepper & Corvi (1995) of East Erikoussa-1 well.

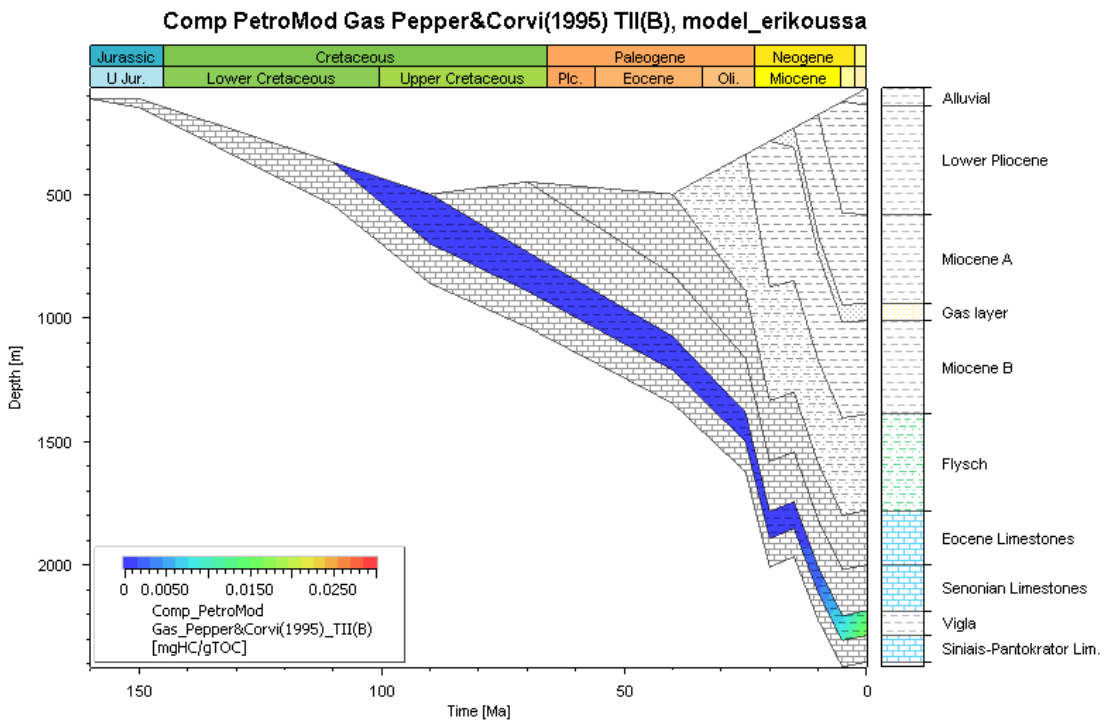


Figure 68: Burial plot with potential generation gas mass overlay by Pepper & Corvi (1995) of East Erikoussa-1 well.

The potential oil (Fig. 69) and gas (Fig. 70) generation mass plots and the burial plot with an expulsion onset overlay (Fig. 71) are displayed below.

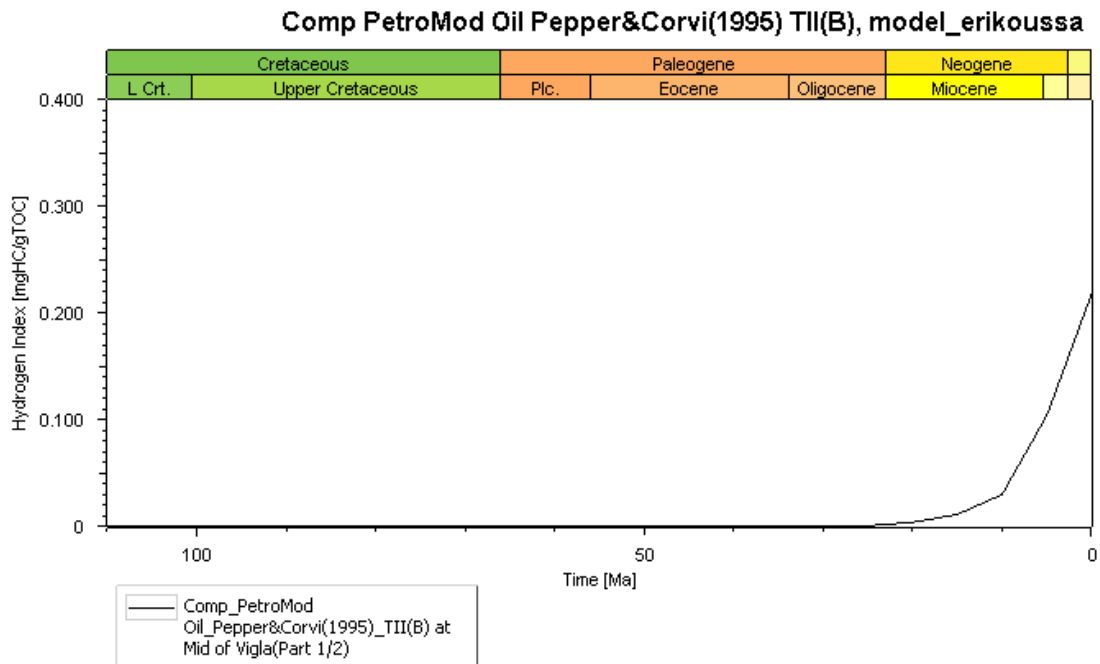


Figure 69: Potential generation oil mass by Pepper & Corvi (1995) vs. time (Ma) plots of the source rock formation of East Erikoussa-1 well.

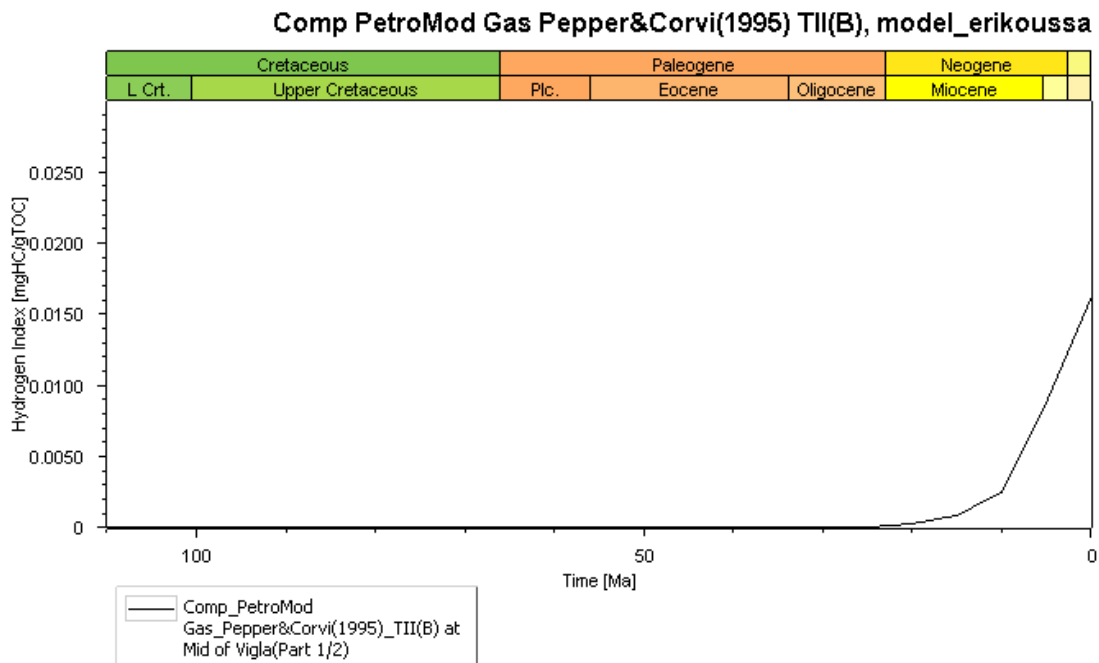


Figure 70: Potential generation gas mass by Pepper & Corvi (1995) vs. time (Ma) plot of the source rock formation of East Erikoussa-1 well.

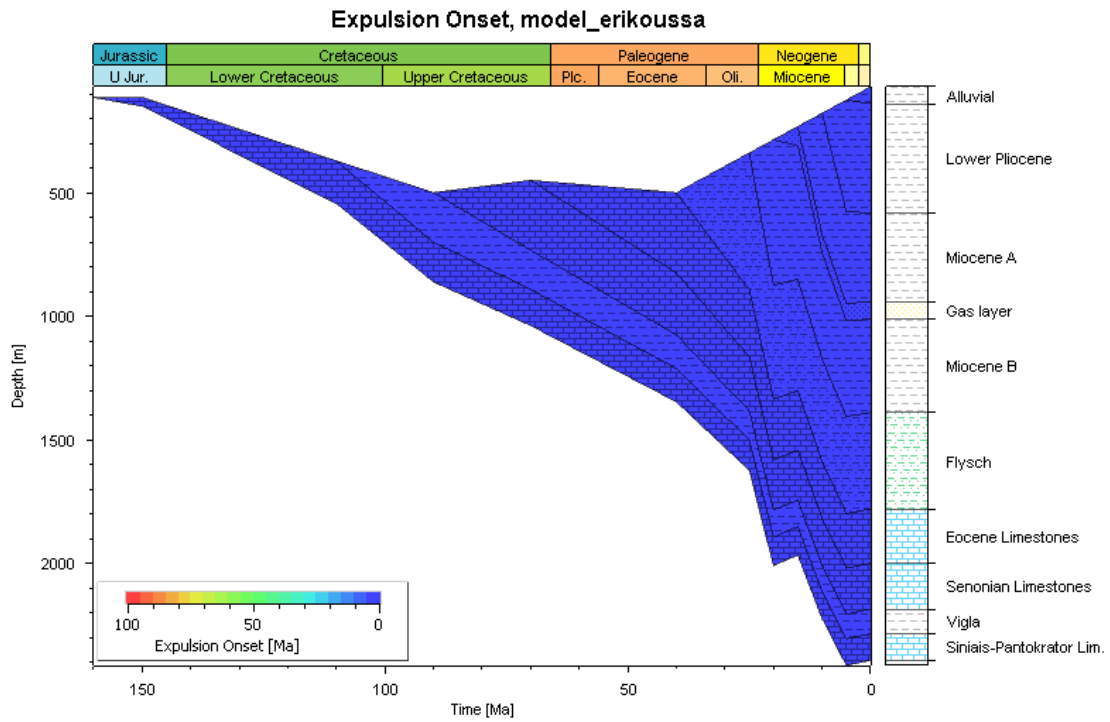


Figure 71: Burial plot of East Erikoussa-1 well with an expulsion onset overlay.

Vigla

The Vigla formation did not enter the hydrocarbon generation range. The potential oil generation mass is 0.22 mgHC/gTOC and the potential gas generation mass is 0.02mgHC/gTOC. The present-day transformation ratio is equal to 0.04% and the present-day vitrinite reflectance value is 0.38%. According to the available results, the source rock formation is immature and it has not reached the peak oil expulsion in the specific area (Fig. 71).

6 CONCLUSIONS

The purpose of this study was to examine the potential source rock formations in two wells, one onshore and one offshore, both located within the wider Ionian paleobasin regime, a well-known sedimentary basin in Greece for its hydrocarbon potential significance, using Schlumberger's PetroMod (version 2017.1) petroleum systems modeling software. Even though, there were assumptions and uncertainties about the models, a reasonable first estimation about thermal history, maturity history, transformation ratio (TR) and potential oil and gas generation was achieved.

6.1 Agios Georgios-3

Agios Georgios-3 is an onshore well with three known source rock formations (Posidonia shales, Vigla shales B, Vigla shales A) of Mesozoic age.

According to the 1D basin modeling output, Posidonia shales formation is the most mature source rock of Agios Georgios-3 well, with the highest transformation ratio and potential oil and gas generation masses. Hydrocarbon generation started at (early) Oligocene. More precisely, the onset of hydrocarbon generation was at 29.53Ma and at 3976m, while the zone of main oil was reached at 16.16Ma and at 4448m. The potential oil generation mass is 281.72mgHC/gTOC and the potential gas generation mass is 7.67mgHC/gTOC. The present-day transformation ratio is equal to 48.95% and the present-day vitrinite reflectance value is 0.77%, showing that the formation has not reached the peak oil expulsion in the specific area.

Vigla formation formed very good hydrocarbon source rocks as well. It consists of two main source rock formation zones, Vigla shales A and Vigla shales B. The second one is more mature than the first, with higher transformation ratio and potential hydrocarbon generation mass than the other. More specifically, the hydrocarbon generation of Vigla shales B source rock formation started at (late) Oligocene. The onset of hydrocarbon generation was at 26.64Ma and at 3857m, while the potential oil and generation masses are 139.67mgHC/gTOC and 2.74mgHC/gTOC respectively. The present-day transformation ratio is equal to 24.05% and the present-day vitrinite reflectance value is 0.69%, showing that Vigla shales B formation has not reached the peak oil expulsion in the specific area.

Vigla shales A is the least mature source rock of Agios Georgios-3 well. The hydrocarbon generation started at Miocene. The onset of hydrocarbon generation was at 18.12Ma and at

3498m, while the potential oil generation mass is 78.01mgHC/gTOC and the potential gas generation mass is 1.49mgHC/gTOC. The present-day transformation ratio is equal to 13.41% and the present-day vitrinite reflectance value is 0.64%. Vigla shales A formation has not reached the peak oil expulsion in the specific area.

Sensitivity analysis results displayed that the thickness of eroded surface at 0m depth affects positively the transformation ratio and potential hydrocarbon generation mass values of the source rock formations, with standard heat flow. In addition, only the heat flow from boundary condition tables plays an important role to the temperature and maturity modeling.

6.2 East Erikoussa-1

East Erikoussa-1 is an offshore well that penetrated only one source rock formation (Vigla shales) of Cretaceous age.

Vigla source rock formation did not enter the hydrocarbon generation range. The potential oil generation mass is 0.22mgHC/gTOC, while the potential gas generation mass is 0.02mgHC/gTOC. The present-day transformation ratio is equal to 0.04% and the present-day vitrinite reflectance value is 0.38%, showing that the formation is an immature source rock that has not reached the peak oil expulsion in the specific area.

6.3 Correlation

As mentioned on the previous chapters, most of the required input data for the paleo-basin modeling of the wells included in this study, are derived from Rigakis (1999) PhD thesis. Age, depth and lithology data imported to the software according to the lithostratigraphic columns of Agios Georgios-3 and East Erikoussa-1 wells which are modified from Rigakis (1999) (Fig. 14; Fig. 17). Erosion surface and thrust sheet depths and thicknesses (Agios Georgios-3 well) are derived from vitrinite reflectance vs. depth and sonic vs. depth diagram (Fig. 15), modified from Rigakis (1999) and Rigakis et al. (2013). Source rocks parameters from Rock Eval analysis, vitrinite reflectance (Agios Georgios-3 well) and geothermal gradient values were also available.

On the other hand, no PWD, SWIT and HF values were available from Rigakis (1999) in order to create the boundary condition tables. The Paleo Water Depth (PWD) values in the models were estimated based on published data. The tables of both wells are based on their

location (in the internal and external part of the Ionian zone for the Agios Georgios-3 and East Erikoussa-1 respectively), the sedimentary facies and the depositional environments in Ionian zones, studies of Getsos et al. (2018) and Kontakiotis et al. (2020). Sediment Water Interface (SWIT) values were calculated by the software, while the paleo-Heat Flow (HF) values were selected according to the study of Mavromatidis (2009) and the primary heat flow map of Greece (Fig. 28) which created by Fytikas and Kolios (1979).

All the geological data which imported to the software were derived from the published open source literature or have been estimated accordingly.

During the modeling process, it was noticed that the Agios Georgios-3 and East Erikoussa-1 wells present differences in the sedimentary sequences, even though both of them are located in the same (Ionian) basin, probably due to their paleogeographic location and/or relevant thrust tectonics affected the area. The lithostratigraphic column of East Erikoussa-1 well (Fig. 17) starts with alluvial sediments at 71m depth. The second and third layers are of Lower Pliocene and Miocene age, followed by the Flysch formation of 390m thickness. Eocene Limestones, Senonian Limestones and Vigla formation have thicknesses equal to 220m, 185m and 100m respectively. The final layer is Siniais-Pantokrator formation at 2285m depth. On the other hand, the lithostratigraphic column of Agios Georgios-3 well (Fig. 14) starts with an erosion surface and the debris layer at 0m depth. The Flysch formation follows with a thickness up to 1750m, while a thrust sheet is detected within it at a stratigraphic level of 1050m. Eocene Limestones, Senonian Limestones and Vigla formation have thicknesses equal to 140m, 580m and 1280m respectively. Posidonia Shales at 3960m and Pantokrator at 4210m depth are the final two layers.

According to the previous lithostatigraphic data, formations of Pliocene and Miocene age are not detected in Agios Georgios-3 well compared with East Erikoussa-1. The Flysch and Vigla formations of Agios Georgios-3 are much thicker than the corresponding formations of East Erikoussa-1. In addition, Posidonia shales formation detected only in Agios Georgios-3 well, while Siniais only in East Erikoussa-1. As mentioned previously, both wells are based in Ionian basin, but Agios Georgios-3 is an onshore well located in internal Ionian zone and East Erikoussa-1 is an offshore well located in external Ionian zone. It is clear that the location and events type (deposition, erosion, thrusting) difference between the wells directly affects the sedimentary sequence in each location.

Bearing the 1D basin modeling results of both wells in mind, we conclude that Agios Georgios-3 well has a thicker Vigla shales formation derived into two mature source rocks

than the Vigla shales formation of East Erikoussa-1 well, which has only one immature source rock. Posidonia shales formation which does not recorded in East Erikoussa-1 well is the most mature source rock formation of Agios Georgios-3 well with the higher transformation ratio (TR) values and potential hydrocarbon generation masses than Vigla shales A and Vigla shales B source rock formations.

REFERENCES

- Al-Hajeri, M.M., Al Saeed, M., Derks, J., Fuchs, T., Hantschel, T., Kauerauf, A., Neumaier, M., Schenk, O., Swientek, O., and Tessen, N. (2009). Basin and petroleum system modeling. *Oilfield Review*, 21(2), pp. 14–29.
- Allen, J.R.L. (1965). A review of the origin and characteristics of recent alluvial sediments. *Sedimentology*, 5: p. 89-191.
- Allen, J.R.L. (1970). Studies in fluvial sedimentation: composition of fining-upwards cyclothemes with special reference to coarse member composition and interpretation. *J. Sediment. Petrol.*, 40: p. 298-323.
- Allen, P.A. and Allen, J.R. (2005). *Basin Analysis: Principles and Applications*. Wiley-Blackwell, 2nd edition.
- Aubouin, J. (1959). Contribution à l' étude géologique de la Grèce septentrionale: Le confins de l' Epire et de la Thessalie. *Annales Géologiques des Pays Helléniques*, 10: 1-484, Athen.
- Aubouin, J. (1965). Geosynclines. *Developments in Geotectonics*, 1: 350 p., (Elsevier) Amsterdam.
- Aubouin, J. and Brunn, J.H. (1985). Zone Ionienne et Zone du Gavrovo en Épire Septentrionale: Le Mitsikéli et le Tymphé. *Ann. Géol. Pays Hell.*, 9:242-248, Athen.
- Avramidis, P. and Zelilidis, A. (2001). The nature of deep-marine sedimentation and palaeocurrent trends as an evidence of Pindos foreland basin fill conditions. *Episodes*, 24, 252–256
- Balarin, M. (1977). Improved approximations of the exponential integral in tempering kinetics. *Journal of Thermal Analysis and Calorimetry* 12, 169–177.
- Barker, C. and Takach, N.E. (1992). Prediction of natural gas composition in ultradeep Sandstone reservoirs. *American Association of Petroleum Geologists Bulletin* 76, 1859–1873.

Beardsmore, G.R. and Cull, J.P. (2001). *Crustal Heat Flow: A Guide to Measurement and Modelling*. Cambridge University Press, Cambridge. 324 p.

Behar, F., Kressmann, S., Rudkiewicz, J.L. and Vandenbroucke, M. (1992). Experimental simulation in a confined system and kinetic modeling of kerogen and oil cracking. *Organic Geochemistry* 19, 173–189.

Behar, F., Vandenbroucke, M., Tang, Y., Marquis, F. and Espitalie, J. (1997). Thermal cracking of kerogen in open and closed systems: determination of kinetic parameters and stoichiometric coefficients for oil and gas generation. *Organic Geochemistry* 26, 321–339.

Bellas, S.M. (1997). Calcareous nannofossils of the Tertiary Flysch (Post Eocene to Early Miocene) of the Ionian Zone in Epirus, NW-Greece: Taxonomy and Biostratigraphical correlations. *Berliner geowissenschaftliche Abhandlungen, E (22)*, I-VIII, 1-173, 9 plates (out of text), Berlin.

Bellas, S.M. and Frydas, D. (1996): Calcareous nannofossil stratigraphy of the Transitional Beds, from carbonates to Flysch, in the Ionian Zone (Eocene/Oligocene of NW-Greece). *Terra Nostra (Schriften der Alfred-Wegener-Stiftung)*, 96/6, 21, Leipzig.

Bellas, S.M., Mertmann, D., Manutsoglu, E., Bartholdy, J. & Frydas, D. (1995): The Oligocene Argyrotopos Profile in the External Ionian Basin (Epirus, Greece): Microfacies and microfossils. *Facies*, 33, 107-120, Erlangen.

Bourli, N., Pantopoulos, G., Maravelis, A.G., Zoumpoulis, E., Iliopoulos, G., Pomoni-Papaioannou, F., Kostopoulou, S. and Zelilidis, A. (2019). Late Cretaceous to early Eocene geological history of the eastern Ionian Basin, southwestern Greece: A sedimentological approach. *Cretac. Res.*, 98, 47–71.

Braun, R.L., Burnham, A.K., Reynolds, J.G. and Clarkson, J.E. (1991). Pyrolysis kinetics for lacustrine and marine source rocks by programmed micropyrolysis. *Energy and Fuels* 5, 192–204.

Bucker, C. and Rybach, L. (1996). A simple method to determine heat production from gamma ray logs. *Marine and Petroleum Geology* 13, 373–375.

Burnham, A.K. and Sweeney, J.J. (1989). A chemical kinetic model of vitrinite maturation and reflectance. *Geochimica et Cosmochimica Acta* 53, 2649–2657.

Butler, B. and Baldwin, C.O. (1985). Compaction curves. *American Association of Petroleum Geologists Bulletin* 69 (4), 622–626.

Cao, S. and Lerche, I. (1989). Basin modeling: Applications of sensitivity analysis. *J. Pet. Sci. Eng.*, 4: 83-104.

Connan, J. (1974). Time-temperature relation in oil genesis. *American Association of Petroleum Geologists Bulletin*, 2516–2521.

Danelian, T. and Baudin, F. (1990). Discovery of an organic-rich carbonated horizon on the top of the radiolarites from Epirus (Ionian zone, Greece): The Paliambela Member. *C.R.Acad.Sci.Paris*, 311, II, 421-428.

Dembicki, Jr.H. (2017). *Practical petroleum geochemistry for exploration and production*. Elsevier.

Dieckmann, V., Horsfield, B. and Schenk, H.J. (2000). Heating rate dependency of petroleum-forming reactions: implications for compositional kinetic predictions. *Organic Geochemistry* 31, 1333–1348.

Doutsos, T., Piper, G., Boronkay, K. and Koukouvelas, I. (1993). Kinematics of the Central Hellenides. *Tectonics* 12, 936–953.

Dow, W. G. (1977). Kerogen studies and geological interpretations, *Journal of Geochemical Exploration*, 7, 79-99.

Erickson, A.J., Simmons, M.G. and Ryan W.B.F. (1976). Review of heat flow data from the Mediterranean and Aegean Seas, in: Biju-Duval, B., Montadert, L. (Eds.), *Int. Symp. on the Strut. Hist. of the Medit. Basin. Split, Yugoslavia*, pp. 263–280.

Esposito, K.J. and Whitney, G. (1995). Thermal effects of thin igneous intrusions on diagenetic reactions in a tertiary basin of southwestern Washington. *United States Geological Survey Bulletin* 2085-C 48.

Falvey, D.A. and Middleton, M.F. (1981). Passive continental margins: evidence for a prebreakup deep crustal metamorphic subsidence mechanism. In: *Oceanologica Acta*, Proceedings of 26th IUGG SP, pp. 103–114.

Fertl, W.H. and Wichmann, P.A. (1977). How to determine static BHT from well log data. *World Oil* 184, 105–106.

Fytikas, M.D. and Kolios, N.P. (1979). Preliminary heat flow map of Greece, in: Cermak, L. Rybach (Eds.), *Terrestrial Heat Flow in Europe*, Springer – Verlag, Berlin Heidelberg, 1979, pp. 197 – 205

Gear, C.W. (1971). *Numerical Initial Value Problems in Ordinary Differential Equations*. Prentice-Hall, Englewood Cliffs, New Jersey. 253 p.

Georgalas, L., Zacharopoulos, A., Angelopoulos, A., Bellas, S., Tripsanas, E., Athanasiadis, I. (2012): New Developments on Exploration & Exploitation of Hydrocarbons in Greece: Invitations to Procedures a) Non-exclusive seismic surveys b) Open Door. *Symposium on Energy*, Athens University, Geology & Geoenvironment Dept., Febr. 17th, Athens, Greece.

Getsos, K., Pomoni-Papaioannou, F. and Zelilidis, A. (2018). Triassic carbonate and evaporite sedimentation in the Ionian zone (Western Greece): Palaeogeographic and palaeoclimatic implication. *Bulletin of the Geological Society of Greece*, 36(2), 699-707.

Gretener, P.E. (1981). *Geothermics, Using Temperature in Hydrocarbon Exploration*. American Association of Petroleum Geologists Education Course Note Series, vol. 17, 156 p.

Hantschel, T. and Kauerauf, A.I. (2009). *Fundamentals of Basin and Petroleum Systems Modeling*. Springer, Berlin.

Horner, D.R. (1951). Pressure build-up in wells. In: *Proceedings of the Third World Petroleum Congress*, Lieden, The Netherlands, Sec. II, pp. 503–521.

Hsu, K., Montadert, L., Garrison, R.E., Fabricius, F.H., Bernoulli, D., Melieres, F., Kidd, R.B., Muller, C., Cita, M., Bizon, G., Wright, R. and Erickson A. (1975). Glomar challenger returns to the Mediterranean Sea. *Geotimes*, 20, pp. 16-19

(IFP) Institute Francais du Petrole (1966). Etude géologique de l'Épire (Grèce nord-occidentale). 306 p., (Edition Technipress) Paris.

Jacobshagen, V. (Ed.) (1986). Geologie von Griechenland.- 363 p., (Gebrüder Borntraeger) Berlin-Stuttgart

Jongsma, D. (1974). Heat flow in the Aegean Sea. *Geophys. J. R. Astron. Soc.*, 37, pp. 337-346.

Karakitsios, V. (1995). The influence of preexisting structure and halokinesis on organic matter preservation and thrust system evolution in the Ionian Basin, Northwest Greece. *AAPG Bulletin*, 79, 960–980.

Karakitsios, V. (2007). Studying the Carbonates from Triassic to Eocene in the Ionian Zone., IAS 2007 25th Meeting (Patras, 2007), Field Trips guide book, Field Trip P 3, pp. 123 141.

Karakitsios, V. (2013). Western Greece and Ionian Sea petroleum systems. *AAPG Bulletin*, 97, (9), 1567-1595.

Karakitsios, V. and Rigakis, N. (1996). New Oil Source Rocks Cut in Greek Ionian Basin. *Oil and Gas Journal*, 94, (7), 56-59.

Karakitsios, V. and Rigakis, N. (2007). Evolution and petroleum potential of Western Greece. *Journal of PetroleumGeology*, 30, (3), 197-218.

Karakitsios, V., Roveri, M., Lugli, S., Vinicio, M., Rocco, G., Antonarakou, A., Triantaphyllou, M., Agiadi, K., Kontakiotis, G. and Kafousia, N. (2017). A record of the Messinian Salinity Crisis in the eastern Ionian tectonically-active domain (Greece, eastern Mediterranean). *Bas. Res.*, 29, 203–233.

Kontakiotis, G., Moforis, L., Karakitsios, V. and Antonarakou, A. (2020). Sedimentary Facies Analysis, Reservoir Characteristics and Paleogeography Significance of the Early Jurassic to Eocene Carbonates in Epirus (Ionian Zone, Western Greece). *J. Mar. Sci. Eng.*, 8, 706.

Larter, S.R., 1989. Chemical models of vitrinite reflectance evolution. *Geologische Rundschau* 78, 349–359.

Lie, Ø., Fürstenau, J., Bellas, S. and Tsifoutidis G. (2013):.Exploration: A Fresh Look at the Oil & Gas Potential of Greece. *GeoExPro*, vol. 10, pp. 46-48, London.

Lopatin, N.V. (1971). Temperature and geologic time as factors in coalification (in Russian): *Akademii Nauk SSSR Izvestiya. Ser Geologicheskaya* 3, 95–106.

Magara, K. (1978). Geological models of petroleum entrapment, Elsevier, Applied Science Publishers (eds.), 328 pp.

Magoon, L.B. and Beaumont, E.A. (2003). Search and Discovery Article #40068 Adaptation and revision for online presentation of Chapter 3, “Petroleum Systems,” by Leslie B. Magoon and Edward A. Beaumont, in *Exploring for Oil and Gas Traps*, Edward A. Beaumont and Norman H. Foster, eds., *Treatise of Petroleum Geology, Handbook of Petroleum Geology*, 1999.

Magoon, L.B. and Dow, W.G. (1994). “The Petroleum System” - In: Magoon, L.B. and Dow, W.G. (eds.): *The Petroleum System - From Source to Trap*. - AAPG Memoir 60: 3 – 24

Maravelis, A., Makrodimitras, G. and Zelilidis, A. (2012). Hydrocarbon prospectivity in Western Greece. *Oil and GasEuropean Journal*, 38, (2), 84-89.

Mavromatidis, A. (2009). ‘Review of Hydrocarbon Prospectivity in the Ionian Basin, Western Greece’: *Energy Sources, Part A: Recovery, Utilization, and Environmental Effects*, 31:7,619-632.

McKenzie, D.P. (1978). Some remarks on the development of sedimentary basins. *Earth Planetary Science Letters* 40, 25–32.

McKenzie, D.P. (1981). The variation of temperature with time and hydrocarbon maturation in sedimentary basins formed by extension. *Earth and Planetary Science Letters* 55, 87–98.

Nakayama, K. (1987). Hydrocarbon-expulsion model and its application to Niigata area, Japan. *American Association of Petroleum Geologists Bulletin* 71, 810–821.

Okosun, E.A., and Osterloff, P. (2014). Ostracod, Diatom and Radiolarian Biostratigraphy of the Niger Delta, Nigeria. *Earth Science Research*; Vol. 3, No. 1; 2014. Published by Canadian Center of Science and Education.

Papadakis, G., Vallianatos, F. and Sammonds, P. (2016). "Non-extensive statistical physics applied to heat flow and the earthquake frequency–magnitude distribution in Greece," *Physica A: Statistical Mechanics and its Applications*, Elsevier, vol. 456(C), pages 135-144.

Papanikolaou, D. (2009). Timing of tectonic emplacement of the ophiolites and terrane paleogeography in the Hellenides. *Lithos*, 108, 262–280.

Pasadakis, N. (2015). “Γεωχημεία Πετρελαίου” (Petroleum Geochemistry), Tziolas Publishing, Greece, p. 270.

Pepper, A.S. and Corvi, P.J. (1995). Simple kinetic models of petroleum formation: Part I—oil and gas generation from kerogen. *Marine and Petroleum Geology* 12, 291–319.

Philp, R.P. (2003). Formation and geochemistry of oil and gas. In: Holland HD, Turekian KK, Mackenzie FT (eds) *Treatise on geochemistry*. Elsevier, Amsterdam, pp. 223-256

Pickard, G.L. (1963). *Descriptive Physical Oceanography*. Pergamon Press, New York. 200 p.

Pollack, H.N. (1982). The heat flow from the continents. *Annual Review of Earth and Planetary Sciences* 10, 459–481.

Rigakis, N. (1999). Contribution to stratigraphic research on wells and outcrops of the Alpine formations in Western Greece, in relation to the petroleum generation efficiency of their organic matter, Ph.D Thesis, University of Athens, p. 255.

Rigakis, N. and Karakitsios, V. (1998). The source rock horizons of the Ionian Basin (NW Greece). *Marine and Petroleum Geology*, 15, 593–617.

Rigakis, N., Karakitsios, V., Marnelis, F., and Sotiropoulos, S. (2013). Geological solutions concluded by petroleum geochemical data in Western Greece. *Bulletin of the Geological Society of Greece*, 47(4), pp. 2131-2143.

Schjeldsøe Berg, M., Fürstenau, J., Bellas, S. (2014). Exploring Greece with a new subsurface perspective. *Offshore Mag.*, (2014), 40-43.

Sclater, J.G. and Christie, P.A.F. (1980). Continental stretching: an explanation of post Mid-Cretaceous subsidence of the Central North Sea. *Journal of Geophysical Research* 85, 3711–3739.

Suzuki, N., Matsubayashi, H. and Waples, D.W. (1993). A simpler kinetic model of vitrinite reflectance. *American Association of Petroleum Geologists Bulletin* 77, 1502–1508.

Sweeney, J.J. and Burnham, A.K. (1990). Evaluation of a simple model of vitrinite reflectance based on chemical kinetics. *American Association of Petroleum Geologists Bulletin* 74, 1559–1570.

Sylwan, C.A., Rodriguez, J.F.R. and Strelkov, E.(2008). Petroleum systems of the Golfo san Jorge Basin, Argentina. In: *7th Congreso de Exploración y Desarrollo de Hidrocarburos, Simposio Sistemas Petroleros de las Cuencas Andinas*. pp. 53–77. (Mar del Plata).

Tegelaar, E.W. and Noble, R.A. (1994). Kinetics of hydrocarbon generation as a function of the molecular structure of kerogen as revealed by pyrolysis-gas chromatography. *Organic Geochemistry* 22, 543–574.

Tissot, B. (1969). Premières données sur les mécanismes et la cinétique de la formation du pétrole dans les bassins sédimentaires. Simulation d'un schema réactionnel sur ordinateur. *Revue Institut Francais Petrole* 24, 470–501.

Tissot, B.P. and Espitalie, J. (1975). L'évolution thermique de la matiere organique des sediments: applications d'une simulation mathematique. *Revue de l'Institut Franccais du Petrole* 30, 743–777.

Tissot, B.P., Pelet, R. and Ungerer, P.H. (1987). Thermal history of sedimentary basins, maturation indices, and kinetics of oil and gas generation. *American Association of Petroleum Geologists Bulletin* 71, 1445–1466.

Turcotte, D.L. (1980). On the thermal evolution of the earth. *Earth and Planetary Science Letters*, 48:53–58.

Ungerer, P., Burrus, J., Doligez, B., Chenet, P.Y. and Bessis, F. (1990). Basin evaluation by integrated two dimensional modelling of heat transfer, fluid flow, hydrocarbon generation and migration: *AAPG Bulletin*, v. 74, pp. 309-335.

Ungerer, P., Espitalie, J., Behar, F. and Eggen, S. (1988b). Modelisation mathemetique des interactions entre craquage thermique et migration lors de la formation du petrole et du gaz. Comptes Rendus de l'Académie des Sciences, Series II 927–934.

Vandenbroucke, M., Behar, F. and Rudkiewicz, J.L. (1999). Kinetic modelling of petroleum formation and cracking: implications from the high pressure/high temperature Elgin Field (UK, North Sea). *Organic Geochemistry* 30, 1105–1125.

Waples, D.W. (1980). Time and temperature in petroleum formation: application of Lopatin's method to petroleum exploration. *American Association of Petroleum Geologists Bulletin* 64 (6), 916–926.

Welte, D.H. and Yalcin, M.N. (1988). Basin modelling - a new comprehensive methodology in petroleum geology. In: Matavelli L, Novelli L (eds) *Advances in organic geochemistry* 13. Pergamon, Oxford, pp. 141-151.

Welte, D.H., Horsfield, B. and Baker, D.R. (1997). *Petroleum and basin evolution*: Springer-Verlag, pp. 1-536.

Wygrala, B.P. (1989). Integrated study of an oil field in the southern Po basin, northern Italy. Diss, Univ Köln, Berichte Kernforschungsanlage Jülich, no 2313, pp. 1–217.

Zelilidis, A., Maravelis, A., Tserolas, P. and Konstantopoulos, P., 2015. An overview of the petroleum systems in the Ionian zone, onshore NW Greece and Albania, *Journal of Petroleum Geology*, 38, 331-348

Zelilidis, A., Piper, D.J.W. and Kontopoulos, N. (2002). Sedimentation and basin evolution of the Oligocene- Miocene Mesohellenic basin, Greece. *AAPG Bulletin*, 86, 161-182.

Zelilidis, A., Piper, D.J.W., Vakalas, I., Avramidis, P. and Getsos, K. (2003). Oil and gas plays in Albania: Do equivalent plays exist in Greece? *Journal of Petroleum Geology*, 26, (1), 29-48.

APPENDIX

Mixed lithologies created for well Agios Georgios-3.

Table A: Lithology of Debris formation.

DEBRIS	LITHOLOGY	PERCENT
	Flysch	80.00
	Conglomerate (typical)	20.00

Table B: Lithology of Flysch formation.

FLYSCH	LITHOLOGY	PERCENT
	Siltstone (organic lean)	50.00
	Clay (base component)	20.00
	Sandstone (typical)	20.00
	Conglomerate (typical)	10.00

Table C: Lithology of Vigla limestones-shales formation.

VIGLA LSTS-SHALES	LITHOLOGY	PERCENT
	Limestone (micrite)	50.00
	Shale (typical)	20.00
	Limestone (organic rich-typical)	10.00
	Marl	10.00
	Chert	10.00

Table D: Lithology of Vigla shales A formation.

VIGLA SHALES A	LITHOLOGY	PERCENT
	Shale (typical)	70.00
	Limestone (micrite)	10.00
	Limestone (organic rich-typical)	10.00
	Marl	5.00
	Chert	5.00

Table E: Lithology of Vigla limestones formation.

VIGLA LSTS	LITHOLOGY	PERCENT
	Limestone (micrite)	80.00
	Dolomite (typical)	20.00

Table F: Lithology of Vigla shales B formation.

VIGLA SHALES B	LITHOLOGY	PERCENT
	Shale (typical)	80.00
	Limestone (micrite)	15.00
	Dolomite (typical)	5.00

Table G: Lithology of Vigla dol. limestones-shales formation.

VIGLA DOL. LSTS-SHALES	LITHOLOGY	PERCENT
	Shale (typical)	43.00
	Limestone (micrite)	30.00
	Dolomite (typical)	25.00
	Chert	2.00

Table H: Lithology of Posidonia formation.

POSIDONIA	LITHOLOGY	PERCENT
	Dolomite (typical)	35.00
	Limestone (micrite)	30.00
	Shale (typical)	20.00
	Marl	10.00
	Chert	5.00

Mixed lithologies created for well East Erikoussa-1.

Table I: Lithology of Alluvial formation.

ALLUVIAL	LITHOLOGY	PERCENT
	Clay (base component)	34.00
	Siltstone (organic lean)	33.00
	Sandstone (typical)	33.00

Table J: Lithology of Pliocene formation.

PLIOCENE	LITHOLOGY	PERCENT
	Clay (base component)	25.00
	Siltstone (organic lean)	25.00
	Conglomerate (typical)	25.00
Coal (pure)	25.00	

Table K: Lithology of Miocene formation.

MIOCENE	LITHOLOGY	PERCENT
	Clay (base component)	80.00
	Siltstone (organic lean)	20.00

Table L: Lithology of Flysch formation.

FLYSCH	LITHOLOGY	PERCENT
	Siltstone (organic lean)	50.00
	Clay (base component)	20.00
	Sandstone (typical)	20.00
Limestone (micrite)	10.00	

Table M: Lithology of Vigla formation.

VIGLA	LITHOLOGY	PERCENT
	Shale (typical)	60.00
	Limestone (micrite)	20.00
	Marl	10.00
Chert	10.00	

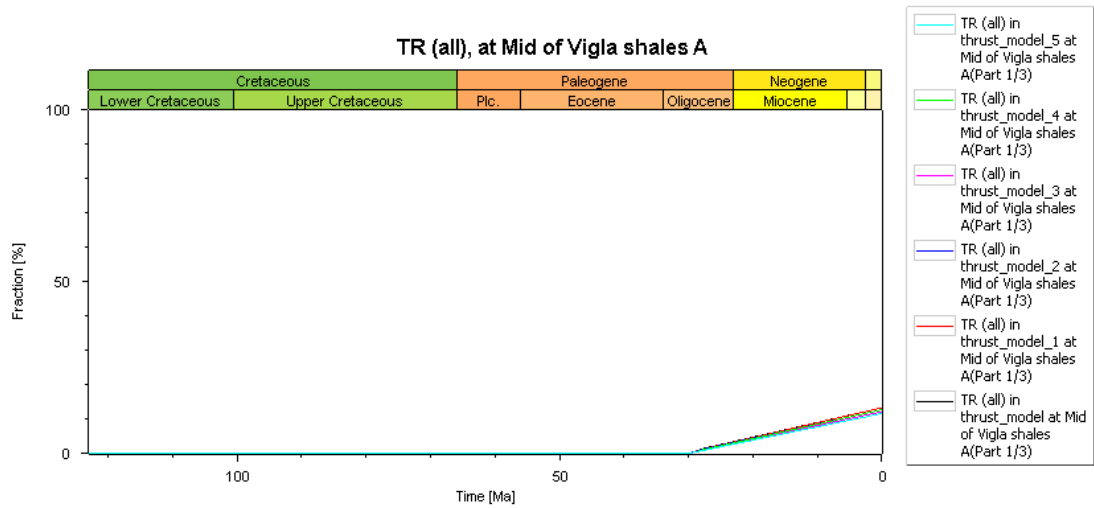


Figure A: Transformation ratio (TR) vs. time (Ma) plots of all thrust models at Vigla shales A formation.

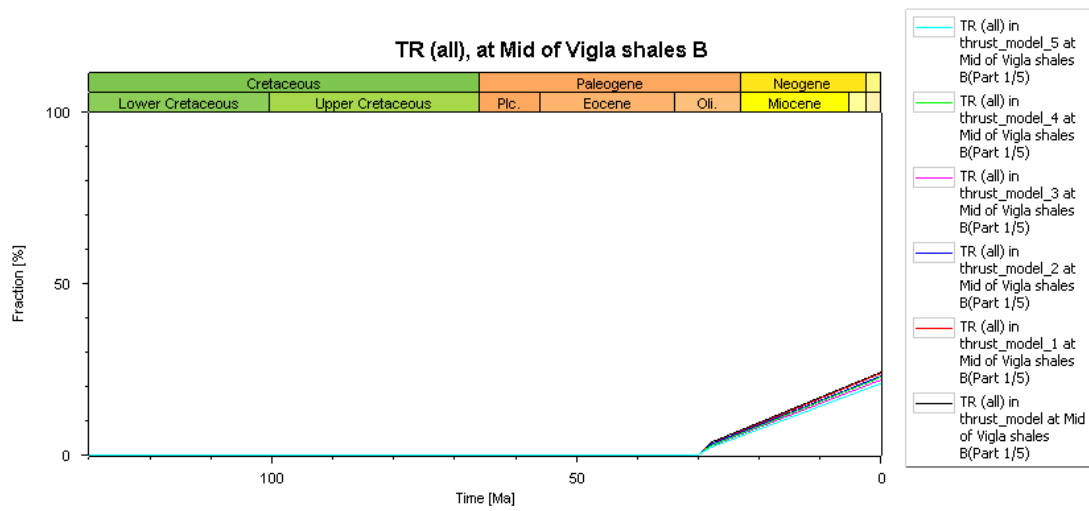


Figure B: Transformation ratio (TR) vs. time (Ma) plots of all thrust models at Vigla shales B formation.

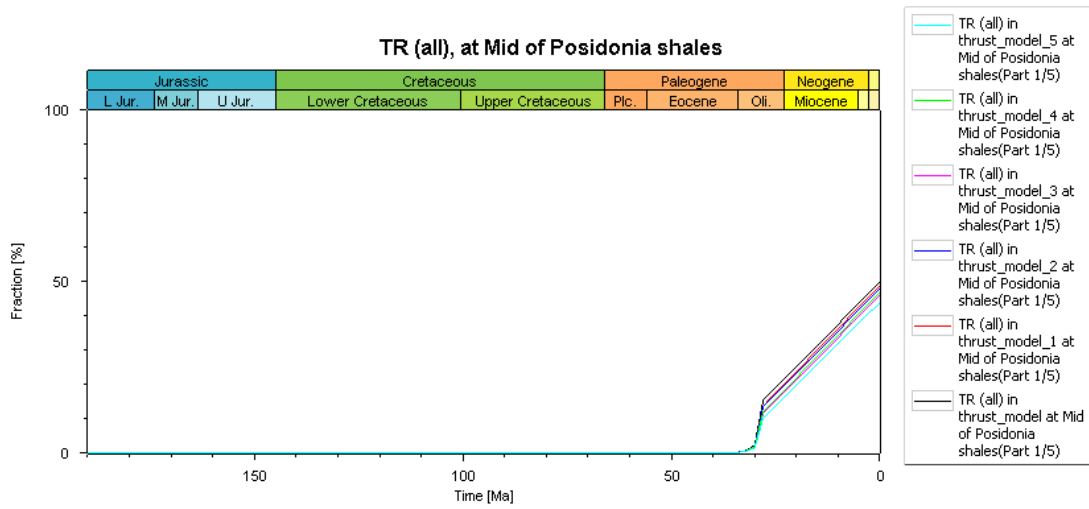


Figure C: Transformation ratio (TR) vs. time (Ma) plots of all thrust models at Posidonia shales formation.

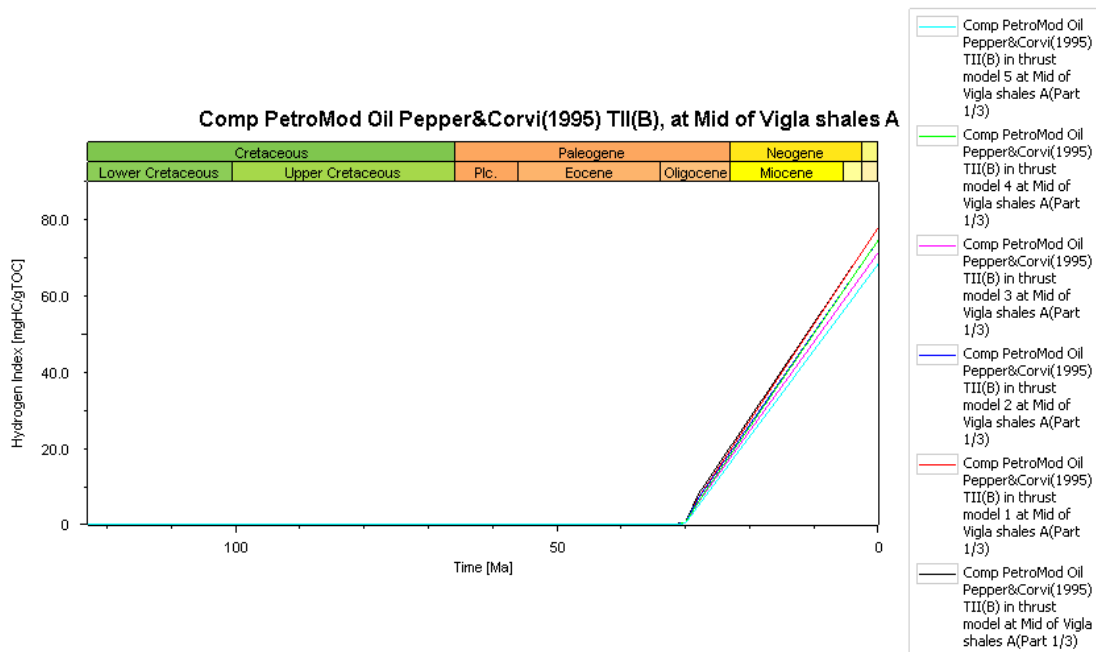


Figure D: Potential oil generation mass by Pepper & Corvi (1995) vs. time (Ma) plots of all thrust models at Vigla shales A formation.

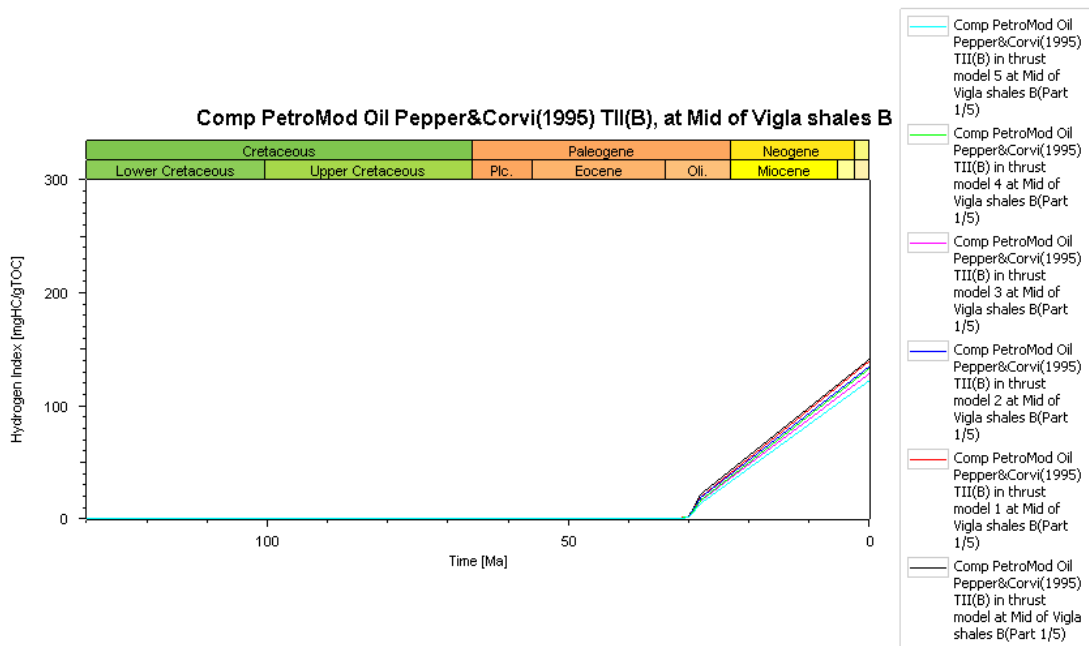


Figure E: Potential oil generation mass by Pepper & Corvi (1995) vs. time (Ma) plots of all thrust models at Vigla shales B formation.

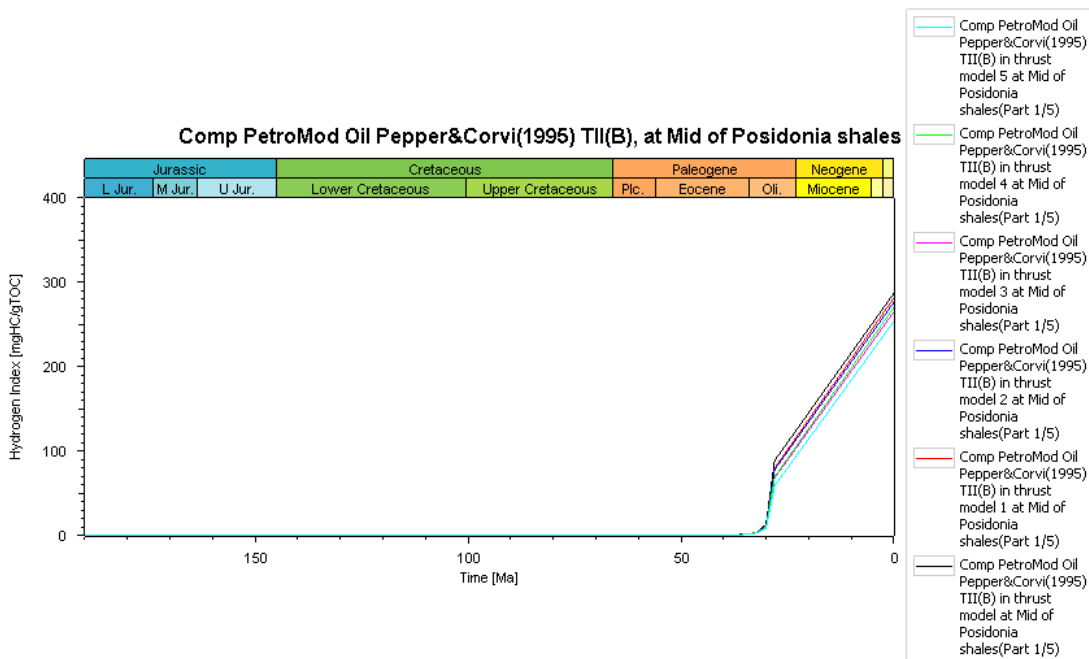


Figure F: Potential oil generation mass by Pepper & Corvi (1995) vs. time (Ma) plots of all thrust models at Posidonia shales formation.

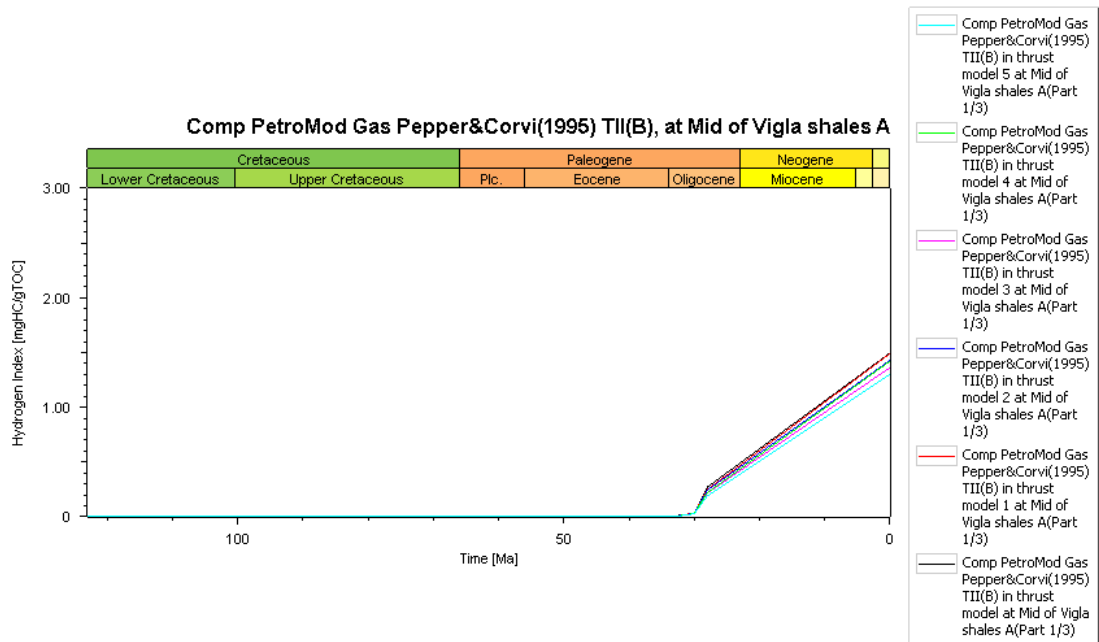


Figure G: Potential gas generation mass by Pepper & Corvi (1995) vs. time (Ma) plots of all thrust models at Vigla shales A formation.

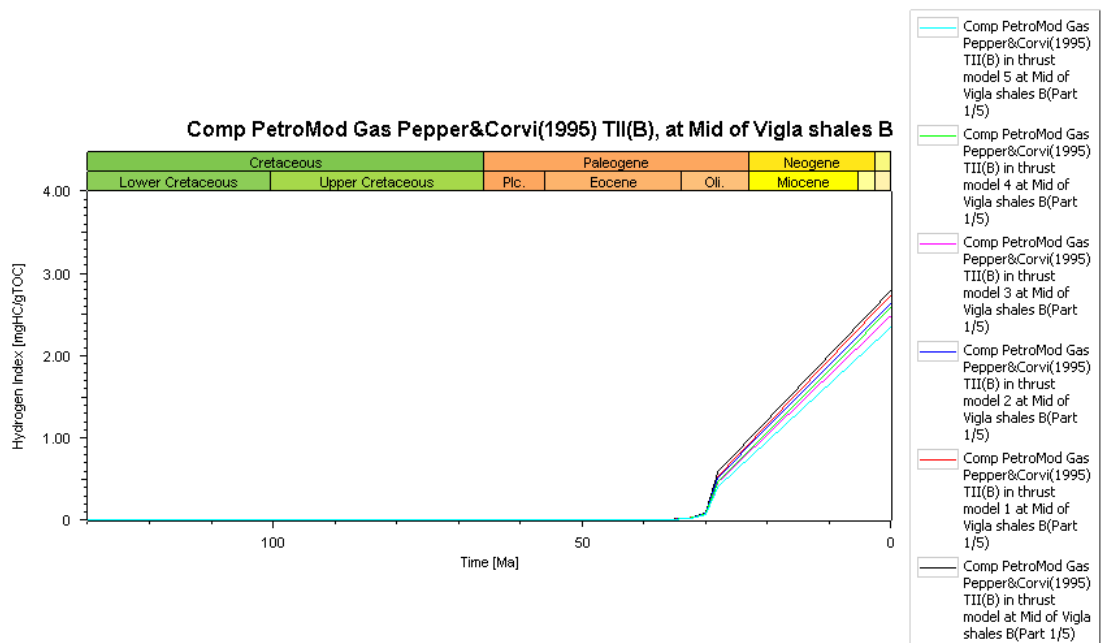


Figure H: Potential gas generation mass by Pepper & Corvi (1995) vs. time (Ma) plots of all thrust models at Vigla shales B formation.

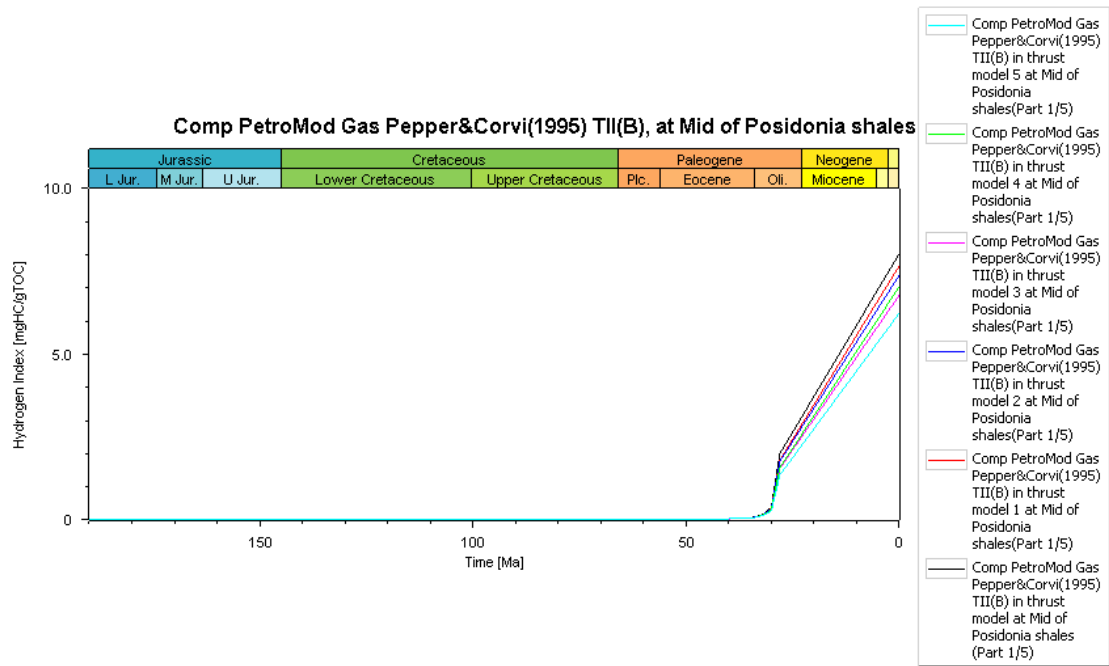


Figure I: Potential gas generation mass by Pepper & Corvi (1995) vs. time (Ma) plots of all thrust models at Posidonia shales formation.